Climatic growth signatures in observed and modelled tree-rings - constraints from a global tree-ring network

Inauguraldissertation
der Philosophisch-naturwissenschaftlichen Fakultät
der Universität Bern

vorgelegt von

Petra Daniela Breitenmoser

von Wetzikon ZH

Leiter der Arbeit:
Prof. Dr. Stefan Brönnimann
Geographisches Institut, Universität Bern

Climatic growth signatures in observed and modelled tree-rings - constraints from a global tree-ring network

Inauguraldissertation
der Philosophisch-naturwissenschaftlichen Fakultät
der Universität Bern

vorgelegt von

Petra Daniela Breitenmoser

von Wetzikon ZH

Leiter der Arbeit:
Prof. Dr. Stefan Brönnimann
Geographisches Institut, Universität Bern

Von der Philosophisch-naturwissenschaftlichen Fakultät angenommen.

Bern, den 28. Februar 2012 Der Dekan:

Prof. Dr. S. Decurtins

Summary

Information derived from tree-rings greatly expanded our understanding of the spectrum of past climate variability and its forcing mechanisms during the last centuries to millennia. Tree-ring archives are spatially widely distributed, annually resolved and dated, and the physiological basis for the response of trees to climate is well founded. This thesis presents three studies analysing climatic growth signatures in observed and modelled tree-rings to deepen our understanding of past climate variability and to develop and test novel reconstruction methods to combine model and proxy data.

Within the first study, solar and volcanic fingerprints were analysed in a near global collection of 17 annually-resolved tree-ring-based climate proxies spanning the past two millennia. Analyses in the frequency domain indicated significant periodicities in the 208-year frequency band, corresponding to the DeVries cycle of solar activity. However, solar-climate associations remained weak. Other forcing factors, namely volcanic activity, appeared to mask the solar signal in space and time. To investigate this hypothesis, volcanic signals were extracted from the temperature proxies using a statistical modelling approach. Wavelet analysis of the volcanic contribution revealed significant periodicities near the DeVries frequency during the Little Ice Age (LIA). This remarkable and coincidental superposition of the signals hindered a clear separation of volcanic and solar forcing during the LIA. Nevertheless, the "volcano free" temperature records showed significant periodicities near the DeVries periodicity during the entire past 1500 years, further pointing to solar mechanisms. Moreover, evidences of synchronous cooling events in respect to highly explosive tropical volcanic eruptions could be described.

In the second study, relationships between climate and tree-ring data were investigated on a global scale using the process-based Vaganov-Shashkin-Lite (VSL) forward model of tree-ring width formation. The VSL model requires as inputs only latitude, monthly mean temperature, and monthly accumulated precipitation. Analysis of the growth response of simulated tree-rings was performed based upon past monthly climate conditions obtained from the CRU TS3.1 data set back to 1901. Key aims were (a) to examine the relations among VSL modelled growth and growth observed in actual tree-ring chronologies at 2287 globally distributed sites and (b) to evaluate the potential of the VSL model to reconstruct past climate. A new assessment of the growth-onset threshold temperature of approximately 4-6 °C for most sites and species using a Bayesian estimation approach provided new quantification for the lower temperature limits where plant growth may be sustained. Results further demonstrated that the VSL model can skilfully simulate site level tree-ring series in response to climate forcing for a wide range of environmental conditions and species. Spatial aggregation of the tree-ring chronologies to reduce non-climatic noise at the site level yielded notable improvements in the coherence between modelled and actual growth and provided a basis for reconstruction methodology.

The third study combines climate model simulations and tree-ring width time series to obtain climate reconstructions. By selecting, for each 6-month-period, the best member among an ensemble of

simulations according to its agreement with observed tree growth, we obtain a reconstruction that is consistent with model physics, forcing, and proxy data. A 30 member initial-condition ensemble performed with the ECHAM5.4 general circulation model for the period 1600-2005 forms the basis of the study. The model was forced with observed and reconstructed sea-surface temperatures as well as with time series of the main external forcing factors. The VSL forward model of tree-ring growth was used to simulate tree growth in these model simulations. Tree-ring growth was simulated at 405 grid points as a function of monthly mean temperature, monthly accumulated precipitation, and latitude. The best member was then selected according to the mean squared error between modelled and observed tree-ring width. The skill of the approach was estimated in the 1911-1970 period using CRU TS3 temperature and precipitation as a reference. The procedure improved the skill compared to the ensemble mean, although correlations are low in some regions, while maintaining physically plausible results. The reconstructions are able to use tree-ring data far away from the more typical locations where growth is limited by one climate parameter. The VSL model makes this possible by explicitly integrating joint temperature and moisture variation in a non-linear way.

These three studies contribute to an enhanced understanding of past climate variability and provide valuable knowledge to the advancement of combining model and proxy data. It could be shown that successful implementation of forward models strongly relies on continued efforts to improve climate models and proxy data. The analogue reconstruction of summer temperature and precipitation represents a first milestone toward more sophisticated data-assimilation oriented approaches. This approach opens great possibilities to study the climate of the past in great detail with all the advantages model data offers.

Contents

List of Figures

List of Tables

Abbreviations

Institutions, scientific programs and projects

ARSTAN	AutoRegressive STANdardization
CPS	Climate Prediction Center
CRU	Climate Research Unit
ECHAM	Atmospheric General Circulation Model (developed at the Max Planck Institute for Meteorology (MPIM)
IPCC	Intergovernmental Panel on Climate Change
ITRDB	International Tree Ring Database
NCCR Climate	National Centre of Competence in Research on Climate
NCDC	National Climate Data Center
NOAA	National Oceanic and Atmospheric Administration
NSF	Swiss National Science Foundation
PALVAREX	Paleoclimate Variability and Extreme Events

Variables and parameters

ASD	Average Sample Depth
CCC400	Model variant of the ECHAM5.4 model
D	Drought
g	Growth parameter
M	Moisture
MSE	Mean square error
MSL	Mean Segment Length
P	Precipitation
T	Temperature
T_1	Growth-onset threshold temperature
TRW	Tree Ring Width
TSI	Total Solar Irradiance

Other abbreviations

AD	Anno Domini
AOD	Aerosol Optical Depth
BHM	Bayesian Hierarchical Model
CGCM	Coupled General Circulation Model
DACP	Dark Age Cold Period
EMIC	Earth system Model of Intermediate Complexity
ENSO	El Niño Southern Oscillation
EPS	Expressed Population Signal
GCM	Global Circulation Model
LIA	Little Ice Age
m.a.s.l.	Meters above sea level
MCA	Medieval Climate Anomaly
MOC	Meridional Overturning Circulation
NAO	North Atlantic Oscillation
NH	Northern Hemisphere
PCA	Principal Component Analysis
RWP	Roman Warm Period
SEA	Superposed Epoch Analysis
SH	Southern Hemisphere
VS	Vaganov-Shashkin
VSL	Vaganov-Shashkin-Lite

Chapter 1

INTRODUCTION

1.1 Relevance of research

Knowledge of past climate variability provides a crucial context for understanding the ongoing and future changes in climate (IPCC, 2007). The detection and attribution of past climatic changes to anthropogenic influences and different natural forcing factors is hence crucial in the debate about the level of mitigation and adaption efforts required (IPCC, 2007). Estimates of such effects on climate provide valuable insights into the complex environmental interactions of forcing factors, either internal or external to the climate system on various temporal and spatial scales (Crowley, 2000; Hegerl et al., 2007a,b, 2011; Wanner et al., 2008). The unprecedented large and fast climate changes in the recent decades, however, were preceded by a regime of comparatively minor changes in external forcing. The detection and understanding of larger spatiotemporal fluctuations need long records along with a dense global network of observations of the climate system. Analysis of climate variability and climate change, therefore, depends strongly on the availability, high temporal resolution, and accuracy of records of meteorological/climatological parameters and climate forcing factors (Hegerl et al., 2007a; Jansen et al., 2007). Direct instrumental or satellite-based measurements, however, are not available in the pre-industrial era. Consequently, these relatively short records cannot cover the full range of natural climate variability and we have to rely either on climate modelling studies or on climatic information stored in natural proxy archives through physical, biological, and/or chemical processes in response to environmental conditions (Gray et al., 2009). One of the most commonly-used climate proxies in climate reconstructions for the past centuries to millennia are the annually formed rings of trees. Climatic information derived from tree-rings has greatly expanded our understanding of the nature and range of past climatic variability, especially in the context of the emerging signals of global climate change (e.g. Hughes, 2002; Jones and Mann, 2004; Jansen et al., 2007).

1.2 Tree-rings in climate reconstructions

Temperature, moisture, and light are the main locally-relevant climatic conditions affecting tree-ring growth (Vaganov et al., 2006; Vaganov et al., 2011) while the climatic imprint in tree-rings is contained in tree-ring width, density, cell diameter, cell wall thickness, and stable isotopes (Vaganov et al., 2011). Of these, tree-ring width is the most widely used variable for climate reconstructions.

The main advantages of tree-rings in comparison to other proxy data are the inexpensive sampling, the relatively easy and precise dating, the temporally stable and high (annual) resolution, the spatially dense and expansive distribution, the length of tree-ring chronologies from decades to millennia, and their high climate sensitivity (Hughes, 2002; Jones et al., 2009). Besides, large efforts were undertaken by the dendro-community to steadily develop a vast network of tree-ring chronologies meeting a common standard. Data can be obtained from the International Tree Ring Database (ITRDB, Grissino-Mayer and Fritts, 1997; http://www.ncdc.noaa.gov/paleo/treering.html). For these reasons, tree-rings are most prominently used in quantitative high-resolution reconstructions of temperature on global, hemispheric, and continental scales (e.g. Jones et al., 1998; Moberg et al., 2005; D'Arrigo et al., 2006; Mann et al., 2008, 2009; Christiansen and Ljungqvist, 2012).

1.2.1 Tree-rings in conventional past climate reconstructions

The use of tree-rings in conventional empirical climate reconstructions requires a transfer function to translate the proxy information into climatic data (commonly temperature or precipitation). However, relationships between tree-growth and climate are complex and classical calibration methods (i.e. establishing a statistical relationship between instrumental and proxy data during their period of overlap) are often inadequate for a few reasons. Firstly, empirical methods generally treat climate as a function of the proxy rather than quantify how proxy signals are driven by climate variability. Secondly, statistical calibration is bound by assumptions of uniformitarianism and stationarity in the climate-growth system - conditions that may not be adequately met in the past (Rutherford et al., 2003; Jones and Mann, 2004; Raible et al., 2006; D'Arrigo et al., 2008). Thirdly, most tree-ring based reconstructions of temperature are limited to regions where growth is primarily limited by cold temperatures - leaving the vast areas of the Earth away from high mountains and high latitude environments poorly represented by high-quality proxy data (Wahl and Frank, 2012).

Hence, empirical methods are often inadequate to represent the complex mechanisms linking tree growth to climate even though it has been demonstrated repeatedly that these linear statistical based reconstructions can effectively capture tree-ring growth - climate relationships at specific locations up to the hemispheric scale (e.g. Fritts et al., 1971, 1976; Rutherford et al., 2003, 2005; Anchukaitis et al., 2006; D'Arrigo et al., 2006; Cook et al., 2007; Mann et al., 2008, 2009). A general review of the state of the art of these reconstruction methods of the last millennium is provided by Jones et al. (2009).

1.2.2 Comparison of tree-ring reconstructions with climate models

Along with these empirical-statistical based methods, dynamical methods are often used to analyse the climate of the past. Simulations using climate models of various complexities are a source to climatic information independent from proxy data and are based on physical principles and external forcing. They are driven by both natural and anthropogenic forcings (e.g. changes in solar irradiance, land cover, atmospheric aerosols, and greenhouse gas concentrations) to simulate past climate variability (e.g. Crowley, 2000; Gonzáles-Rouco et al., 2003; Ammann et al., 2007; Jansen et al., 2007; Gao et al., 2008; Wanner et al., 2008; Steinhilber et al., 2009; Jungclaus et al., 2010). Therefore, models help to quantitatively understand the mechanisms of past climatic changes and to place the recent 20th and 21st century warming trends into a longer-term perspective (IPCC, 2007; Wanner et al., 2008).

Comparisons of large-scale analyses of multi-proxy reconstructions with simulations using global climate models (GCMs) and systematic model intercomparisons have greatly improved our understanding of externally and internally forced past climate variability (Crowley, 2000; Hegerl et al., 2003; Shindell et al., 2003; Ammann et al., 2007; Jansen et al., 2007a; Wanner et al., 2008; Gray et al., 2009; Wahl and Frank, 2012). It has been shown, for instance, that the nature and scale of hemispheric-scale climate variability on Northern Hemisphere temperature over the past millennia were greatly consistent in the output of forced climate models and with proxy reconstructions that did not make use of forcing information (Jansen et al., 2007 and references therein). Likewise, comparison of simulated and reconstructed climate to estimate natural (i.e. solar and volcanic) external forcings, have provided significant understanding of past forced responses of climate (Haigh, 1996; Robock, 2000; Shindell et al., 2001, 2003; Waple et al., 2002).

However, high-resolution climate reconstructions, which are largely based on tree-ring width chronologies, and state-of-the-art coupled general circulation model (CGCM) simulations, only cover the last few centuries to millennia, limiting the evaluation of variance on long time scales. Limitations related to the removal of biological age-trends in tree-ring width reconstructions further limit the evaluation of low-frequency climate variability (e.g. Moberg et al., 2005). Additionally, there is an ongoing debate on how an incomplete understanding of processes incorporated in climate models might affect uncertainties in the amplitude and spatial pattern of different external forcings and its associated climatic response (e.g. Anchukaitis et al., 2012; Driscoll et al., in press; Mann et al., 2012). Hence, it is most challenging to determine whether a difference between model result and observation is related to model bias or due to different realisation of internal variability in models and reality.

1.2.3 New climate reconstruction approaches

In recent years, new approaches have found an increasingly important role in palaeoclimate reconstruction efforts, combining process knowledge and proxy data to achieve improved reconstructions (e.g. Guiot et al., 2009; Hughes and Ammann, 2009; Goosse et al., 2010; Widmann et al., 2009; Franke et al., 2011; Bhend et al., 2012). These techniques are sometimes referred to as data assimilation approaches but this term is not yet standard in palaeoclimatology. According to this definition, there is a wide spectrum of assimilation-like approaches and common to all these approaches is that they are especially designed to combine the individual strengths of reconstructions based on proxy data and model simulations to achieve improved past climate reconstructions. Doing

so, these approaches offer a more complete and quantitative understanding of processes linking proxy information, such as tree-ring growth, with environmental variables, including the evaluation of uncertainties. Hughes and Ammann (2009) provide a good overview of different techniques which are briefly discussed here. In the broadest sense, these range from primarily observed data-dependent approaches to those that explicitly combine existing understanding of proxy information and of climate with treatment of various causes of uncertainty. Figure 1 summarises the relationships between these approaches requiring detailed process understanding and those depending on increasing amounts of proxy data.

Multi-proxy cross-validation & climate field reconstructions

These approaches are entirely oriented to the observed proxy data without explicit use of process models within the reconstruction process. The multi-proxy cross-validation approach is based on the consistency in timing and absolute amplitude of change in proxies observed in different parts of the climate system. This technique is especially useful if one proxy can be used to predict another, completely independent proxy which would reduce uncertainty, especially if the second proxy is indicative of another environmental quantity (Briffa et al., 2008; Hughes and Ammann, 2009). Climate field reconstructions, on the other hand, use large-scale spatial coherence among different proxy records in a network. The underlying main patterns of climate variability are represented by the system's preferred dynamics even though no model-data are used (Mann et al., 1998; Hughes and Ammann, 2009).

Pseudoproxy experiments

So-called pseudoproxy experiments may mimic the characteristics of observed proxy data, such as annual tree-ring width (e.g. Mann and Rutherford, 2002; Bhend et al., 2012; Smerdon, 2012). These experiments add systematically stochastic noise to time series of the model simulation, and thus, provide an objective way into the performance of reconstructions methods (e.g. Mann et al., 2007; Riedwyl et al., 2009; Smerdon et al., 2010).

Inverse approaches & Bayesian hierarchical models (BHMs)

Inverse reconstruction approaches conventionally involve linear, empirical regression-based techniques. Yet inverse modelling offers a new approach in which process-based forward models (section 1.3) are used to infer past climate variables from tree-ring width data (ter Braak, 1995; Vaganov et al., 2006; Hughes and Ammann, 2009; Guiot et al., 2009). Hence, we are able to calculate tree-ring growth for any tree and year for which we have climate data. The greatest strengths of this approach is the explicit treatment of non-linearity and that it is based on the process-based understanding of the climate-tree ring growth relationship (Vaganov et al., 2006).

Inverse modelling can be approached in various ways. One possibility is in the framework of using Bayesian hierarchical modelling (BHM) in which complexities and uncertainties for different palaeoclimate records and climate dynamics at various levels can be flexibly incorporated (Tingley et al., 2012). For instance, it is basically possible to embed the ensemble-Kalman filter within a full climate model (Hughes and Ammann, 2009). This integrating character allows much more robust inferences in comparison to traditional reconstruction approaches (Guiot et al., 2009; Hughes and

Ammann, 2009; Tingley et al., 2012). The main advantages of BHM for climate reconstructions over traditional regression-based techniques are 1) the separation of the process descriptions and the proxy climate records. At the same time, it is possible to use different, completely independent proxy records, 2) the combination of multiple sources of uncertainty within a Markov chain Monte Carlo method and other re-sampling approaches, and 3) the ability to assimilate understanding of proxy formation processes through mechanistic models for palaeoclimate reconstructions (Guiot et al., 2009; Garreta et al., 2010; Tingley et al., 2012). The methodological background and a detailed review of published literature of BHM applied to palaeoclimate data can be found in Tingley et al., 2012 and references therein).

Proxy surrogate reconstructions

Proxy surrogate reconstructions search for the closest model states (analogues) that are most similar with proxy data at predefined locations and at specific times (Graham et al., 2007; Franke et al., 2011). While this approach is computationally very efficient and does not seem to underestimate past climate variability (Zorita and von Storch, 1999), remaining challenges include the loss of temporal continuity when the model output is temporally reordered, possible inconsistencies with the forcings, and the large number of degrees of freedom in the climate system when searching an appropriate analogue (van den Dool, 1994).

Particle filter

This method also combines proxy data and model simulations by searching the closest analogues, but assures temporal continuity. Out of a large ensemble of model simulations, at each comparison step only the best members are retained (and multiplied by adding perturbations) while the other members are stopped. Due to computational constraints, this approach is currently only feasibly for earth system model of intermediate complexity (EMICs) (Goosse et al., 2006).

Transient climate model simulations

Transient climate model simulations are constrained by (often proxy-based) information on the boundary conditions, i.e., the climate forcings, but not by information on the state of the climate. In the absence of any climate state information but available forcing information, an ensemble of climate model simulations may provide the best possible estimation of the climate state.

Ensemble Kalman filters

Data assimilation approaches such as Kalman filtering or 4D-Var are widely used in atmospheric sciences. In these approaches the model state vector (termed background) is corrected towards the observations in short intervals and based on the background error covariance matrix. The corrected model state then becomes the initial condition for the next (short) interval. For palaeoclimatic purposes, however, the application of these methods is not straight forward due to (i) the gap in time scales between typical model forecasting steps and proxy resolution, (ii) the difficulty of finding suitable observation operators and (iii) the sparsity of information. In recent years, several approaches have been developed that are based on similar ideas (e.g. Goosse et al., 2006, 2010; Widmann et al.,

2009; Compo et al., 2011; Bhend et al., 2012). However, these approaches are computationally very intensive to run with state of the art GCMs (Hughes and Ammann, 2009).

One of the big advantages of many of the presented data assimilation methods over statistical methods is that many of the former do not require a stationarity assumption. An essential prerequisite in this case, is that that the key processes responsible for the formation of a proxy, such as a tree-ring, are well enough understood to be modelled effectively using a proxy forward model (Vaganov et al., 2006; Hughes and Ammann, 2009; Tingley et al., 2012). Stationarity assumptions still will be present in that model, but will have far less weight than in conventional reconstruction approaches.
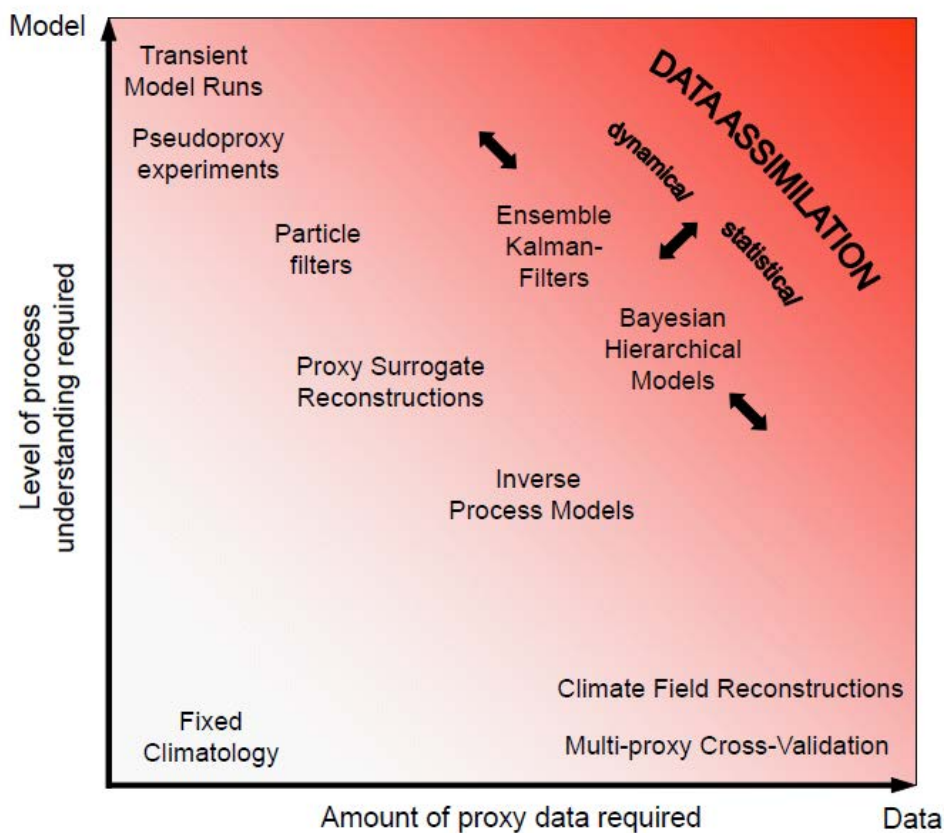
Figure 1.1: *Schematic illustration of the relationships between methods requiring progressively more process understanding and those depending on increasing amounts of data (adapted from Hughes and Ammann (2009)).*

1.3 Forward models of tree-ring growth

A profound understanding of the relationships between climate and tree-ring width along with the inherent uncertainties is fundamental for climate reconstructions. Forward models of tree-ring growth provide one tool suitable for climate reconstruction. One of the greatest strengths of these models is the explicit treatment of non-linearity and that the parameters have a clear biological or physical meaning. The most sophisticated of these models are the TREERING model (Fritts et al., 1999) and the MAIDEN model (Misson, 2004) which describe quantitatively and in detail anatomical wood

formation processes, carbon storage and biological processes like rates of photosynthesis and transpiration in response to environmental influences. These comprehensive models, however, need precise site-by-site measurements on stand characteristics such as crown structure or biomass as well as daily meteorological inputs (Fritts et al., 1999; Misson, 2004; Vaganov et al., 2006, 2011). While these complex models offer valuable insights into the formation of tree-rings, requirements of local stand data make them too complicated for use in palaeoclimate reconstructions.

Efforts to simplify these models focus on the cambial zone as the main target of environmental control on seasonal tree-ring formation and the subsequent transformation of these signals into further processes of cell differentiation (enlargement and cell wall thickening) (Vaganov et al., 2006, 2011). The Vaganov-Shashkin model (Vaganov et al., 2006), for instance, is specially designed to describe weather and climate-driven tree-ring variability. It computes rates of cell growth and division from temperature and precipitation series on a daily resolution, but still contains more than forty tunable parameters (Evans et al., 2006; Vaganov et al., 2006; 2011). Such requirements limit model verification by comparison with dendrochronological data.

Tolwinski-Ward et al. (2011) developed a simplified and more efficient alternative version of this model, the so-called Vaganov-Shashkin-Lite (VSL) model. It calculates monthly growth rates only from monthly temperature and precipitation along with solar irradiance. This model is simple and efficient in terms of its monthly resolution and relatively few tunable parameters, but complex in terms of its non-linear transformation of climate variability into a tree-ring index. These characteristics make this model especially suited for palaeoclimatic use because it is as simple as possible but still captures all essential relationships between climate and the formation of tree-rings. Hence, the VSL model is an ideal candidate of a forward model to gain estimates of past climate variables within an inverse modelling approach. Please refer to Chapters 3 and 4 for a detailed description of the VSL model and its use in a new palaeoclimatic reconstruction approach.

1.3.1 Forward modelling of tree-ring growth in a climate reconstruction approach

A forward model with a sufficient process-based understanding of the formation of climate/tree-ring growth relationship can be used to compare with existing observed tree-ring chronologies for the same time period allowing the examination of uncertainties in both the tree-ring data and the model (e.g. Evans et al., 2006; Tolwinski-Ward et al., 2011). Figure 2 schematically illustrates the use of the VSL model as a forward model in a climate reconstruction approach. In principle, this approach describes the use of a forward model of tree-ring growth to simulate tree-ring series using model ensemble simulations. These simulated series are then compared quantitatively with existing observed tree-ring chronologies to identify the best agreement. Selection of the best ensemble member (analogue) for each year yields the final climate reconstruction which can then be compared with existing climate observations in a validation period. Uncertainties in both the model and the tree-ring data can be examined. It is the advantage of this method that the method provides the full, physically consistent model output (in our case 6-hourly, global, 3-dimensional multi-variable fields). Climate can be studied in detail at sites and with variables that are not directly available from proxy data though using the best analogue of model ensemble simulations at a very high resolution and which is consistent with model physics and climate forcing.
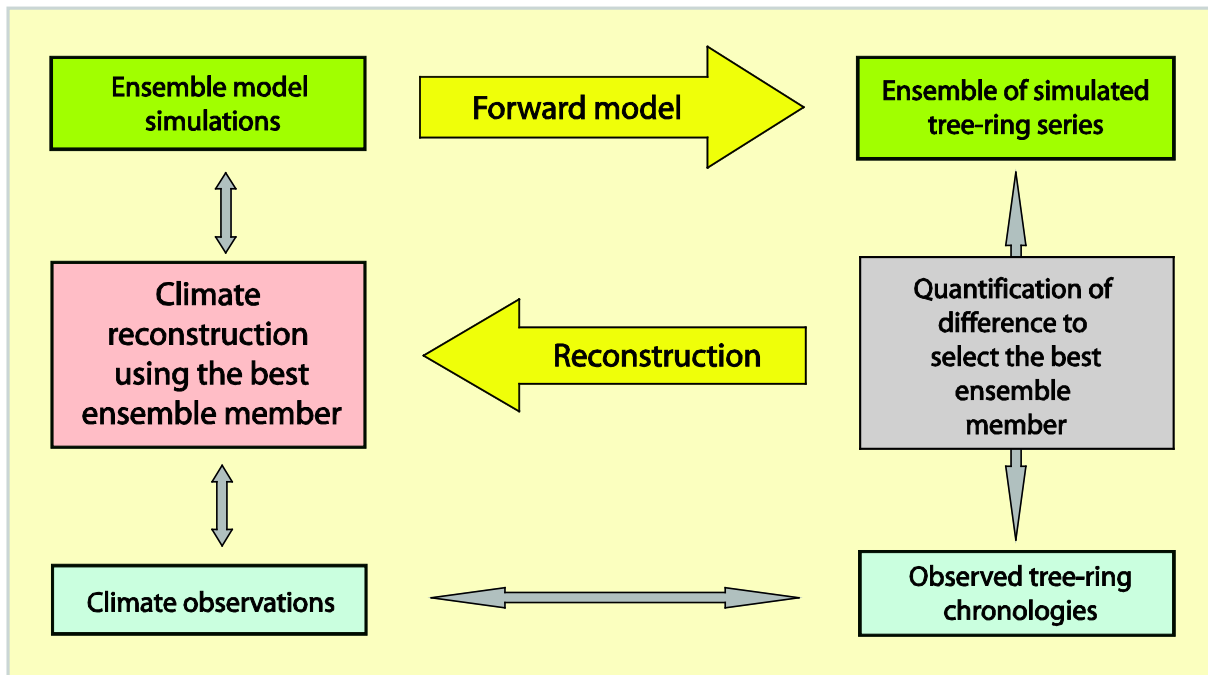
Figure 1.2: *Schematic illustration of a possible use of a process-based forward model in a climate reconstruction. Comparisons between two boxes are represented with grey bars. A detailed description of this approach can be found in Chapter 4.*

1.4 Objectives of the PhD thesis

The main objectives of this PhD thesis are:

- Compile all presently available long-term tree-ring data covering the past about 2000 years, to separate the effects of volcanic and solar activity on temperature from the tree-ring proxies with a statistical model, and to investigate the variability of the Sun-volcano climate relationship especially in terms of the about 200 years De-Vries periodicity,
- Examine the Vaganov-Shashkin-Lite (VSL) model's ability to skilfully link climate and tree-ring formation across the globe and to identify large-scale patterns of the climatic drivers of tree growth,
- Apply the VSL forward model of tree-ring width formation in a new analogue approach to proof concept to reconstruct past summer season temperature and precipitation.

1.5 Outline of the PhD thesis

This thesis is organised as follows: Chapter 1 gives a general introduction to the scientific background and framework of this thesis. In Chapter 2, tree-ring chronologies covering the past approximately 2000 years are evaluated in terms of possible solar and volcanic fingerprints and a statistical model to separate the effects of volcanic activity on temperature are presented (Breitenmoser et al., 2012). In Chapter 3, the Vaganov-Shashkin-Lite (VSL) forward model of tree-ring growth is examined with respect to its ability to skilfully link climate and tree-ring formation across the global. In Chapter 4, the

VSL model is used as an observation operator in a new analogue approach to proof concept to reconstruct past summer season temperature and precipitation from ensemble member simulations of an ECHAM5.4 general circulation model variant. Concluding remarks and recommendations for possible future research are finally in Chapter 5.

References

Ammann, C. M., Joos, F., Schimel, D. S., Otto-Bliesner, B. L., and Tomas, R. A., 2007. Solar influence on climate during the past millennium: Results from transient simulations with the NCAR Climate System Model. P. Natl. Acad. Sci. USA **104**, 3713-3718.

Anchukaitis, K. J., Evans, M. N., Kaplan, A., Vaganov, E. A., Hughes, M. K., Grissino-Mayer, H. D., and Cane, M. A., 2006. Forward modeling of regional scale tree-ring patterns in the southeastern United States and the recent influence of summer drought. Geophys. Res. Lett. **33**, L04705, doi:10.1029/2005GL025050.

Anchukaitis, K. J., Breitenmoser, P., Briffa, K. R., Buchwal, A., Büntgen, U., Cook, E. R., D'Arrigo, R. D., Esper, J., Evans, M. N., Frank, D., Grudd, H., Gunnarson, B. E., Hughes, M. K., Kirdyanov, A. V., Körner, C., Krusic, P.J., Luckman, B., Melvin, T. M., Salzer, M. W., Shashkin, A. V., Timmreck, C., Vaganova E. A., and Wilson, R. J. S., 2012. Tree rings and volcanic cooling. Nature Geoscience, doi:10.1038/ngeo1645.

Bhend, J., Franke, J., Folini, D., Wild, M., and Brönnimann, S., 2012. An ensemble-based approach to climate reconstructions. Clim. Past **8**, 963-976.

Breitenmoser, P., Beer, J., Brönnimann, S., Frank, D., Steinhilber, F., and Wanner, H., 2012. Solar and volcanic fingerprints in tree-ring chronologies over the past 2000 years. Palaeogeog. Palaeclim. Palaeoeco. **313-314**, 127-139.

Briffa, K. R, Shishov, V. V., Melvin, T. M., Vaganov, E. A., Grudd, H., Hantemirov, R. M., Eronen, M., and Naurzbaev, M. M., 2008. Trends in recent temperature and radial tree growth spanning 2000 years across northwest Eurasia. Philos. Trans. R. Soc. B **363**, 2271-2284.

Christiansen, B. and Ljungqvist, F. C., 2012. The extra-tropical Northern Hemisphere temperature in the last two millennia: reconstructions of low-frequency variability. Clim. Past **8**, 765-786.

Compo, G. P.,Whitaker, J. S., Sardeshmukh, P. D., Matsui, N., Allan, R. J., Yin, X., Gleason, Jr. B. E., Vose, R. S., Rutledge, G., Bessemoulin, P., Brönnimann, S., Brunet, M., Crouthamel, R. I., Grant, A. N., Groisman, P. Y., Jones, P. D., Kruk, M. C., Krüger, A. C., Marshall, G. J., Maugeri, M., Mok, H. Y., Nordli, Ø., Ross, T. F., Trigo, R. M., Wang, X. L., Woodruff, S. D, and Worley, S, J., 2011. The Twentieth Century Reanalysis Project. Q. J. R. Meteorol. Soc. **137**, 1-28.

Cook, E. R., Seager, R., Cane, M. A., and Stahle, D. W., 2007. North American drought: reconstructions, causes, and consequences. Earth-Sci. Rev. **81**, 93-134.

Crowley, T. J., 2000. Causes of climate change over the past 1000 years. Science **289**, 270-277.

D'Arrigo, R., Wilson, R., and Jacoby, G., 2006. On the long-term context for late twentieth century warming. J. Geophys. Res-Atmos. **111**, D03103, doi:10.1029/2005jd006352.

D'Arrigo, R., Wilson, R., and Cherubini, P., 2008. On the 'Divergence Problem' in Northern Forests: A review of the tree-ring evidence and possible causes. Global Planet. Change **60**, 289-305.

Driscoll, S., Bozzo, A., Gray, L. J., Robock, A., and Stenchikov, G., 2012. Coupled Model Intercomparison Project 5 (CMIP5) simulations of climate following volcanic eruptions. J. Geophys. Res., doi:10.1029/2012JD017607, in press.

Evans, M. N., Reichert, B. K., Kaplan, A., Anchukaitis, K. J., Vaganov, E. A., Hughes, M. K., and Cane, M. A., 2006. A forward modeling approach to paleoclimatic interpretation of tree-ring data. J. Geophys. Res. **111**, G03008, doi:10.1029/2006JG000166.

Franke, J., Gonzáles-Rouco, J. F., Frank, D., and Graham, N. E., 2011. 200 years of European temperature variability: insights from and tests of the Proxy Surrogate Reconstruction Analog Method. Clim. Dyn. **37**, 133-150.

Fritts, H. C., 1976. Tree rings and climate, Academic Press, London, UK.

Fritts, H. C., Blasing, T. J., Hayden, B. P., and Kutzbach, J. E., 1971. Multivariate techniques for specifying tree-growth and climate relationships and for reconstructing anomalies in paleoclimate. J. Appl. Meteorol. **10** (5), 845-864.

Fritts, H. C., Shashkin, A., and Downes, G.,1999. A simulation model of conifer ring growth and cell structure. In: Wimmer, R. and Vetter, R. (eds.). Tree Ring Analysis, Cambridge University Press.

Gao, C. C., Robock, A., and Ammann, C., 2008. Volcanic forcing of climate over the past 1500 years: An improved ice core-based index for climate models. J. Geophys. Res.-Atm. **113**, D23111, doi:10.1029/2008jd010239.

Garreta, V., Miller, P., Guiot, J., C. Hely, C., Brewer, S., Sykes, M., and Litt, T., 2010. A method for climate and vegetation reconstruction through the inversion of a dynamic vegetation model. Clim. Dyn. **35**, 371-389.

Gonzáles-Rouco, F., von Storch, H., and Zorita, E., 2003. Deep soil temperature as proxy for surface air-temperature in a coupled model simulation of the last thousand years. Geophys. Res. Lett., **30**(21), 2116, doi1029/203GL018264.

Goosse, H., Renssen, H., Timmermann, A., Bradley, R. S., and Mann, M. E., 2006. Using paleoclimate proxydata to select optimal realisations in an ensemble of simulations of the climate of the past millennium. Clim. Dyn. **27**(2–3), 165-184.

Goosse, H., Crespin, E., de Montety, A., Mann, M. E., Renssen, H., and Timmermann, A., 2010. Reconstructing surface temperature changes over the past 600 years using climate model simulations with data assimilation. J. Geophys. Res. **115**, D09108, doi:10.1029/2009JD012737.

Grissino-Mayer, H. D. and Fritts, H. C., 1997. The International Tree-Ring Data Bank: an enhanced global database serving the global scientific community. Holocene **7**, 235-238.

Graham, N. E., Hughes, M. K., Ammann, C. M., Cobb, K. M., Hoerling, M. P., Kennett, D. J., Kennett, J. P., Rein, B., Stott, L., Wigand, P. E., and Xu, T., 2007. Tropical pacific mid-latitude teleconnections in medieval times. Clim. Change **83**, 241-285.

Gray, L. J., Beer, J., Geller, M., Haigh, J. D., Lockwood, M., Matthes, K., Cubasch, U., Fleitmann, D., Harrison, G., Hood, L., Luterbacher, J., Meehl, G. A., Shindell, D., Van Geel, B., and White, W., 2010. Solar influences on climate. Rev. Geophys. **48**, RG4001, doi:10.1029/2009 RG000282.

Guiot, J., Wu, H. B., Garreta, V., Hatte, C., and Magny, M., 2009. A few prospective ideas on climate reconstruction: from a statistical single proxy approach towards a multi-proxy and dynamical approach, Clim. Past. **5**, 571-583.

Haigh, J. D., 1996. The impact of solar variability on climate. Science **272**, 981-984.

Hegerl, G. C., Zwiers, F. W., Braconnot, P., Gillet, N. P., Luo, Y., Marengo, J. A., Orsini, J. A., Nicholls, N., Penner, J. E., and Stott, P. A., 2007a. Understanding and attributing climate change. In: Solomon, S., Qin, D., Manning, M., Chen, Z., Marquis, M., Averyt, K., Tignor, M., and Miller, H. (eds.), Climate Change 2007: The physical science basis, Contribution of working group I to the Fourth Assessment Report of the Intergovernmental Panel on Climate Change, Cambridge University Press, Cambridge, United Kingdom and New York, NY, USA.

Hegerl, G. C., Crowley, T. J., Allen, M., Hyde, W. T., Pollack, H. N., Smerdon, J., and Zorita, E., 2007b. Detection of human influence on a new, validated 1500-year temperature reconstruction. J. Clim. **20**, 650-666.

Hegerl, G., Luterbacher, J., González-Rouco, F., Tett, S. F. B., Crowley, T., and Xoplaki, E., 2011. Influence of human and natural forcing on European seasonal temperatures. Nature Geosci. **4**, 99-103.

Hughes, M. K., 2002. Dendrochronology in climatology – the state of the art. Dendrochronologia **20**, 95-116.

Hughes, M. K. and Ammann, C. M., 2009. The Future of the Past-an Earth System Framework for High Resolution Paleoclimatology: Editorial Essay. Climatic Change **94**, 247-259.

IPCC, 2007. Climate Change 2007: The physical science basis. Contribution of working group I to the Forth Assessment Report of the Intergovernmental Panel on Climate Change. In: Solomon, S., Qin, D., Manning, M., Chen, Z., Marquis, M., Averyt, K. B., Tignor, M., Miller, H. L. (eds), Cambridge University Press, Cambridge, United Kingdom and New York, NY, USA.

Jansen, E., Overpeck, J., Briffa, K., Duplessy, J., Joos, F., Masson-Delmotte, V., Olago, D., Otto-Bliesner, B., Peltier, W., Rahmstorf, S., Ramesh, R., Raynaud, D., Rind, D., Solomina, O., Villalba, R., and Zhang, D., 2007. Paleoclimate. In: Solomon, S., Qin, D., Manning, M., Chen, Z., Marquis, M., Averyt, K., Tignor, M., and Miller, H. (eds.), Climate Change 2007: The physical science basis, Contribution of working group I to the Fourth Assessment Report of the Intergovernmental Panel on Climate Change, Cambridge University Press, Cambridge, United Kingdom and New York, NY, USA.

Jones, P. D., Briffa, K. R., Barnett, T., and Tett, S., 1998. High-resolution paleoclimatic records for the last millennium: Interpretation, Integration and comparison with general circulation model control-run temperatures. Holocene **8**, 455-471, doi:10.1191/095968398667194956.

Jones, P. D. and Mann, M. E., 2004. Climate over past millennia. Rev. Geophys. **42**, RG2002, doi:10.1029/2002GL016635.

Jones, P. D., Briffa, K. R., Osborn, T. J., Lough, J. M., van Ommen, T. D., Vinther, B. M., Luterbacher, J., Wahl, E. R., Zwiers, F. W., Mann, M. E., Schmidt, G. A., Ammann, C. M., Buckley, B. M., Cobb, K. M., Esper, J., Goosse, H., Graham, N., Jansen, E., Kiefer, T., Kull, C., Küttel, M., Mosley-Thompson, E., Overpeck, J. T., Riedwyl, N., Schulz, M., Tudhope, A. W., Villalba, R., Wanner, H., Wolff, E., and Xoplaki, E., 2009. High-resolution palaeoclimatology of the last millennium: a review of current status and future prospects. Holocene **19**(1), 3-49.

Jungclaus, J. H., Lorenz, S. J., Timmreck, C., Reick, C. H., Brovkin, V., Six, K., Segschneider, J., Giorgetta, M. A., Crowley, T. J., Pongratz, J., Krivova, N. A., Vieira, L. E., Solanki, S. K., Klocke, D., Botzet, M., Esch, M., Gayler, V., Haak, H., Raddatz, T. J., Roeckner, E., Schnur, R., Widmann, H., Claussen, M., Stevens, B., and Marotzke, J., 2010. Climate and carbon-cycle variability over the last millennium. Clim. Past **6**, 723-737, doi:10.5194/cp-6-723-2010.

Mann, M. E., Bradley, R. S., and Hughes, M. K., 1998. Global-scale temperature patterns and climate forcing over the past six centuries. Nature **392**(6678), 779-787.

Mann, M. E. and Rutherford, S., 2002. Climate reconstruction using "pseudoproxies". Geophys. Res. Lett. **29**, doi:10.1029/2001GL014554.

Mann, M. E., Rutherford, S., Wahl, E., and Ammann, C., 2007. Robustness of proxy-based climate field reconstruction methods. J. Geophys. Res. **112**, D12109, doi:10.1029/2006JD008272.

Mann, M. E., Zhang, Z. H., Hughes, M. K., Bradley, R. S., Miller, S. K., Rutherford, S., and Ni, F. B., 2008. Proxy-based reconstructions of hemispheric and global surface temperature variations over the past two millennia. P. Natl. Acad. Sci. USA **105** (36), 13252-13257.

Mann, M. E., Zhang, Z. H., Rutherford, S., Bradley, R. S., Hughes, M. K., Shindell, D., Ammann, C., Faluvegi, G., and Ni, F., 2009. Global signatures and dynamical origins of the Little Ice Age and Medieval Climate Anomaly. Science **326** (5957), 1256-1260.

Mann, M. E., Fuentes, J. D., and Rutherford, S., 2012. Underestimation of volcanic cooling in tree-ring based reconstructions of hemispheric temperatures. Nat. Geosc., doi:10.1038/NGEO1394.

Misson, L., 2004. MAIDEN: a model for analyzing ecosystem processes in dendroecology. Can. J. For. Res. **34**, 874-887.

Moberg, A., Sonechkin, D., Holmgren, K., Datsenko, N., and Karlén, W., 2005. Highly variable Northern Hemisphere temperatures reconstructed from low- and high resolution proxy data. Nature **433**, 613-617, doi:10.1038/nature03265.

Raible, C. C., Casty, C., Luterbacher, J., Pauling, A., Esper, J., Frank, D., Büntgen, U., Roesch, A. C., Tschuck, P., Wild, M., Vidale, P.-L., Schär, C., and Wanner, H., 2006. Climate variability - observations, reconstructions, and model simulations for the Atlantic-European and Alpine region from 1500-2100 AD. Clim. Change **79**, 9-29.

Riedwyl, N., Küttel, M., Luterbacher, J., and Wanner, H., 2009. Comparison of climate field reconstruction techniques: application to Europe. Climate Dynam. **32**, 381-395.

Robock, A., 2000. Volcanic eruptions and climate. Rev. Geophys. **38**, 191-219.

Rutherford, S., Mann, M. E., Delworth, T. L., and Stouffer, R. J., 2003. Climate field reconstruction under stationary and nonstationary forcing. J. Climate **16**(3), 462-479.

Rutherford, S., Mann, M. E., Osborn, T. J., Briffa, K. R., Jones, P. D., Bradley, R. S., and Hughes, M. K., 2005. Proxy-based Northern Hemisphere surface temperature reconstructions: Sensitivity to method, predictor network, target season, and target domain. J. Climate **18**, 2308-2329.

Shindell, D. T., Schmidt, G. A., Mann, M. E., Rind, D., and Waple, A., 2001. Solar forcing of regional climate change during the Maunder minimum. Science **294**, 2149-2152.

Shindell, D. T., Schmidt, G. A., Miller, R. L., and Mann, M. E., 2003. Volcanic and solar forcing of climate change during the preindustrial era. J.Clim. **16**(24), 4094-4107.

Smerdon, J. E., 2012. Climate models as a test bed for climate reconstruction methods: pseudoproxy experiments. WIREs Clim. Change **3**, 63-77.

Smerdon, J. E., Kaplan, A., Chang, D., and Evans, M. N., 2010. A pseudoproxy evaluation of the CCA and RegEM methods for reconstructing climate fields of the last millennium. J. Climate **23**, 4856-4880.

Steinhilber, F., Beer, J., and Fröhlich, C., 2009. Total solar irradiance during the Holocene. Geophys. Res. Lett. **36**, L19704. doi:10.1029/2009gl040142.

ter Braak, C., 1995. Non-linear methods for multivariate statistical calibration and their use in palaeoecology: a comparison of inverse (k-nearest neighbours, partial least squares and weighted averaging partial least squares) and classical approaches. Chemometr. Intell. Lab. **28**, 165-180.

Tingley, M. P., Craigmile, P. F., Haran, M., Li, B., Mannshardt, E., and Rajaratnam, B., 2012. Piecing together the past: statistical insights into paleoclimatic reconstructions. Quaterny Sci. Rev. **35**, 1-22.

Tolwinski-Ward, S. E., Evans, M. N., Hughes, M. K., and Anchukaitis, K. J., 2011. An efficient forward model of the climate controls on interannual variation in tree-ring width. Clim. Dyn. **36**, 2419-2439.

Vaganov, E. A., Hughes M. K., and Shashkin, A. V., 2006. Growth dynamics of conifer tree rings. In: Growth dynamics of tree rings: Images of past and future environments. Ecological studies **183**, Springer, New York, NY, USA.

Vaganov, E. A., Anchukaitis, K. J., and Evans, M. N., 2011. How well understood are the processes that create dendroclimatic records? A mechanistic model of climatic control on conifer tree-ring growth dynamics. In: Dendroclimatology, Developments in Paleoenvironmental Research **11**, Hughes, M. K., Swetnam, T., Diaz, H. (eds.), Springer, New York, NY, USA.

van den Dool, H., 1994. Searching for analogues, how long must we wait? Tellus A **46**, 314–324.

Wahl, E. and Frank, D., 2012. Evidence of environmental change from annually-resolved proxies with particular reference to dendroclimatology and the last millennium. In: Matthews, J. A. (ed.), The SAGE handbook of environmental change **1**. Sage, 320-344.

Wanner, H., Beer, J., Bütikofer, J., Crowley, T. J., Cubasch, U., Flückiger, J., Goosse, H., Grosjean, M., Joos, F., Kaplan, J. O., Küttel, M., Müller, S. A., Prentice, I. C., Solomina, O., Stocker, T. F., Tarasov, P., Wagner, M., and Widmann, M., 2008. Mid- to Late Holocene climate change: an overview. Quaterny Sci. Rev. **27**, 1791-1828.

Waple, A. M., Mann, M. E., and Bradley, R. S., 2002. Long-term patterns of solar irradiance forcing in model experiments and proxy based surface temperature reconstructions. Clim. Dyn. **18**, 563-578.

Widmann, M., Goosse, H., van der Schrier, G., Schnur, R., and Barkmeijer, J., 2009. Using data assimilation to study extratropical Northern Hemisphere climate over the last millennium. Clim. Past **6**, 627-644.

Zorita, E, and von Storch, H., 1999. The analog method as a simple statistical downscaling technique: comparison with more complicated methods. J. Clim. **12**(8), 2474-2489.

Chapter 2

SOLAR AND VOLCANIC FINGERPRINTS IN TREE-RING CHRONOLOGIES OVER THE PAST 2000 YEARS

Petra **Breitenmoser** [1,2], Jürg **Beer** [4], Stefan **Brönnimann** [1,2], David **Frank** [2,4], Friedhelm **Steinhilber** [3], Heinz **Wanner** [2]

[1] *Institute of Geography, Climatology and Meteorology, University of Bern, Switzerland*

[2] *Oeschger Centre for Climate Change Research, University of Bern, Switzerland*

[3] *Swiss Federal Institute of Aquatic Science and Technology (EAWAG), Dübendorf, Switzerland*

[4] *Swiss Federal Institute for Forest, Snow and Landscape Research (WSL), Birmensdorf, Switzerland*

Abstract

The Sun is the main driver of Earth's climate, yet the Sun's role in forcing decadal-to-centennial climate variations has remained controversial, especially in the context of understanding contributions of natural climate forcings to continuing global warming. To properly address long-term fingerprints of solar forcing on climate, long-term, very high-resolution, globally distributed climate proxy records are necessary. In this study we compile and evaluate a near global collection of annually-resolved tree-ring-based climate proxies spanning the past two millennia. We statistically assess these records in both the time and frequency domains for solar forcing (i.e. Total Solar Irradiance; TSI) and climate variability with emphasis on centennial time scales. Analyses in the frequency domain indicate significant periodicities in the 208-year frequency band, corresponding to the DeVries cycle of solar activity. Additionally, results from superposed epoch analysis (SEA) point toward a

possible solar contribution in the temperature and precipitation series. However, solar-climate associations remain weak, with for example no clear linkage distinguishable in the southwestern United States drought records at centennial time scales. Other forcing factors, namely volcanic activity, appear to mask the solar signal in space and time. To investigate this hypothesis, we attempted to extract volcanic signals from the temperature proxies using a statistical modelling approach. Wavelet analysis of the volcanic contribution reveals significant periodicities near the DeVries frequency during the Little Ice Age (LIA). This remarkable and coincidental superposition of the signals makes it very difficult to separate volcanic and solar forcing during the LIA. Nevertheless, the "volcano free" temperature records show significant periodicities near the DeVries periodicity during the entire past 1500 years, further pointing to solar mechanisms and emphasising the need for solar related studies in the absence of strong multi-decadal volcanic forcing.

2.1 Introduction

The Sun's role in climate variability has been a much discussed topic (e.g. Crowley, 2000; Rind, 2002; Shindell et al., 2003; Ammann et al., 2007; Gray et al., 2010; Haigh et al., 2010; Lean, 2010). The recent low and long-lasting minimum of solar cycle 23 - superimposed on generally high background solar activity during the past ~60 years (Abreu et al., 2008) - has put a renewed focus on the relationship between solar variability and its influence on climate on decadal to millennial time scales during the past, present, and future.

While variations in total solar irradiance (TSI) can only be measured quantitatively since the satellite era, changes in solar activity are captured in a number of proxies and measures including cosmic ray neutron monitor counts, measurements of geomagnetic disturbance (aa-index), the incidence of aurorae, observations of sunspots, or concentrations of [10]Be in ice cores and ^{14}C in tree-rings, respectively (Gray et al., 2010). However, only reconstructions based on the cosmogenic radionuclides allow the study of the evolution of solar magnetic activity beyond multi-centennial time-scales in a quantitative manner (e.g. Stuiver and Quay, 1980; Muscheler et al., 2004; Vonmoos et al., 2006). For instance, Solanki et al. (2004) and Usoskin et al. (2006) reconstructed the decadal averaged sunspot number for the past approximately 10,000 years from measurements of [14]C. A different approach, using the [10]Be record to reconstruct Total Solar Irradiance (TSI) during the past 9300 years, was applied by Steinhilber et al. (2009). A TSI reconstruction using ^{14}C has recently been published by Vieira et al. (2011), generally confirming the [10]Be record.

Although only the 11- and 22-year solar periodicities (the so-called Schwabe and Hale cycle, respectively) can be observed in instrumental-meteorological records, other solar cycles are known, e.g. at ~90 years (Gleissberg), ~208 years (DeVries cycle, a.k.a. Suess cycle), ~1000 years (Eddy cycle, Abreu et al., 2010), and ~2300 years (Hallstatt cycle) (e.g. Stuiver and Braziunas, 1989; Damon and Sonett, 1991). Of these the DeVries cycle is very prominent during the Holocene and is the focus of our study. This particular frequency has been identified in essentially all long-term proxy records of solar activity using a variety of spectral

techniques, record lengths, and detrending approaches (e.g. Eddy, 1976; Stuiver and Braziunas, 1989; Damon and Sonett, 1991; Wagner et al., 2001; Vonmoos et al., 2006). The well-known, grand solar minima during the second millennium AD, in particular the Oort, the Wolf, the Spörer, and the Maunder minima, closely correspond to minima of the 208-year oscillation (Fig. 2.1b).

This ~200 year pacing cannot only be found in solar activity reconstructions but has also been identified in a range of climate proxies from different archives such as glacier variations (Denton and Karlén, 1973; Wiles et al., 2004; Nussbaumer et al., 2011), monsoon intensity changes (e.g. Fleitmann et al., 2003; Gupta et al., 2005; Wang et al., 2005; Liu et al., 2009) or other climate-linked processes (e.g. Sonett and Suess, 1984; Haug et al., 2001; Hodell et al., 2001; Schimmelmann et al., 2003; Raspopov et al., 2008; Eichler et al., 2009). Due to these (mostly spectral) coincidences, this 208-year periodicity is thus often considered to be of solar origin in spite of the fact that the underlying processes are still not completely understood and that the alleged solar signal exhibits large spatial and temporal variability, highlighting the importance of internal variability in the climate system. A global overview compiling all presently available high-resolution, long term tree-ring data in terms of the DeVries cycle of solar activity is missing.

Besides solar forcing, volcanism is considered to be one of the primary agents for global, decadal-scale climate variability during the pre-industrial era (Crowley, 2000; Hegerl et al., 2003; Shindell et al., 2003; Stenchikov et al., 2009; Thompson et al., 2009) and, hence, also needs consideration. Finally, it needs to be kept in mind that the ~200 year cycle, with decade-long periods of strong changes, interferes with the "greenhouse time scale", making a distinction between anthropogenic and natural changes on this time scale during the past century difficult.

There are a number of different proxy archives providing information on the climate of the past (e.g. Jones et al., 2009). Reconstructions from trees have advantages over other proxies, including their i) wide spatial distribution, ii) annual resolution, iii) calendar-exact dating, and iv) high climate sensitivity making them one of the most important archives for reconstructing past climate (Frank et al., 2010). When analysing ultra-long tree chronologies (>~1500 years), preservation of lower frequencies is a critical issue. The necessary removal of biological age trends and the potential loss of lower frequency variability due to the short-length of tree segments contributing to the chronology require explicit consideration. Therefore, care must be taken to preserve variability at centennial or greater time scales needed for this study. A common technique of tree-ring standardisation used to overcome this problem is Regional Curve Standardisation (RCS) (Briffa et al., 1992; Cook et al., 1995; Esper et al., 2002, 2003).

In this study, a global overview and evaluation of all presently available long term tree-ring data is given. We investigate temporal and spatial variability of the Sun-climate relationship especially in terms of the ~200-year variability during the past two millennia using seventeen near worldwide distributed tree chronologies. First, we perform analysis in the frequency domain (i.e. frequency, phase, and amplitude) of the reconstruction of Total Solar Irradiance (TSI) and the ultra-long tree chronologies using Fourier spectral analysis, different wavelet

transforms, and band-pass filtering. Examination on the relationship between grand solar minima and concurring climate variability in the tree time series is then performed using Superposed Epoch Analysis (SEA). Strong decadal-scale volcanic forcing played an important role in climate variability on a global scale during the pre-industrial era of the Late Holocene (Crowley, 2000; Shindell et al., 2003) and is hence also considered in our analysis.

2.2 Data and methods

Centennial-scale climate variability during the past approximately two millennia was examined using reconstructions of the solar and volcanic forcing (Fig. 2.1), as well as the climate response derived from tree chronologies (Table 2.1, Fig. 2.2). Note that analysis using tree data is biased towards the warm season when tree-growth processes are most active and temperature is significantly influenced by solar radiation and local/regional climate processes. Accordingly, the larger-scale and dynamical processes that may occur in response to solar (and volcanic) forcing during winter are not given weight in this study.
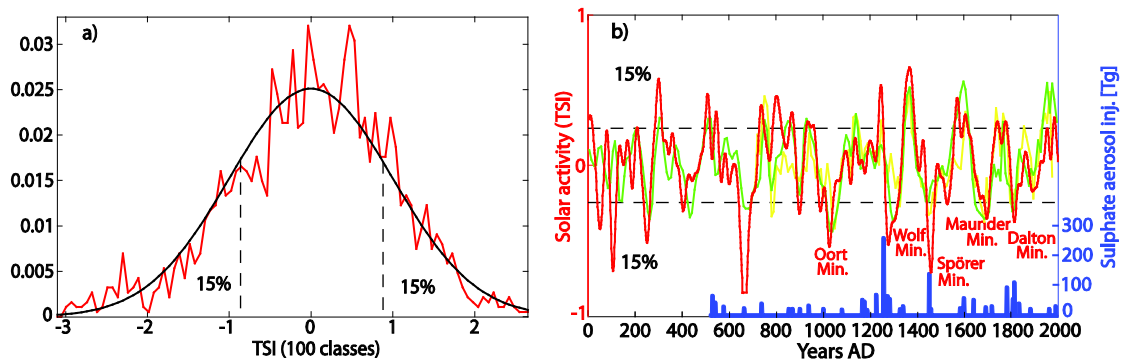
Fig. 2.1: *(a) Probability distribution for the high-pass filtered (700 years) reconstruction of Total Solar Irradiance (TSI) from Steinhilber et al. (2009), compared with a normal distribution (black line). The threshold for grand solar extrema is indicated by horizontal dashed lines. (b) Comparison of different high-pass filtered (700 years) TSI reconstructions and total global stratospheric sulphate aerosol injection from medium to large volcanic eruptions with >20 Tg (blue bars) (Gao et al., 2008). The TSI reconstructions by Steinhilber et al. (2009) (red line) and Delaygue and Bard (2010) (yellow line) are based on measurements of the cosmogenic radionuclide ^{10}Be from ice cores while the TSI reconstructions by Vieira et al. (2011) (green line) is based on the cosmogenic radionuclide ^{14}C from trees. These long-term records are very similar in the frequency domain, but differences exist in the amplitudes, where most uncertainties are inherent to the reconstructions.*

2.2.1 Solar forcing

As a measure for solar activity, we have used the 9,300-year long reconstruction of Total Solar Irradiance (TSI) from Steinhilber et al. (2009). This record is based on measurements of the cosmogenic radionuclide [10]Be in polar ice cores and the observationally derived relationship between TSI and the open solar magnetic field. The data are 40-year running means and were resampled to a 5-year time resolution, implying this record is only suitable to study the solar-terrestrial relationships on multi-decadal and longer time scales. Figure 2.1b compares the TSI from Steinhilber et al. (2009) with two other recent TSI reconstructions by Delaygue and Bard (2010), and Vieira et al. (2011).

The high-pass filtered (700 years) TSI reconstruction can be roughly approximated by a Gaussian distribution. Further, we define grand solar minima (maxima) as intervals when TSI is within the bottom (top) 15% of the Gaussian distribution, respectively. According to this criterion, the Sun spends 70% of the time in a normal state outside grand extrema (Fig. 2.1). Although somewhat arbitrary, our definition of grand solar extrema largely follows Abreu et al. (2008) who applied a threshold of 20% to the Gaussian distribution of the solar modulation function Φ from Steinhilber et al. (2008). In this study, we focus on grand solar minima, which typically last several decades and are characterised by a decrease of TSI by approximately 1 Wm^2 compared to the mean TSI during the most recent 30 years.

2.2.2 Volcanic forcing

Information on the volcanic forcing is taken from Gao et al. (2008) who generated a volcanic forcing index over the past 1500 years using a total of 54 sulphate ice core records from Antarctica and Greenland. We set a threshold for global total stratospheric sulphate aerosol injection values at >20 Tg to only consider medium to large volcanic eruptions (Fig. 2.1b). For comparison, the Pinatubo eruption in 1991 had a global total stratospheric sulphate injection of 30 Tg.

2.2.3 Tree chronologies

As measures of long-term climatic changes that occurred during the past approximately 2000 years, we used information derived from tree-rings. Yet, there are only a few tree chronologies that extend back more than 1000 years, but even so, simple criteria were applied to limit potential biases resulting from the selection of these records. These include:

a)   Annually resolved, calendrically dated, and globally distributed ultra-long (>~1500 years) tree-ring chronologies with no data gaps.

b)   Consistent interpretation of a climatic variable assigned to a time series. The target climatic parameters are temperature, precipitation, and drought.

c)   The presence of low-frequency signals. This was defined as >10% variance contained at time scales >100 years, as derived from the correlation between the low-pass filtered (100 years) and unfiltered time series.

d)   Sample depth (number of samples from trees used for every point in time) of a chronology is always ≥5.

Table 2.1 lists 17 tree chronologies which fulfil these criteria and Figure 2.11 shows each of these reconstructions. Their locations are shown on the map in Figure 2.2. Analysis is not restricted to temperature-sensitive tree-ring data because any significant changes in the atmospheric circulation due to solar modulation would most likely also impact other climate parameters.

Table 2.1: *Site description, period covered references, and sources for the tree reconstructions used for our analysis.*

Site, region, country	Period	Proxy for	Reference	Source
Torneträsk, NW Sweden	500-2004 AD	Temperature	Grudd (2008)	ftp://ftp.ncdc.noaa.gov/pub/data/paleo/treering/reconstructions/europe/sweden/tornetrask-temperature2008.txt
Central Europe	499 BC-2003 AD	Temperature	Büntgen et al. (2011)	ftp://ftp.ncdc.noaa.gov/pub/data/paleo/treering/reconstructions/europe/buentgen2011europe.txt
Central Europe	398 BC-2008 AD	Precipitation	Büntgen et al. (2011)	ftp://ftp.ncdc.noaa.gov/pub/data/paleo/treering/reconstructions/europe/buentgen2011europe.txt
Yamal, NW Siberia, Russia	1-1996 AD	Temperature	Briffa (2000)	Ljungqvist (2009): ftp://ftp.ncdc.noaa.gov/pub/data/paleo/contributions_by_author/ljungqvist2009/ljungqvist2009recons.txt
Taimyr peninsula, N Siberia, Russia	1-1996 AD	Temperature	Naurzbaev et al. (2002)	Ljungqvist (2009): ftp://ftp.ncdc.noaa.gov/pub/data/paleo/contributions_by_author/ljungqvist2009/ljungqvist2009recons.txt
Indigirka river region, far-NE Russia	1-1993 AD	Temperature	Moberg et al. (2005)	Moberg et al. (2005, 2006), Siderova and Naurzbaev (2002)
Solongotyn Davaa (Sol Dav), Mongolia	262-1999 AD	Temperature	D'Arrigo et al. (2001)	Ljungqvist (2009): ftp://ftp.ncdc.noaa.gov/pub/data/paleo/contributions_by_author/ljungqvist2009/ljungqvist2009recons.txt
NE Qinghai, Qinghai-Tibetan Plateau, China	515 BC-1993 AD	Precipitation	Sheppard et al. (2004)	ITRDB chin006, ftp://ftp.ncdc.noaa.gov/pub/data/paleo/treering/measurements/asia/chin006.rwl
Methusaleh Walk, California, USA	0-1979 AD	Drought	Cook et al. (2004)	ITRDB ca535, standardized by Edward R. Cook (LDEO)
Indian Garden, Nevada, USA	0-1980 AD	Drought	Cook et al. (2004)	ITRDB nv515, standardized by Edward R. Cook (LDEO)
Spruce Mountain, Nevada, USA	553-1985 AD	Drought	Mann et al. (2008)	ITRDB nv514, ftp://ftp.ncdc.noaa.gov/pub/data/paleo/treering/chronologies/northamerica/usa/nv514.crn
Mammoth Creek, Utah, USA	487-1989 AD	Drought	Cook et al. (2004)	ITRDB ut509, standardized by Edward R. Cook (LDEO)
El Malpais Nat. Mon., New Mexico, USA	103-1992 AD	Drought	Grissino-Mayer (1996)	ITRDB nm580, ftp://ftp.ncdc.noaa.gov/pub/data/paleo/treering/reconstructions/new mexico/malpais_recon.txt
Princeton bristlecone pine, Colorado, USA	0-1992 AD	Drought	Cook et al. (2004)	Connie Woodhouse (LTRR, U Arizona), standardized by Edward R. Cook (LDEO)
Mt. Read, W Tasmania, Australia	1600 BC-1991 AD	Temperature	Cook et al. (2000)	ftp://ftp.ncdc.noaa.gov/pub/data/paleo/treering/reconstructions/tasmania/tasmania_recon.txt
La Esperanza, N Patagonia, Argentina	182-1995 AD	Temperature	Mann et al. (2008)	ftp://ftp.ncdc.noaa.gov/pub/data/paleo/treering/chronologies/southamerica/arge092.crn
Puerto Café, N Patagonia, Argentina	427-1992 AD	Temperature	Mann et al. (2008)	ftp://ftp.ncdc.noaa.gov/pub/data/paleo/treering/chronologies/southamerica/arge093.crn
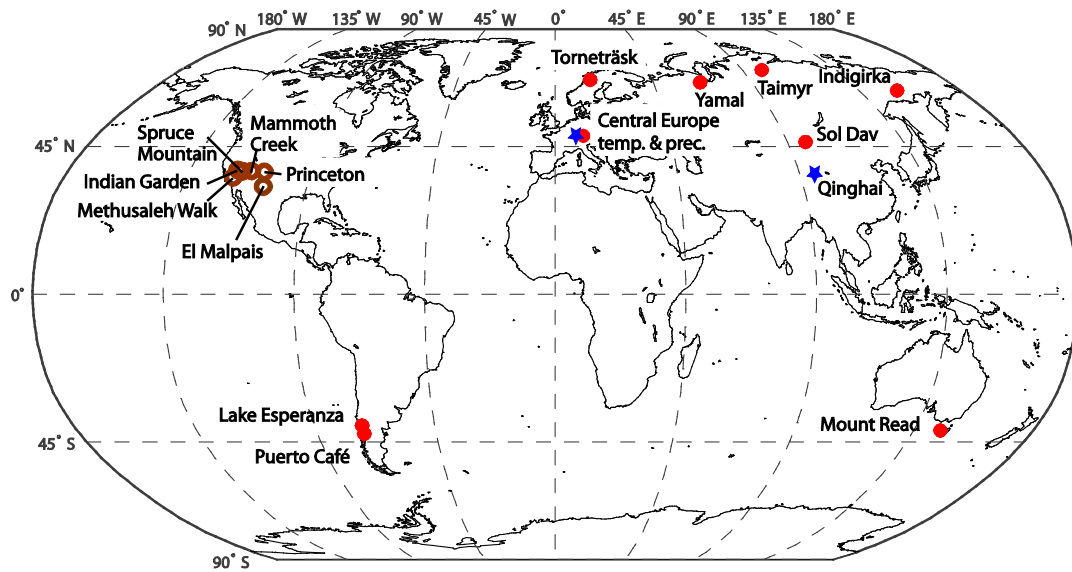
Fig. 2.2: *Global overview on the ultra-long tree proxy records used for analysis, with the climatic variable assigned as following: red dots - summer temperature, blue stars – precipitation, and brown circles - drought.*

2.2.4 Methods

Analysis was performed on individual, standardised series. In addition, the same analyses were performed on aggregated series to capture more fully the climate signature in a proxy network. We also used the average of all standardised temperature, all precipitation, and all drought series, respectively.

The averaging assumes a globally uniform signal and averages out regional variations, which might not be related to solar forcing. Since radiative energy is directly absorbed by oceans and land surfaces and in the lower atmosphere by water vapour and by CO_2, a direct positive link between TSI and global temperature is a reasonable first order approximation (Waple et al., 2002; Meehl et al., 2009; de Wit and Watermann, 2010). For precipitation and drought, such an a priori assumption cannot be made, but in these cases the proxy distribution is spatially much more limited, and so is the representation of the average.

Principal component analysis (PCA) is used to detect climate signals that have a specific spatial pattern, i.e., the signal does not have to be globally uniform. In principle, PCA reduces the dimensionality of a data set consisting of a large number of interrelated variables. This transformation is defined in such a way that the leading principal component accounts for most of the variance contained in all the original variables. The following principal components explain less of the total variance and represent mutually orthogonal signal components. Methodological details and applications of PCA in atmospheric sciences can be found in Wilks (2011). PCA is applied to the temperature, precipitation, and drought series separately.

Two independent approaches were employed in order to assess the temporal and spatial effects of mean tree-ring growth responses to solar and volcanic forcing. First, frequency domain analyses were performed using spectral and wavelet techniques, as well as band-pass filtering at centennial time-scales. Special emphasis was paid to the DeVries periodicity of solar activity at 208 years, its temporal behaviour, and how the phase and amplitude of solar activity relate to the climate proxies. Second, superposed epoch analysis (SEA) or compositing was used, following the methodologies adopted in previous work (e.g. Cook et al., 1997; Adams et al., 2003; Salzer and Hughes, 2007). The main idea is that SEA isolates signals that are difficult to detect against relatively large background noise. Through application of composites, this noise should cancel out and the climate response (if present) should emerge in the average. In detail, SEA cuts the time series into sub-series centred around defined key years of solar minima or volcanic eruptions and specified years immediately before and after these key years. These resulting climate sub-series of the individual time series are subsequently superposed and averaged together. The mean pattern emerging is examined for statistical significance using a Monte Carlo resampling procedure based on 10,000 random surrogates derived from permutation of sub-series. The distribution of randomly generated composites provided the 2σ-confidence bounds. We used SEA on the standardised and high-pass filtered time series (cut-off frequency 700 years) (Figs. 2.6, 2.7) and in the range of periods 180-230 years band-pass filtered time series (Fig. 2.5)

2.3   Results and discussion

2.3.1. Analysis in the frequency domain

Spectral analysis

First, we performed spectral analyses of the data sets listed in Table 2.1 in order to analyse which frequencies are significant in the tree-ring reconstructions and whether a global or regional pattern emerges. All reconstructions were high-pass filtered (cut-off frequency 700 years) and then processed with the same spectral analysis method (REDFIT; Schulz and Mudelsee, 2002).
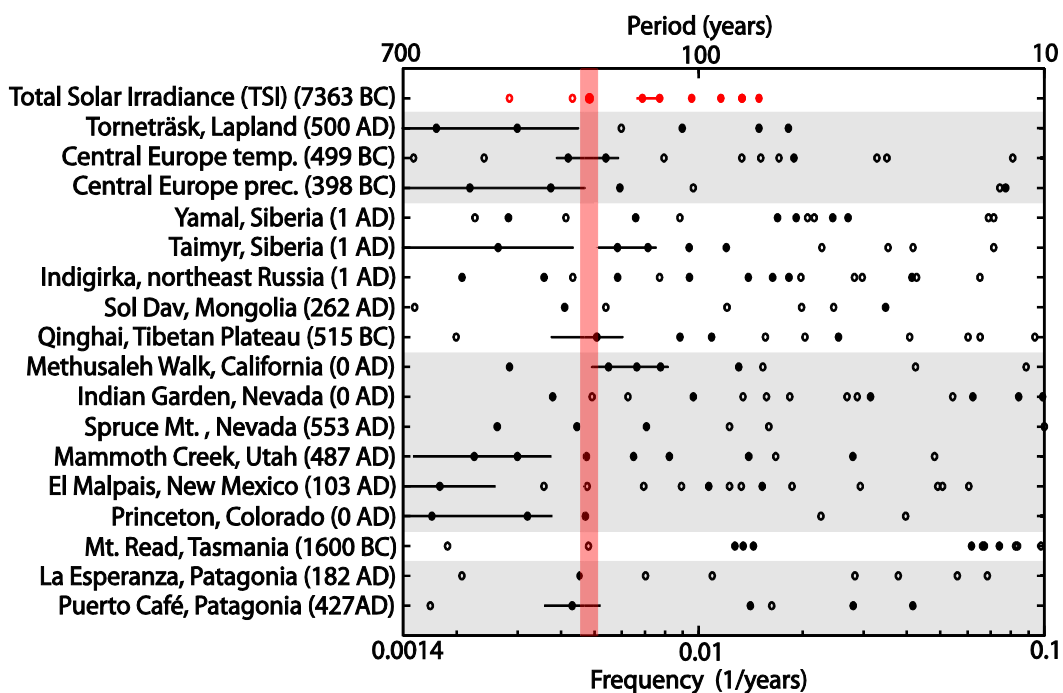
Fig. 2.3: *Overview of the spectral characteristics of TSI (red dots, until frequency 70 years) and the regionally sorted tree-ring data sets used in this study (Table 2.1). Filled (unfilled) circles mark the 99% (95%) significance level, and horizontal black lines denote broad peaks. The red box indicates the 208-year (±10 years) solar cycle. Note the logarithmic x-axis.*

Figure 2.3 displays the overview of the spectral characteristics of the regionally arranged climate time series used in our analyses. Results show a weak clustering of significant spectral behaviour at approximately 210 years, especially in the North American drought records. However, there is no obvious pattern with consistent periodicities.

The lack of strict spectral coherence is consistent with observations by Wanner et al. (2008) who described a broad band of quasi-periodic variability being typical of Holocene climate records. Significant internal dynamic variability, frequency-dependent phase shifts in the

environmental response to a forcing, threshold events, regionality, as well as non-linearity and non-stationarity of the climate system with feedback processes, and the influence of other forcings contribute to the complexity of correlating specific periodicities in climate proxies with solar forcing (Raspopov et al., 2008; Wanner et al., 2008). Hence, it would be unrealistic to assume strict agreement in the frequency domain, even if solar variability was the only driver of Earth's climate, which it certainly is not.

Moreover, it is important to mention that the solar DeVries cycle is not stationary over time. For instance, the 208-year cycle is not significant between approximately 800 and 1200 AD (see wavelet power spectrum of TSI in Fig. 2.13). Hence, it may be difficult to find a solar-climate relationship in this frequency range during certain periods in time.

Principal Component Analysis (PCA) was undertaken to extract the dominant modes of variability from the proxy network due to a common external forcing. The standardised time components (scores) of the principal components were spectrally analysed using the above mentioned method for the AD 553-1979 period common across the proxy network. The leading principal components for temperature and drought account for 20.4%, and 36.6%, respectively, of the total variability. The leading principal component for precipitation mainly describes the record from Central Europe, accounting for 51% of the total variability. Spectral analysis shows a significant (95% confidence-level) 208-year periodicity in all the subsets. In contrast to the inconclusive spectral results of the individual time-series, results from PCA suggest that the dominant modes, which capture much of the variance of the tree-ring records, may be related to climate anomalies generated by solar variability close to the DeVries periodicity.

Phase relationships

Radiative energy is absorbed by oceans and land surfaces and in the lower troposphere by water vapour and by CO_2. Hence, a direct link between TSI and tropospheric temperature can be established and the attenuation of the radiative forcing may lead to a lagged temperature and precipitation response (de Wit and Watermann, 2010). The thermal inertia of the ocean and the land surface are prominent candidates for decadal scale lagged responses of the climate system to solar forcing (Perry, 2007). Indeed, Perry (2007) finds lags between 0 and 70 years between solar forcing and various globally distributed hydroclimatic time series during the past approximately 150 years. Likewise, model simulations predict lags of 0-20 years attributable to the thermal inertia of the climate system, with longer lags for lower frequency components in the forcing (Rind et al., 1999; Shindell et al., 2001; Weber et al., 2004). Moreover, comparison between Northern Hemisphere temperature and solar activity reconstructions and climate model experiments showed lags of up to 30 years for the time period 1650-1850 (Waple et al., 2002). Another comparison between a temperature proxy from the continental Siberian Altai and a solar activity reconstruction reveals lags of 10-30 years over the past 750 years (Eichler et al., 2009).

To reveal the time-dependent characteristics of the relationship between the DeVries periodicity and climatic variation in our study, 180-230 year band-pass filtering, as well as continuous wavelet (Torrence and Compo, 1998) and cross-wavelet transformations (Grinsted et al., 2004) was performed on all data series. The result of the band-pass filtering is illustrated in Figure 2.4 and of the wavelet analyses in Figures 2.13 and 2.14 in the appendix.

The 180-230 band-pass signal accounts for 23.6% of the TSI variance, confirming the prominent role of the De Vries cycle. On the other hand, this 180-230 band-pass signal represents between 1.36% (El Malpais) and 18.9% (Indigirka) of the variance in the unfiltered time-series. Both band-pass filtering and wavelet analysis give evidence that the frequency amplitude of the records has varied in time. Lowest, yet significant amplitude changes in TSI are evident in the middle of the first millennium, whereas the most pronounced ~200-year oscillations are observed in the Little Ice Age between approximately 1300 and 1700 AD. Moreover, there is generally a better coincidence between TSI and the temperature and precipitation time series in this frequency band during times of high solar variability in the second millennium AD (Figs. 2.4a-d, 2.13, 2.14). Another distinct feature in Fig. 2.4 is the decreased coherence between the records during the first millennium which can be related to a reduced variability during earlier times. Likewise, a decreased chronology quality may also be the result of a reduced sample replication further back in time. We tried to address this aspect of reduced sample depth, which is common in tree-ring data, by selecting only chronologies with at least five tree samples (Frank et al. 2007b). In a more regional perspective, TSI and the Asian temperature and precipitation records visually agree well from approximately AD 700 onwards (Fig. 2.4a). With the exception of the southern hemispheric temperature and the central Asian temperature time series, no significant common high power can be found close to the DeVries frequency during the time around 1000 AD (Fig. 2.14).

Cross-correlation analysis (Table 2.2) reveals that eight time series, the leading temperature principal component, and the second principal component of the precipitation subset correlate significantly (above the 90% confidence level) with TSI, but there are considerable differences in the phase relationships. Moreover, analysis of the 180-230 year band pass-filtered series indicates that the climate response to any assumed solar 208-year pacing has, at best, regional characteristics and considerable temporal phase shifts (Table 2.2, see also 2.14). Nevertheless, the results from PCA suggest a relationship between TSI and the dominant modes of temperature/ precipitation in this frequency range. The climate response is found to lag the solar forcing by +10 years on average, which conforms to our physical understanding of solar-temperature links. However, individual negative phase shifts occur, demonstrating the uncertainty of the data and method.
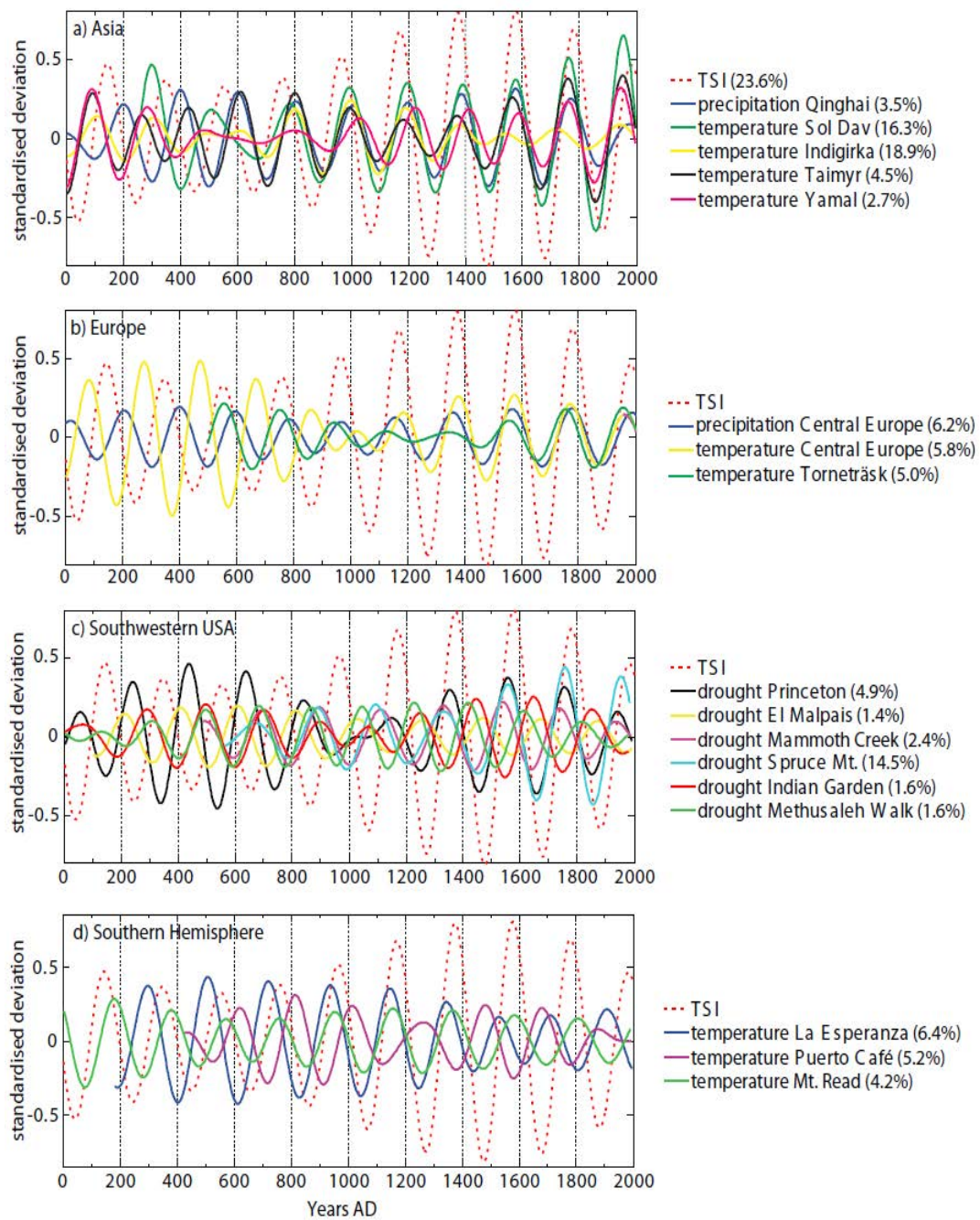
Fig. 2.4: *Band-pass filtered TSI (dotted red line) and climate data series in the range of periods 180-230 years for (a) Asia, (b) Europe, (c) southwestern United States, and (d) Southern Hemisphere. The values in the brackets describe the variability in the band-pass filtered time series in relation to the corresponding unfiltered data series for the displayed time intervals.*

Table 2.2: *Pearson correlation coefficients (r) and temporal shifts of the phase (Δt) in years rounded to the next decade between TSI and the band-pass filtered (180-230 years) chronologies presented in Figure 2.4 and the leading principal components of the temperature, precipitation, and drought series, respectively. The significance of the values is * for the 90%, ** for the 95%, and *** for the 99% confidence level (all in bold). A Fourier approach of estimation of the number of degrees of freedom, as outlined in Yan et al. (2004), was considered for the determination of the statistical significance of correlation between the band-pass filtered time series. Positive (negative) Δt expresses a lead (lag) of TSI in relation to the climate proxies. Note that two entries are given for some series when either a negative lag or an anticorrelation may be probable.*

TSI correlation with	r		Δt (years)
Torneträsk summer temperature	**0.73**	*	**-20**
	-0.78	*	**80**
Central Europe, summer temperature	0.32		-30
	-0.34		60
Central Europe, precipitation	0.49		10
Yamal, summer temperature	0.30		10
Taimyr, summer temperature	0.45		0
Indigirka, summer temperature	0.43		10
Sol Dav, summer temperature	**0.76**	*	**0**
Qinghai, annual precipitation	**0.72**	*	**20**
Methusaleh Walk, drought	0.43		60
Indian Garden, drought	0.54		90
Spruce Mountain, drought	**0.73**	*	**-40**
	-0.77	*	**70**
Mammoth Creek, drought	**0.93**	***	**-50**
	-0.92	***	**50**
El Malpais, drought	**0.75**	**	**80**
Princeton, drought	0.21		-40
	-0.24		60
Mt. Read, summer temperature	**0.85**	***	**20**
La Esperanza, summer temperature	**0.75**	*	**-40**
	-0.70		60
Puerto Café, summer temperature	0.67		90
"Temperature" PC 1	**0.76**	*	**0**
"Precipitation" PC 2	**0.93**	***	**10**
"Drought" PC 1	0.36		40

2.3.2 Superposed epoch analysis (SEA)

SEA was performed on the 40-700 years band-pass filtered time series over the common time interval with respect to key years during the grand solar minima centred at AD 662, 897, 1028, 1282, 1458, 1698, and 1817. Results show significant climatic responses near year t+6, i.e. the climate follows the sun with a lag of 6 years, for temperature (Fig. 2.5a) and t+13 years for precipitation (Fig. 2.5b), implying generally cooler and drier conditions, respectively. SEA of the drought series, on the other hand, does not contain clear evidence of a Sun-drought linkage at multidecadal-to-centennial time scales (Fig. 2.5c).
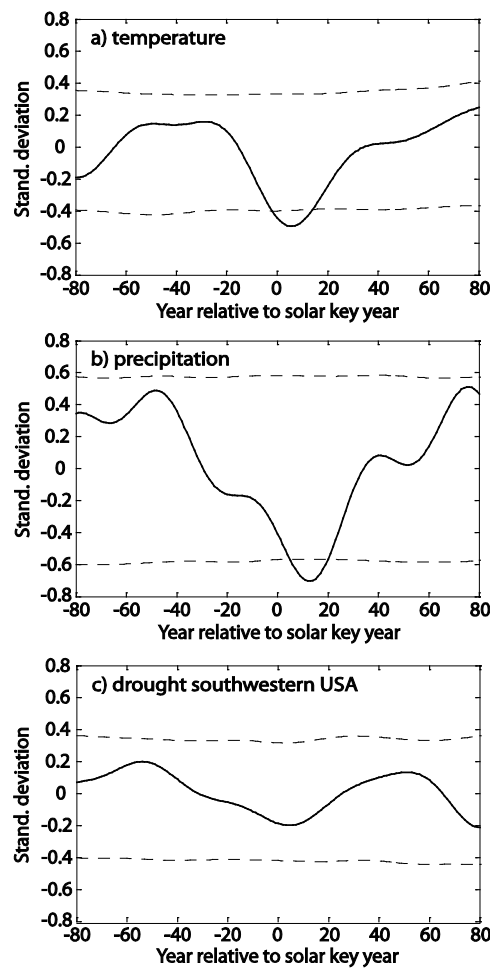
Fig. 2.5: *SEA composites on band-pass filtered (40-700 years) time series based on key years (= year 0) during grand solar minima centred at AD 662, 897, 1028, 1282, 1458, 1698, and 1817 considering (a) all temperature series; (b) only precipitation time series; and (c) only the southwestern USA drought time series. Note that positive/negative values indicate warmer/colder and wetter/drier, respectively. Dashed lines are the 2σ-confidence limits that were established by randomly sampling the key years 10,000 times. The SEA units are standard normal deviates.*

In order to explore the climate response to solar forcing in different time intervals individually, the key years of the grand solar minima were grouped into the four well-known climate epochs of the past 2000 years; the Roman Warm Period (RWP; until ~450 AD), the Dark Age Cold Period (DACP; ~450-950 AD), the Medieval Climate Anomaly (MCA; ~950-1250 AD), and the Little Ice Age (LIA; ~1250-1850 AD) (Fig. 2.6). The RWP and the MCA are generally considered to have been episodes of above average temperatures, while the DACP and the LIA were episodes of cooler climatic conditions (e.g. Lamb, 1977; Stine, 1994; Moberg et al., 2005; Ljungqvist, 2010).

The most striking negative temperature response can be found during the LIA, with values culminating in the first two decades after the key years of grand solar minima. Comparison with the corresponding SEA composite of TSI for the same episode shows a similar pattern (Fig. 2.6d). The temperature response in relation to grand solar minima for the other three climate episodes is less obvious (Fig 2.6a-c). Interestingly, significantly positive temperatures can be observed in the years around lag zero during the RWP. The same pattern, although not significant, can be visually identified for the MCA (Fig. 2.6a,b).
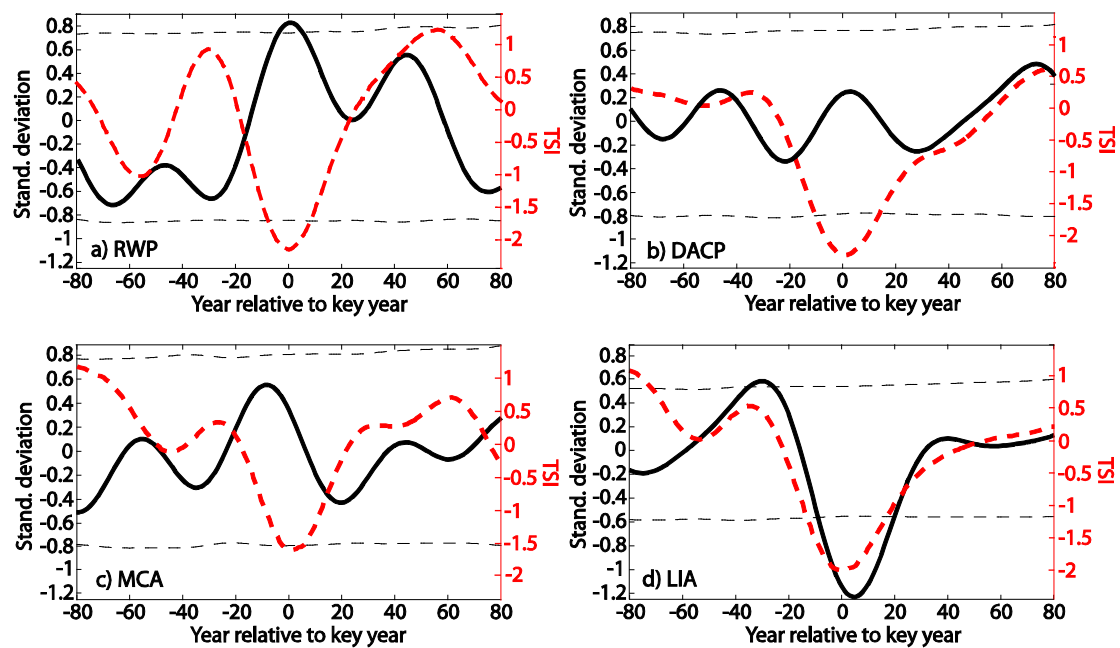
Fig. 2.6: *SEA composites (black line) on the band-pass filtered (40-700 years) records reaching back at least to 1 AD, with the temperature series from Central Europe, Yamal, Taimyr, Indigirka, and Tasmania with grand solar minima falling within the RWP (panel a; solar minima 102 and 242 AD); DACP (panel b; solar minima 397 and 662 AD); MCA (panel c; solar minima 897 and 1028 AD); LIA (panel d; solar minima 1282, 1458, 1698, and 1817 AD). The red line shows the corresponding SEA composite for TSI during the four time intervals. The dashed lines are the 2σ-confidence limits which were established by randomly sampling the key years 10,000 times. The SEA units are standard normal deviates.*

The lack of coherence among the subperiods could be due to small sample size both in terms of solar minima (i.e. RWP, DACP, and MCA each comprise only two grand solar minima; LIA comprises four minima) and due to the small number of chronologies (only five data series with decreasing data quality back in time cover the full range of 2000 years). It could also be due to a spatially non-uniform regional signal. For instance, the significantly higher values during the RWP near lag-0 may be an expression of a more regional warming response to decreased solar forcing. That solar irradiance variability can lead to both positive and negative temperature responses in different regions was revealed in model simulation predictions of the temperature responses of the atmosphere-ocean system to long-term variations (T > 40 years) in solar irradiance by Waple et al. (2002). Additionally, our results are biased towards the Northern Hemisphere, with a regional focus on northern Russia for the temperature proxies.

SEA of the precipitation and drought series during the four time intervals does not show significant climate responses in respect to solar minima. The only exception is significantly reduced precipitation during the LIA, which is especially evident in the record from the Qinghai-Tibetan Plateau.

2.3.3 Influence of volcanic forcing

The question remains why the SEA temperature and precipitation responses during the LIA are so strikingly different compared to the other climate episodes. Besides solar forcing, volcanism could have played a significant role in climate variability on a global scale during the pre-industrial era of the Late Holocene. The short-term, radiatively induced summer cooling effect of large explosive tropical eruptions is well understood, as discussed by Crowley, (2000), Robock, (2000), or Shindell et al., (2003) and direct effects of this summer cooling in trees are reduced ring widths. Yet, the climatic impact of these eruptions may be underestimated from tree ring data due to enhanced tree growth induced by additional diffuse radiation stimulating photosynthesis and hence counteracting some of the summer cooling (Robock 2005). The general pattern of low volcanic activity during the MCA and high activity during the LIA have been described previously in e.g. Jones et al. (1995), Robock (2005), Gao et al. (2006, 2008), Cole-Dai et al. (2009), and Timmreck et al. (2009). Figure 2.7 shows the result of SEA on all temperature time series using volcanic key years during (Fig. 2.7a) and before (Fig. 2.7b) the LIA – here defined as the period between the mid-13th and 19th century. It is evident that the temperature response to medium to large volcanic activity was more distinct during the LIA, with particularly the years around 1452/59 and 1809/15 having a profound negative impact on summer temperatures, even at the decadal scale. This longer-term volcanic influence on climate can be explained by the ocean integration of volcanic radiative cooling (Stenchikov et al., 2009; Thompson et al., 2009) as well as the influence of closely spaced eruptions (for instance the eruptions at 1809 and 1815), and the effect of averaging different time series in the SEA.
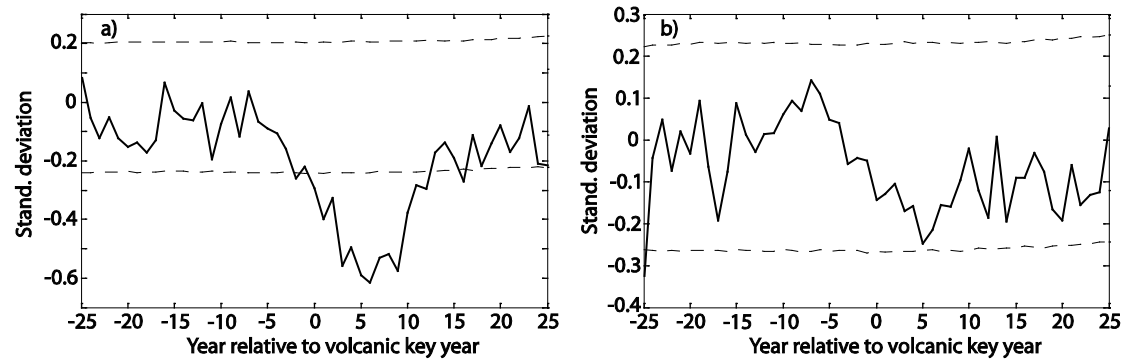
Fig. 2.7: *SEA composites on the unfiltered temperature proxy records centred at years of volcanic eruptions >20 Tg (a) during the LIA (AD 1258, 1275, 1284, 1341, 1452, 1459, 1584, 1600, 1641, 1693, 1719, 1783, 1809, 1815, 1835, 1883); and (b) outside the LIA (AD 529, 541, 577, 664, 738, 854, 870, 901, 939, 1167, 1176, 1227). The dashed lines are the 2σ-confidence limits which were established by randomly sampling the key years 10,000 times. The SEA units are standard normal deviates.*

In order to further examine the solar and volcanic contributions, we attempt to separate the temperature proxies into volcanic and residual (i.e., "volcano free") signals. The following equation describes the volcanic effect on temperature (T) at year t:

$$T(t) = T(t-1)^* e^{-a\Delta t} - b^* AOD$$

In other words, the volcanic effect on temperature linearly depends on the volcanic anomaly of the previous year (which decays and can be interpreted as oceanic memory) and on the short-wave cooling induced by volcanic forcing of the current year (using the conversion of aerosol loading data from Gao et al. (2008) into aerosol optical depth (AOD) (Stothers, 1984)). The parameters "a" (i.e., the decay time or memory) and "b" (i.e., the sensitivity) of the function are fitted to each temperature series by the method of least squares. The volcanic effect on precipitation and drought is calculated likewise. Using these fitted curves, it is now possible to separate each proxy series into a volcanic and a "volcano free" residual component. Figure 2.12 in the supplementary material (green lines) illustrates the separation of the Central European temperature series into a volcanic component and into a residual "volcano free" component using the parameters a = 0.1 yr^{-1}, and b = 2.6 K.

The volcanic climate effect of the three largest tropical volcanic eruptions during the past 1500 years (i.e. the unknown 1258 eruption, the 1452/53 Kuwae eruption, and the 1815 Tambora eruption) is shown in Figure 2.8. The Yamal chronology is influenced the most by volcanic forcing. Least volcanic influence is reflected in the southern hemispheric records, with the chronology from Tasmania even responding with slightly enhanced temperatures (< 0.1K) (not shown). Results for precipitation and drought are less straightforward (Fig. 2.8 b,d,f).

Only precipitation over the Qinghai-Tibetan Plateau and drought recorded at the Princeton and El Malpais chronologies show a negative volcanic effect (i.e. drier). The volcanic influence in the other precipitation and drought series is slightly positive, but the values remain <0.1 standardised units (not shown). Likewise, low statistical significance for summer precipitation changes in the first few years following 15 major tropical volcanic eruptions over the past half millennium was demonstrated in an analysis by Fischer et al., (2007). Moreover, large spatial precipitation variability complicates a clear detection of a volcanic precipitation signal from the background noise. While most of the analysed southwestern USA drought reconstructions do not contain a clear volcanic signal, higher-elevation and more temperature-limited bristlecone pines in the same area, on the contrary, indeed show a volcanic imprint (Salzer and Hughes, 2007).
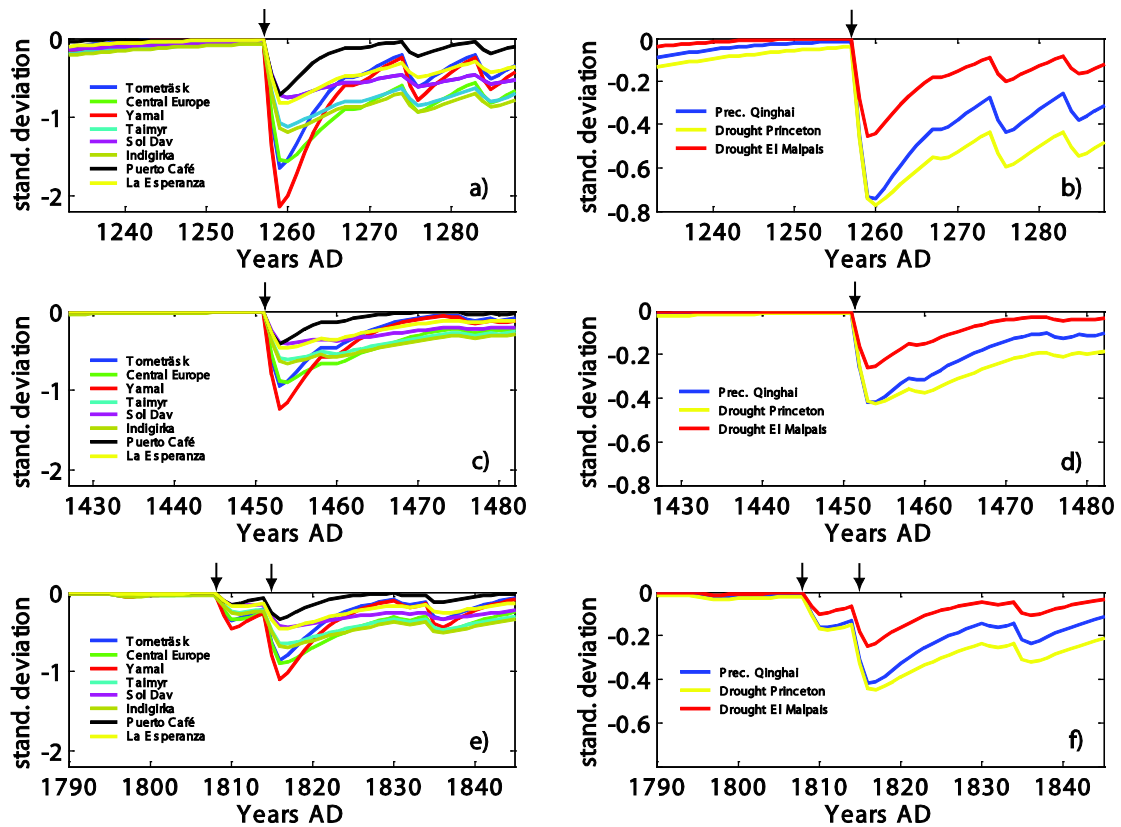
Fig. 2.8: *Volcanic climate effects of the three largest tropical volcanic eruptions during the past 1500 years. The left panels (a, c, e) show the volcanic temperature components while the right panels (b, d, f) give the precipitation/drought components for the unknown 1258 eruption (a, b), the 1452/53 Kuwae eruption (c, d), and the unreported 1809 and 1815 Tambora eruptions (e, f). Note that the parameters in the statistical model were fitted in the common period AD 553-1979.*

In a next step, SEA was applied on the volcanic component and on the 40-700 years band-pass filtered residual time series using solar key years (Fig. 2.9). The volcanic component shows a distinct temperature decrease during solar key years due to a coincidence between solar and volcanic forcing (Fig. 2.9a). This finding is reflected in the pacing of grand solar minima during the LIA (AD 1282, 1458, 1698, and 1817) largely coinciding (defined as ±25 years around key year of solar minima) with years of medium to large volcanic activity (AD 1258, 1275, 1284, 1452, 1459, 1693, 1719, 1809, 1815, and 1835) (see Figure 1b).
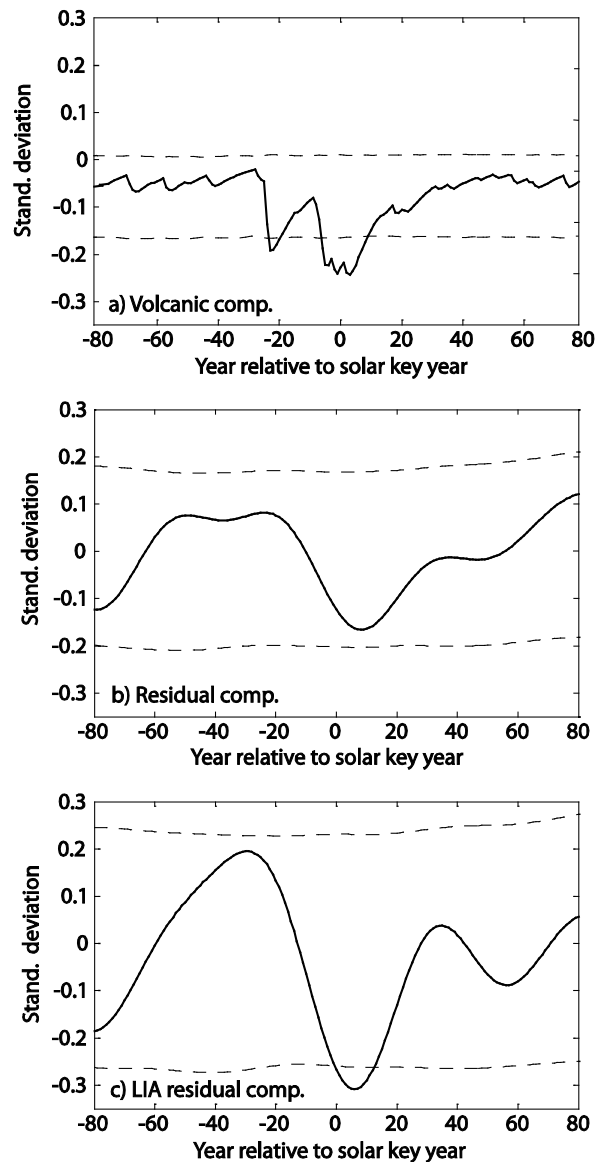
Fig. 2.9: *SEA composites centred at years of solar minima (AD 662, 897, 1028, 1282, 1458, 1698, 1817) (a) on the volcanic temperature component; (b) on 40-700 years band-pass filtered, averaged residual "volcano free" temperature component; and (c) as in b), but centred at years of solar minima only during the LIA. The dashed lines are the 2σ-confidence limits which were established by randomly sampling the key years 10,000 times. The SEA units are standard normal deviates.*

Figure 2.10 gives the power spectrum of the Morlet wavelet for the volcanic (Fig. 2.10a) and residual "volcano free" contributions averaged over all series (Fig. 2.10b). The volcanic component reveals significant periodicities near the DeVries frequency during the LIA. Note also the disturbances of the large volcanic eruptions at AD 1258, 1452/1453 and 1815 which are evident at higher frequencies. The "volcano free" contribution, on the other hand, depicts a band of continuously high power near the 208-year solar cycle.
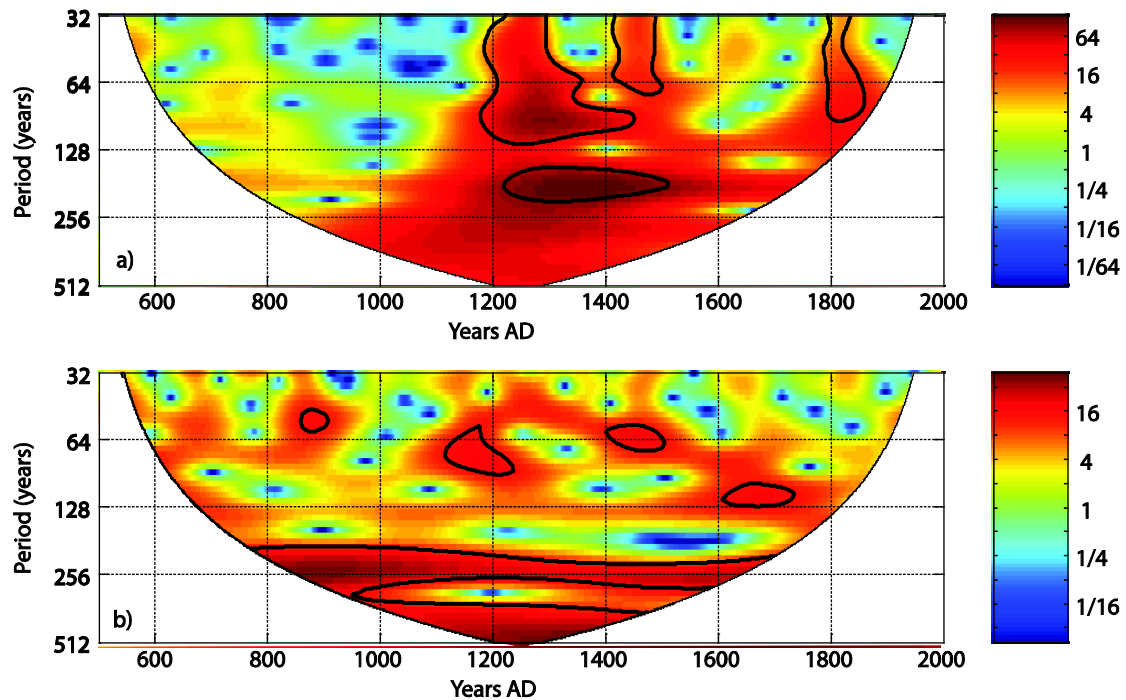
Fig. 2.10: *Wavelet power spectrum (Morlet) of a) the volcanic contributions and b) the averaged residual "volcano free" contribution. Occurrence of periods with respect to time is given by red to yellow colours. Thick black contours designate the 95% confidence level using a red noise background. The region outside the cone of influence (COI) is shown in white.*

If the difference between the LIA and the other episodes is due to coincidence with volcanic eruptions during the LIA, then the residual "volcano free" contribution series should look similar in the SEAs for the LIA and the other periods. However, comparing the residual temperature component of all series (Fig. 2.9b) with the temperature average of all series (Fig. 2.5a,) we find that the response to solar minima is no longer statistically significant at the 95% level (it is significant at the 90% level for a lag of +8 years). For the LIA subperiod, results are still significant (Fig. 2.9c). Hence, the separation of the volcanic and residual contributions seems to be more successful for the other climate episodes with generally lower volcanic activity, emphasising the need for solar related climate studies in the absence of strong multi-decadal volcanic forcing.

While this method which fits parameters a and b over the whole common period provides a good estimation of the volcanic effect, it may not be ideal for some of the eruptions. A further sensitivity study was done using constant parameters a but allowing parameters b to vary from eruption to eruption. This method will overfit the volcanic effect and thus the residuals will be free of any volcanic signal, although the solar signal may also be reduced. Nevertheless, the wavelet spectrum from this sensitivity analysis of the volcano-free contribution of the averaged temperature series is still significant at the De Vries cycle, indicating a solar effect after removal of the volcanic forcing signal.

2.3.4 Other influences, phase relationships, and limitations

Results have shown indications both for and against a solar fingerprint in tree-ring reconstructions. However, the influence of other forcing factors and internal oscillations of the climate system and the interplay with solar radiation changes are difficult to incorporate in this analysis. Nevertheless, some possible alternative explanations for some of the observed results are discussed in this section, especially in terms of the relationships between "solar forcing – climate response" and the "climate variability - tree growth".

The influences of climate on tree growth may be non-stationary and may also contribute to some uncertainty in the lagged solar-climate relationships. If the so-called "Divergence Problem" (i.e. the disagreement between instrumental temperature measurements and tree-ring reconstructions concentrated towards the Northern Hemisphere boreal forest zone since the 1960s) indeed represents a shift towards reduced temperature and increased precipitation control on tree growth (D'Arrigo et al. 2006; Esper and Frank 2009) and especially if such instabilities occurred throughout the past two millennia, then changes in phase lags may also be observed. The basic problem of variable climate-growth relationships is based on the assumption of stationarity and possible threshold levels, but the varying relationships over time are difficult to identify (Briffa et al., 2004; D'Arrigo et al., 2006; Frank et al., 2007a; Jones et al., 2009; Loehle, 2009; Esper and Frank 2009; Salzer et al., 2009). In our analysis, however, no significant lag differences between temperature and precipitation series can be distinguished, but the result may not be representative as only two precipitation records were considered.

Nevertheless, possible changing relationships between solar activity and climate, as well between climate variability and tree growth at the lower elevation sites from arid/semiarid southwestern USA might be expressed in the results of the cross-correlation and wavelet analysis (Table 2.2, 2.14), yet further analysis is necessary to explore this problem in more detail, especially in terms of changing oceanic influences on tree growth over time. Possibly, the positive relationship which is based on the correlation established between the bidecadal drought occurrences in the western United States since 1700 and years of Hale solar cycle minima (i.e. low solar activity = dry) by Cook et al. (1997) might not apply for centennial-scale solar forcing and southwestern US drought. An indication for a more complex relationship

might be found in the climate during the Medieval Climate Anomaly (MCA). Both MCA grand solar minima (centred at AD 897 and 1028) fall within the exceptional Stine (1994) megadrought affecting California/Nevada lasting from AD 832-1074 (Cook et al., 2004, 2007, 2010). This finding is congruent with diverse evidence for widespread hydrological anomalies (see references in Seager et al., 2007) which suggest that changes in the frequency and persistence of circulation regimes (such as a more positive NAO index in the North Atlantic or prevailing La Niña-like conditions possibly induced by increased solar activity and/or lack of strong volcanism) may have accounted for the climate in this period (Hughes and Diaz, 1994; Mann et al., 2005; Emile-Geay et al., 2007, 2008; Trouet et al., 2009; Cook et al., 2010; Graham et al., 2010). Moreover, Weber et al. (2004) emphasise in their modelling study that solar forcing in the range of 200-250 years could amplify an internal damped mode of the Meridional Overturning Circulation (MOC) which would give rise to a stronger response of the MOC at that time scale. Nonetheless, results from band-pass filtering and wavelet analysis in the range of the DeVries periodicity give evidence of lower variability in the southwestern US records, implying that solar forcing in this frequency band might not have been the main and/or direct cause for the droughts. Moreover, results from SEA on the drought series only show a tendency (significant at the 90% confidence level at year t+20 years) towards drier conditions during the MCA. On the other hand, solar forcing (in other frequencies) may still have influenced the climatic background conditions in such a way that solar activity changes were able to contribute to climate variability during the MCA through other processes (such as prevailing La Niña-like conditions).

Additionally, it needs to be kept in mind that the Pearson correlation coefficient only examines the linear relationship between two factors and that filtering and dating inaccuracies particularly in the TSI chronology hamper the precise determination of lagged correlation. For the time window considered, these uncertainties can amount to as much as 40 years, but are generally lower. This might explain the negative values found in some of the Sun-climate relationships.

Finally, it needs to be mentioned that solar forcing of Earth's climate is not restricted to the frequencies emphasised in this study. Possibly, the interplay with other solar frequencies, such as the ~2300-year Hallstatt cycle (Damon and Sonett, 1991), may modulate the 208-year period in a way that the forcing in the ~200-year band gets attenuated or intensified. For instance, it has been found that grand solar minima have largely occurred in clusters corresponding to the Hallstatt cycle minima during the past 9300 years (Steinhilber et al., 2010). The last cluster lasted from AD 1300-1800 and included the Dalton, Maunder, and Spörer Minima (Peristykh and Damon, 2003; McCracken and Beer, 2007; Steinhilber et al., 2010). However, effects of millennial-scale solar forcing cannot be analysed using the presently available tree chronologies due to the limited length of the reconstructions and the problem of the preservation of the lower frequencies.

2.4 Conclusion

Solar and volcanic fingerprints have been identified in various proxies from different climate archives, but a global-scale, very high-resolution, long-term evaluation of presently available tree-ring data has been missing so far. This study examined the Sun-volcano-climate relationship using globally distributed and annually resolved tree-ring chronologies during the past two millennia. Special emphasis was put on the effect of the 208-year solar activity cycle (the so-called DeVries cycle) on mean tree-ring growth response to investigate regional and temporal imprints of long-term solar activity variations. The target climatic parameters are summer surface temperature, precipitation, and drought whereas the reconstruction of solar activity (here Total Solar Irradiance; TSI) is based on measurements of the cosmogenic isotope ^{10}Be from ice cores.

The effect of multidecadal-to-centennial scale solar variability on climate was studied using two methods: analysis in the frequency domain and superposed epoch analysis (SEA). Spectral and wavelet analysis of solar activity show significant peaks near the DeVries cycle. This periodicity is found in some (10 out of 17 proxy series), though not in all of the series and aggregate series such as the first principal component of the temperature subset and the second principal component of the precipitation subset. The De Vries signature in the temperature proxies also remains after subtracting the volcanic signature, which was found to interfere with the De Vries cycle. Likewise, solar fingerprints at this period might be manifested in the temperature-sensitive proxies and in the Qinghai precipitation record which show significant response lags of approximately 0-20 years relative to solar forcing. This finding is in agreement with a high positive correlation established between the strength of the Asian summer monsoon and solar irradiance in Central Asia (Gupta et al., 2005; Liu et al., 2009). SEA of the temperature-sensitive tree chronologies composited with respect to grand solar minima depict a lag of approximately 10 years relative to solar forcing, pointing to a possible solar imprint. This lag relation is physically plausible and supported by model studies by Waple et al. (2002).

The present study performed principal component analysis in the time domain in order to extract the dominant modes of climate variability contained in the time series. Future analyses may be performed in the frequency domain, as discussed and applied in climate studies by Mann and Park (1999), or Apipattanavis et al. (2009). This method has the advantage that narrowband frequency domain structures can be better isolated compared to the traditional time-domain techniques (Mann and Park, 1999) and hence, the phase relationships between TSI and the time series could be better preserved.

Other forcing factors, namely volcanic activity, may mask the solar signal in space and time. Hence, we separated volcanic and other signals in the temperature time series using a statistical approach. Results from wavelet analysis and SEA reveal significant periodicities near the solar DeVries frequency in the volcanic and residual "volcano free" contributions during the LIA, making a clear separation of the solar and volcanic forcing signals difficult. Nevertheless, the "volcano free" temperatures show significant periodicities near the DeVries frequency during the entire past 1500 years, pointing to a solar imprint on global climate. This

finding emphasises the need for solar related climate studies with focus on periods characterised by an absence of strong multi-decadal volcanic forcing.

Acknowledgements

References

Abreu, J. A., Beer, J., Steinhilber, F., Tobias, S. M., Weiss, N. O., 2008. For how long will the current grand maximum of solar activity persist? Geophys. Res. Lett. **35**, L20109, doi:10.1029/2008gl035442.

Abreu, J. A., Beer, J., Ferriz-Mas, A., 2010. Past and future solar activity from cosmogenic radionuclides. In: Cranmer, S. R., Hoeksema, J. R., Kohl, J. L. (Eds.), SOHO-23: Understanding a peculiar solar minimum. ASP Conference Series, **428**.

Adams, J. B., Mann, M. E., Ammann, C. M., 2003. Proxy evidence for an El Nino-like response to volcanic forcing. Nature **426**, 274-278.

Ammann, C. M., Joos, F., Schimel, D. S., Otto-Bliesner, B. L., Tomas, R. A., 2007. Solar influence on climate during the past millennium: Results from transient simulations with the NCAR Climate System Model. Proc. Natl. Acad. Sci. **104**(10), 3713-3718.

Apipattanavis, S., McCabe, G. J., Rajagopalan, B., Gangopadhyay, S., 2009. Joint spatiotemporal variability of global sea surface temperatures and global palmer drought severity index values. J. Clim. **22**, 6251-6267.

Briffa, K. R., 2000. Annual climate variability in the Holocene: interpreting the message of ancient trees. Quaternary Sci. Rev. **19**, 87-105.

Briffa, K. R., Jones, P. D., Bartholin, T. S., Eckstein, D., Schweingruber, F. H., Karlén, W., Zetterberg, P., Eronen, M., 1992. Fennoscandian summers from AD 500: Temperature changes on short and long timescales. Clim. Dyn. **7**(3), 111-119.

Briffa, K. R., Osborn, T. J., Schweingruber, F. H., 2004. Large-scale temperature inferences from tree rings: a review. Global Planet. Change **40**, 11-26.

Büntgen, U., Tegel, W., Nicolussi, K., McCormick, M., Frank, D., Trouet, V., Kaplan, J.O., Herzig, F., Heussner, K.-U., Wanner, H., Luterbacher, J., Esper, J., 2011. 2500 years of European climate variability and human susceptibility. Science **331**(6017), 578-582.

Cole-Dai, J., Ferris, D., Lanciki, A., Savarino, J., Baroni, M., Thiemens, M. H., 2009. Cold decade (AD 1810-1819) caused by Tambora (1815) and another (1809) stratospheric volcanic eruption. Geophys. Res. Lett.**36**, L22703, doi:10.1029/2009gl040882.

Cook, E. R., Briffa, K. R., Meko, D. M., Graybill, D. A., Funkhouser, G., 1995. The segment length curse in long tree-ring chronology development for paleoclimate studies. Holocene **5**(2), 229-237.

Cook, E. R., Meko, D. M., Stockton, C. W., 1997. A new assessment of possible solar and lunar forcing of the bidecadal drought rhythm in the western United States. J. Clim. **10**, 1343-1356.

Cook, E. R., Buckley, B. M., D'Arrigo, R. D., Peterson, M. J., 2000. Warm-season temperatures since 1600 BC reconstructed from Tasmanian tree rings and their relationship to large-scale sea surface temperature anomalies. Clim. Dyn. **16**, 79-91.

Cook, E. R., Woodhouse, C. A., Eakin, C. M., Meko, D. M., Stahle, D. W., 2004. Long-term aridity changes in the western United States. Science **306**, 1015-1018.

Cook, E. R., Seager, R., Cane, M. A., Stahle, D. W., 2007. North American drought: Reconstructions, causes, and consequences. Earth-Sci Rev. **81**, 93-134.

Cook, E. R., Seager, R., Heim, R. R., Vose, R. S., Herweijer, C., Woodhouse, C., 2010. Megadroughts in North America: placing IPCC projections of hydroclimatic change in a long-term palaeoclimate context. J. Quaternary Sci. **25**, 48-61.

Crowley, T. J., 2000. Causes of climate change over the past 1000 years. Science **289**, 270-277.

Damon, P. E., Sonett, C. P., 1991. Solar and terrestrial componants of the atmospheric 14C variation spectrum. In: Sonett, C. P., Giampapa, M. S., Matthews, M. S. (Eds.). The Sun in time. University of Arizona Press, Tucson, pp. 360-388.

D'Arrigo, R., Jacoby, G., Frank, D., Pederson, N., Cook, E., Buckley, B., Nachin, B., Mijiddorj, R., Dugarjav, C., 2001. 1738 years of Mongolian temperature variability inferred from a tree-ring width chronology of Siberian pine. Geophys. Res. Lett. **28**(3), 543-546.

D'Arrigo, R., Wilson, R., Jacoby, G., 2006. On the long-term context for late twentieth century warming. J. Geophys. Res. **111**, D03103, doi:10.1029/2005jd006352.

Delaygue, G. and Bard, E., (2010). An Antarctic view of beryllium-10 and solar activity for the past millennium. Clim. Dyn. **36**, 2201-2218.

de Wit, T. D., Watermann, J., 2010. Solar forcing of the terrestrial atmosphere. CR. Geosci. **342**, 259-272.

Denton, G. H., Karlén, W., 1973. Holocene climatic variations-their pattern and possible cause. Quaternary Res. **3**(2), 155-205.

Eddy, J. A., 1976. The Maunder Minimum. Science **192**, 1189-1202.

Eichler, A., Olivier, S., Henderson, K., Laube, A., Beer, J., Papina, T., Gaggeler, H. W., Schwikowski, M., 2009. Temperature response in the Altai region lags solar forcing. Geophys. Res. Lett. **36**, L01808, doi:10.1029/2008gl03593.

Emile-Geay, J., Cane, M., Seager, R., Kaplan, A., Almasi, P., 2007. El Nino as a mediator of the solar influence on climate. Paleoceanography **22**(3), Pa3210, doi:10.1029/2006 pa001304.

Emile-Geay, J., Seager, R., Cane, M. A., Cook, E. R., Haug, G. H., 2008. Volcanoes and ENSO over the past millennium. J. Clim. **21**, 3134-3148.

Esper, J., Cook, E. R., Schweingruber, F. H., 2002. Low-frequency signals in long tree-ring chronologies for reconstructing past temperature variability. Science **295**, 2250-2253.

Esper, J., Cook, E. R., Krusic, P. J., Peters, K., Schweingruber, F. H., 2003. Tests of the RCS method for preserving low-frequency variability in long tree-ring chronologies. Tree-Ring Research **59**(2), 81-98.

Esper, J., Frank, D., 2009. Divergence pitfalls in tree-ring research. Climatic Change **94**, 261-266.

Fischer, E. M., Luterbacher, J., Zorita, E., Tett, S. F. B., Casty, C., Wanner, H., 2007. European climate response to tropical volcanic eruptions over the last half millennium. Geophys. Res. Lett. **34**, L05707, doi:10.1029/2006GL027992.

Fleitmann, D., Burns, S. J., Mudelsee, M., Neff, U., Kramers, J., Mangini, A., Matter, A., 2003. Holocene forcing of the Indian monsoon recorded in a stalagmite from Southern Oman. Science **300**, 1737-1739.

Frank, D., Büntgen, U., Böhm, R., Maugeri, M., Esper, J., 2007a. Warmer early instrumental measurements versus colder reconstructed temperatures: shooting at a moving target. Quaternary Sci. Rev. 26, 3298-3310.

Frank, D., Esper, J., Cook, E. ., 2007b. Adjustment for proxy number and coherence in a large-scale temperature reconstruction. Geophys. Res. Lett. **34**, L16709, doi:10.1029/2007GL030571.

Frank, D., Esper, J., Zorita, E., Wilson, R., 2010. A noodle, hockey stick, and spaghetti plate: a perspective on high-resolution paleoclimatology. WIREs Clim. Change **1**(4), 507-516.

Gao, C. C., Robock, A., Self, S., Witter, J. B., Steffenson, J. P., Clausen, H. B., Siggaard-Andersen, M. L., Johnsen, S., Mayewski, P. A., Ammann, C., 2006. The 1452 or 1453 AD Kuwae eruption signal derived from multiple ice core records: Greatest volcanic sulfate event of the past 700 years. J. Geophys. Res. **111**, D12107, doi:10.1029/2005jd006710.

Gao, C. C., Robock, A., Ammann, C., 2008. Volcanic forcing of climate over the past 1500 years: An improved ice core-based index for climate models. J. Geophys. Res. **113**, D23111, doi:10.1029/2008jd010239.

Graham, N. E., Ammann, C. M., Fleitmann, D., Cobb, K. M., Luterbacher, J., 2010. Support for global climate reorganization during the ''Medieval Climate Anomaly''. Clim. Dyn. **37**, 1217-1245.

Gray, L. J., Beer, J., Geller, M., Haigh, J. D., Lockwood, M., Matthes, K., Cubasch, U., Fleitmann, D., Harrison, G., Hood, L., Luterbacher, J., Meehl, G. A., Shindell, D., Van

Geel, B., White, W., 2010. Solar influences on climate. Rev. Geophys. **48**, RG4001, doi:10.1029/2009RG000282.

Grinsted, A., Moore, J. C., Jevrejeva, S., 2004. Application of the cross wavelet transform and wavelet coherence to geophysical time series. Nonlinear Proc. in Geophys. **11**, 561-566.

Grissino-Mayer, H. D., 1996. A 2129-year reconstruction of precipitation for northwestern New Mexico, USA. In: Dean, J. S., Meko, D. M., Swetnam, T. W. (Eds.), Tree Rings, Environment and Humanity. Radiocarbon, Tucson, pp. 191-204.

Grudd, H., 2008. Torneträsk tree-ring width and density AD 500-2004: a test of climatic sensitivity and a new 1500-year reconstruction of north Fennoscandian summers. Clim. Dyn. **31**, 843-857.

Gupta, A. K., Das, M., Anderson, D. M., 2005. Solar influence on the Indian summer monsoon during the Holocene. Geophys. Res. Lett. **32**, L17703, doi:10.1029/2005gl022685.

Haigh, J. D., Winning, A. R., Toumi, R., Harder, J. W., 2010. An influence of solar spectral variations on radiative forcing of climate. Nature **467**, 696-699.

Haug, G. H., Hughen, K. A., Sigman, D. M., Peterson, L. C., Rohl, U., 2001. Southward migration of the intertropical convergence zone through the Holocene. Science **293**, 1304-1308.

Hegerl, G. C., Crowley, T. J, Baum, S. K., Kwang-Yul, K., Hyde, W. T., 2003. Detection of volcanic, solar and greenhouse gas signals in paleo-reconstructions of Northern Hemisphere temperature. Geophys. Res. Lett. **30**(5), 1242, doi:10.1029/2002GL016635.

Hodell, D. A., Brenner, M., Curtis, J. H., Guilderson, T., 2001. Solar forcing of drought frequency in the Maya lowlands. Science **292**, 1367-1370.

Hughes, M. K., Diaz, H. F., 1994. Was there a Medieval Warm Period, and if so, where and when. Climatic Change **26**, 109-142.

Jones, P. D., Briffa, K. R., Schweingruber, F. H., 1995. Tree-ring evidence of the widespread effects of explosive volcanic eruptions. Geophys. Res. Lett. **22**(11), 1333-1336.

Jones, P. D., Briffa, K. R., Osborn, T. J., Lough, J. M., van Ommen, T. D., Vinther, B. M., Luterbacher, J., Wahl, E. R., Zwiers, F. W., Mann, M. E., Schmidt, G. A., Ammann, C. M., Buckley, B. M., Cobb, K. M., Esper, J., Goosse, H., Graham, N., Jansen, E., Kiefer, T., Kull, C., Küttel, M., Mosley-Thompson, E., Overpeck, J. T., Riedwyl, N., Schulz, M., Tudhope, A. W., Villalba, R., Wanner, H., Wolff, E., Xoplaki, E., 2009. High-resolution palaeoclimatology of the last millennium: a review of current status and future prospects. Holocene **19**(1), 3-49.

Lamb, H. H., 1977. Climate: Present, Past and Future – Volume 2: Climatic history and the future. Methuen, London. 837 pp.

Lean, J. L., 2010. Cycles and trends in solar irradiance and climate. WIREs Clim. Change **1**(1), 111-122.

Liu, X. Q., Dong, H. L., Yang, X. D., Herzschuh, U., Zhang, E. L., Stuut, J. B. W., Wang, Y. B., 2009. Late Holocene forcing of the Asian winter and summer monsoon as evidenced

by proxy records from the northern Qinghai-Tibetan Plateau. Earth Planet. Sci. Lett **280**, 276-284.

Ljungqvist, F. C., 2009. Temperature proxy records covering the last two millennia: A tabular and visual overview. Geogr. Ann. A. **91** (1), 11-29.

Ljungqvist, F. C., 2010. A new reconstruction of temperature variability in the extra-tropical northern hemisphere during the last two millennia. Geogr. Ann. A. **92**(3), 339-351.

Loehle, C., 2009. A mathematical analysis of the divergence problem in dendroclimatology. Climatic Change **94**, 233-245.

Mann, M. E. and Park, L., 1999. Oscillatory spatiotermporal signal detection in climate studies. Adv. Geophys. **41**, 1-131.

Mann, M. E., Cane, M. A., Zebiak, S. E., Clement, A., 2005. Volcanic and solar forcing of the tropical Pacific over the past 1000 years. J. Clim. **18**(3), 447-456.

Mann, M. E., Zhang, Z. H., Hughes, M. K., Bradley, R. S., Miller, S. K., Rutherford, S., Ni, F. B., 2008. Proxy-based reconstructions of hemispheric and global surface temperature variations over the past two millennia. Proc. Natl. Acad. Sci. **105**(36), 13252-13257.

McCracken, K. G., Beer, J., 2007. Long-term changes in the cosmic ray intensity at Earth, 1428-2005. J. Geophys. Res. **112**, A10101, doi:10.1029/2006ja012117.

Meehl, G.A., Arblaster, J.M., Matthes, K., Sassi, F., van Loon, H., 2009. Amplifying the Pacific climate system response to a small 11-year solar cycle forcing. Science **325**, 1114-1118.

Moberg, A., Sonechkin, D. M., Holmgren, K., Datsenko, N. M., Karlén, W., 2005. Highly variable Northern Hemisphere temperatures reconstructed from low- and high-resolution proxy data. Nature **433**, 613-617.

Moberg, A., Sonechkin, D. M., Holmgren, K., Datsenko, N. M., Karlén, W., Lauritzen, S. E., 2006. Corrigendum: Highly variable Northern Hemisphere temperatures reconstructed from low- and high-resolution proxy data (vol 433, pg 613, 2005). Nature **439**, 1014.

Muscheler, R., Beer, J., Wagner, G., Laj, C., Kissel, C., Raisbeck, G. M., Yiou, F., Kubik, P. W., 2004. Changes in the carbon cycle during the last deglaciation as indicated by the comparison of Be-10 and C-14 records. Earth Planet. Sci. Lett **219**, 325-340.

Naurzbaev, M. M., Vaganov, E. A., Sidorova, O. V., Schweingruber, F. H., 2002. Summer temperatures in eastern Taimyr inferred from a 2427-year late-Holocene tree-ring chronology and earlier floating series. Holocene **12**(6), 727-736.

Nussbaumer, S. U., Steinhilber, F., Trachsel, M., Breitenmoser, P., Beer, J., Blass, A., Grosjean, M., Hafner, A., Holzhauser, H., Wanner, H., Zumbühl, H.J., 2011. Alpine climate during the Holocene: a comparison between records of glaciers, lake sediments and solar activity. J. Quaternary Sci. **26**(7), 703-713.

Peristykh, A. N., Damon, P. E., 2003. Persistence of the Gleissberg 88-year solar cycle over the last similar to 12,000 years: Evidence from cosmogenic isotopes. J. Geophys. Res. **108**, 1003, doi:10.1029/2002ja009390.

Perry, C. A., 2007. Evidence for a physical linkage between galactic cosmic rays and regional climate time series. Adv. Space Res. **40**(3), 353-364.

Raspopov, O. M., Dergachev, V. A., Esperc, J., Kozyreva, O. V., Frank, D., Ogurtsov, M., Kolstrom, T., Shao, X., 2008. The influence of the de Vries (similar to 200-year) solar cycle on climate variations: Results from the Central Asian Mountains and their global link. Palaeogeogr. Palaeoclimatol. Palaeoecol. **259**, 6-16.

Rind, D., 2002. Climatology - The sun's role in climate variations. Science **296**, 673-677.

Rind, D., Lean, J., Healy, R., 1999. Simulated time-dependent climate response to solar radiative forcing since 1600. J. Geophys. Res. **104**, 1973-1990.

Robock, A., 2000. Volcanic eruptions and climate. Rev. Geophys. **3**(8), 191-219.

Robock, A., 2005. Cooling following large volcanic eruptions corrected for the effect of diffuse radiation on tree rings. Geophys. Res. Lett. **32**(6), L06702, doi:10.1029/2004GL022116.

Salzer, M. W., Hughes, M. K., 2007. Bristlecone pine tree rings and volcanic eruptions over the last 5000 yr. Quatern. Res. **67**(1), 57-68.

Salzer, M. W., Hughes, M. K., Bunn, A. G., Kipfmueller, K. F., 2009. Recent unprecedented tree-ring growth in bristlecone pine at the highest elevations and possible causes. Proc. Natl. Acad. Sci. USA 106(48), 20348-20353.

Schimmelmann, A., Lange, C. B., Meggers, B. J., 2003. Palaeoclimatic and archaeological evidence for a similar to 200-yr recurrence of floods and droughts linking California, Mesoamerica and South America over the past 2000 years. Holocene **13**(3), 763-778.

Schulz, M., Mudelsee, M., 2002. REDFIT: estimating red-noise spectra directly from unevenly spaced paleoclimatic time series. Comput. Geosci. **28**(3), 421-426.

Seager, R., Graham, N., Herweijer, C., Gordon, A. L., Kushnir, Y., Cook, E., 2007. Blueprints for Medieval hydroclimate. Quaternary Sci. Rev. **26**, 2322-2336.

Sheppard, P. R., Tarasov, P. E., Graumlich, L. J., Heussner, K.-U., Wagner, M., Österle, H., and Thompson, L. G., 2004. Annual precipitation since 515 BC reconstructed from living and fossil juniper growth of northeastern Qinghai Province, China. Clim. Dynam. **23**, 869-881.

Shindell, D. T., Schmidt, G. A., Mann, M. E., Rind, D., Waple, A., 2001. Solar forcing of regional climate change during the maunder minimum. Science **294**, 2149-2152.

Shindell, D. T., Schmidt, G. A., Miller, R. L., Mann, M. E., 2003. Volcanic and solar forcing of climate change during the preindustrial era. J. Clim. **16**(24), 4094-4107.

Sidorova, O. V., Naurzbaev, M. M., 2002. Response of Larix cajanderi to climatic changes at the upper timberline and in the Indigirka River Valley. Lesovedenie **2**, 73-75.

Solanki, S. K., Usoskin, I. G., Kromer, B., Schussler, M., Beer, J., 2004. Unusual activity of the Sun during recent decades compared to the previous 11,000 years. Nature **431**, 1084-1087.

Sonett, C. P., Suess, H. E., 1984. Correlation of bristlecone pine ring widths with atmospheric C-14 variations - A climate-Sun relation. Nature **307**, 141-143.

Stenchikov, G., Delworth, T. L., Ramaswamy, V., Stouffer, R. J., Wittenberg, A., Zeng, F., 2009. Volcanic signals in oceans. J. Geophys. Res. **114**, D16104, doi:10.1029/2008JD011673.

Steinhilber, F., Abreu, J., Beer, J., 2008. Solar modulation during the Holocene. Astrophys. Space Sci. **4**, 1-6.

Steinhilber, F., Beer, J., Fröhlich, C., 2009. Total solar irradiance during the Holocene. Geophys. Res. Lett. **36**, L19704, doi:10.1029/2009gl040142.

Steinhilber, F., Abreu, J.A., Beer, J., McCracken, K. G., 2010. Interplanetary magnetic field during the past 9300 years inferred from cosmogenic radionuclides. J. Geophys. Res. **115**, A01104, doi:10.1029/2009ja014193.

Stine, S., 1994. Extreme and persistent drought in California and Patagonia during medieval time. Nature **369**, 546-549.

Stothers, R. B., 1984. The great Tambora eruption in 1815 and its aftermath. Science **224**(4654), 1191-1198.

Stuiver, M., Quay, P. D., 1980. Changes in atmospheric C-14 attributed to a variable sun. Science **207**, 11-19.

Stuiver, M., Braziunas, T. F., 1989. Atmospheric C-14 and century-scale solar oscillations. Nature **338**, 405-408.

Thompson, D. W. J., Wallace, J. M., Jones, P. D., Kennedy, J. J., 2009. Identifying signatures of natural climate variability in time series of global-mean surface temperature: methodology and insights. J. Clim. **22**(22), 6120-6141.

Timmreck, C., Lorenz, S. J., Crowley, T. J., Kinne, S., Raddatz, T. J., Thomas, M. A., Jungclaus, J. H., 2009. Limited temperature response to the very large AD 1258 volcanic eruption. Geophys. Res. Lett. **36**, L21708, doi:10.1029/2009gl040083.

Torrence, C., Compo, G. P., 1998. A practical guide to wavelet analysis. Bulletin of the American Meteorological Society **79**(1), 61-78.

Trouet, V., Esper, J., Graham, N. E., Baker, A., Scourse, J. D., Frank, D. C., 2009. Persistent Positive North Atlantic Oscillation Mode Dominated the Medieval Climate Anomaly. Science **324**, 78-80.

Usoskin, I. G., Solanki, S. K., Korte, M., 2006. Solar activity reconstructed over the last 7000 years: The influence of geomagnetic field changes. Geophys. Res. Lett. **33**, L08103, doi:10.1029/2006gl025921.

Vieira, L. E. A., Solanki, S. K., Krivova, N. A., Usoskin, I., 2011. Evolution of the solar irradiance during the Holocene. Astron. Astrophys. **531**(A6), doi:10.1051/0004-6361/201015843.

Vonmoos, M., Beer, J., Muscheler, R., 2006. Large variations in Holocene solar activity: Constraints from Be-10 in the Greenland Ice Core Project ice core. J. Geophys. Res. **111**, A10105, doi:10.1029/2005ja011500.

Wagner, G., Beer, J., Masarik, J., Muscheler, R., Kubik, P. W., Mende, W., Laj, C., Raisbeck, G. M., Yiou, F., 2001. Presence of the solar de Vries cycle (similar to 205 years) during the last ice age. Geophys. Res. Lett. **28**(2), 303-306.

Wang, Y. J., Cheng, H., Edwards, R. L., He, Y. Q., Kong, X. G., An, Z. S., Wu, J. Y., Kelly, M. J., Dykoski, C. A., Li, X. D., 2005. The Holocene Asian monsoon: Links to solar changes and North Atlantic climate. Science **308**, 854-857.

Wanner, H., Beer, J., Bütikofer, J., Crowley, T. J., Cubasch, U., Flückiger, J., Goosse, H., Grosjean, M., Joos, F., Kaplan, J. O., Küttel, M., Müller, S. A., Prentice, I. C., Solomina, O., Stocker, T. F., Tarasov, P., Wagner, M., Widmann, M., 2008. Mid- to Late Holocene climate change: an overview. Quaternary Sci. Rev. **27**, 1791-1828.

Waple, A. M., Mann, M. E., Bradley, R. S., 2002. Long-term patterns of solar irradiance forcing in model experiments and proxy based surface temperature reconstructions. Clim. Dyn. **18**, 563-578.

Weber, S. L., Crowley, T. J., van der Schrier, G., 2004. Solar irradiance forcing of centennial climate variability during the Holocene. Clim. Dyn. **22**, 539-553.

Wiles, G. C., D'Arrigo, R. D., Villalba, R., Calkin, P. E., Barclay, D. J., 2004. Century-scale solar variability and Alaskan temperature change over the past millennium. Geophys. Res. Lett. **31**(15), L15203, doi:10.1029/2004gl020050.

Wilks, D. S., 2011. Statistical methods in the atmospheric sciences, vol. 100, third ed. Elsevier Academic Press, Amsterdam. 704 pp.

Yan, H. M., Zhong, M., Zhu, Y. Z., 2004. Determination of the degree of freedom of digital filtered time series with an application to the correlation analysis between the length of day and the southern oscillation index. Chinese Astron. and Astr. **28**(1), 120-126.

2.5 Appendix
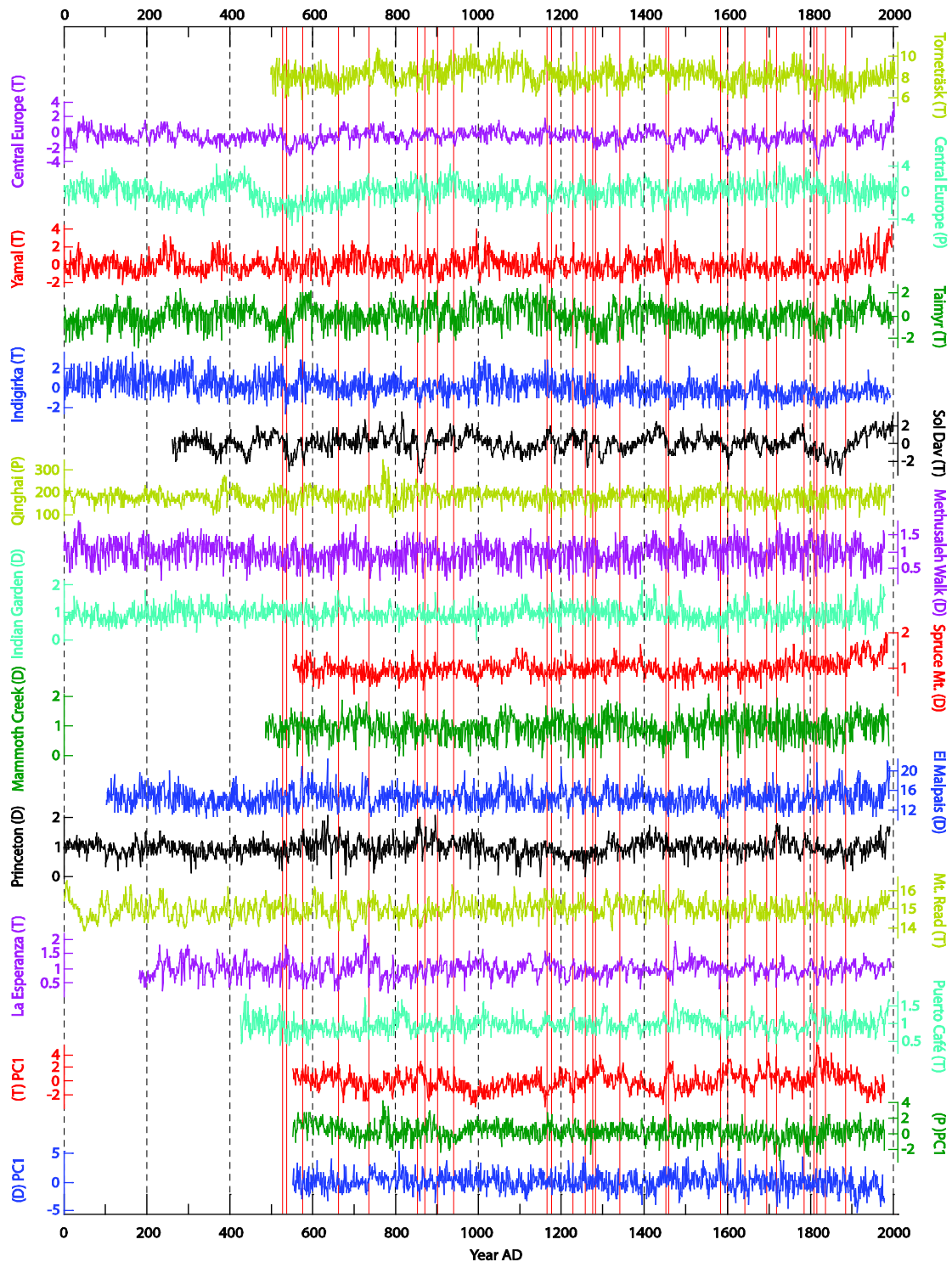
Fig. 2.11: *Raw climate reconstructions (see references in Table 2.1) and the leading principal component (PC) series for temperature (T), precipitation (P), and drought (D). Vertical red lines mark the major volcanic eruptions used for the analyses at AD 529, 541, 577, 664, 738, 854, 870, 901, 939, 1167, 1176, 1227, 1258, 1275, 1284, 1341, 1452, 1459, 1584, 1600, 1641, 1693, 1719, 1783, 1809, 1815, 1835, and 1883.*
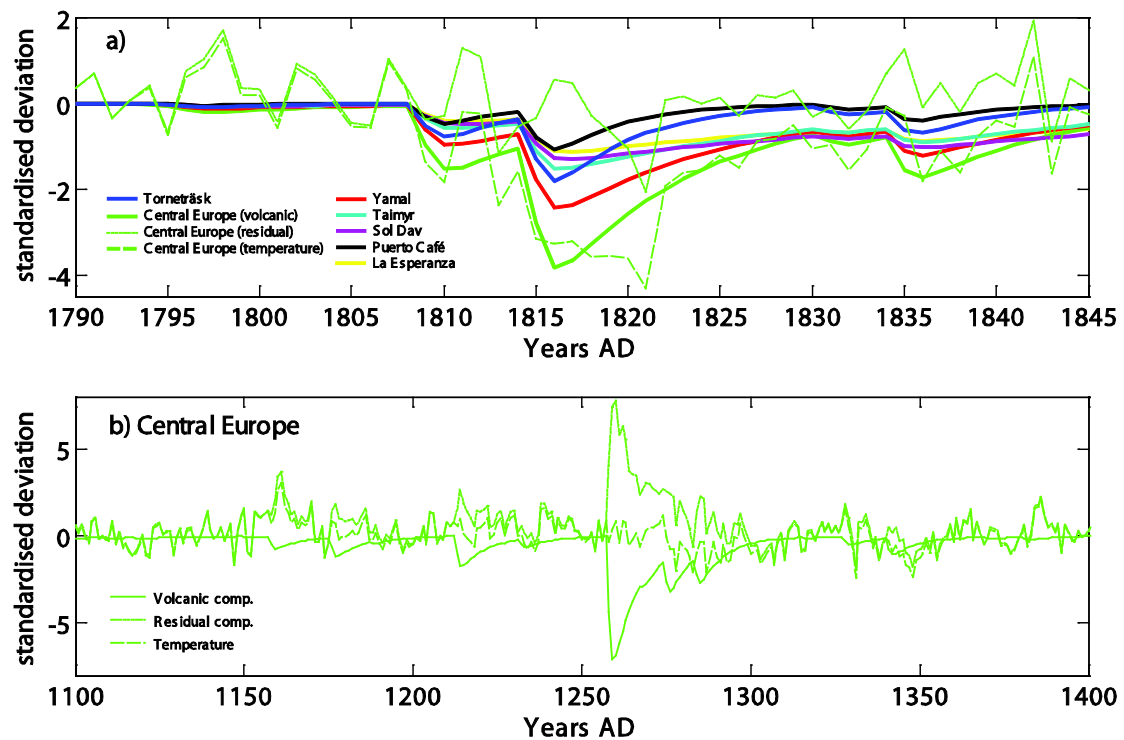
Fig. 2.12: *Volcanic temperature effect with parameters of the statistical model fitted during the AD 1790-1845 period and then applied for the common period AD 553-1979. a) Volcanic temperature effects as well as the Central European residual component (dotted green line) for the unreported 1809 and 1815 Tambora eruptions. Compare with Figure 2.8e. The series from Tasmania (slightly enhanced temperatures) and from Indigirka (unreasonable high memory effect) are not shown. b) Example of the Central European record using the parameters a = 0.1 yr⁻¹ and b = 7.3 K, which leads to a largely overestimated volcanic forcing term. This figure clearly illustrates the dependence of the volcanic forcing term on the time interval used for fitting the parameters in the statistical model. In comparison to the results presented in Figure 2.8, fitting over a specific time interval - which is characterised by large volcanic activity - leads to a more pronounced volcanic temperature influence.*
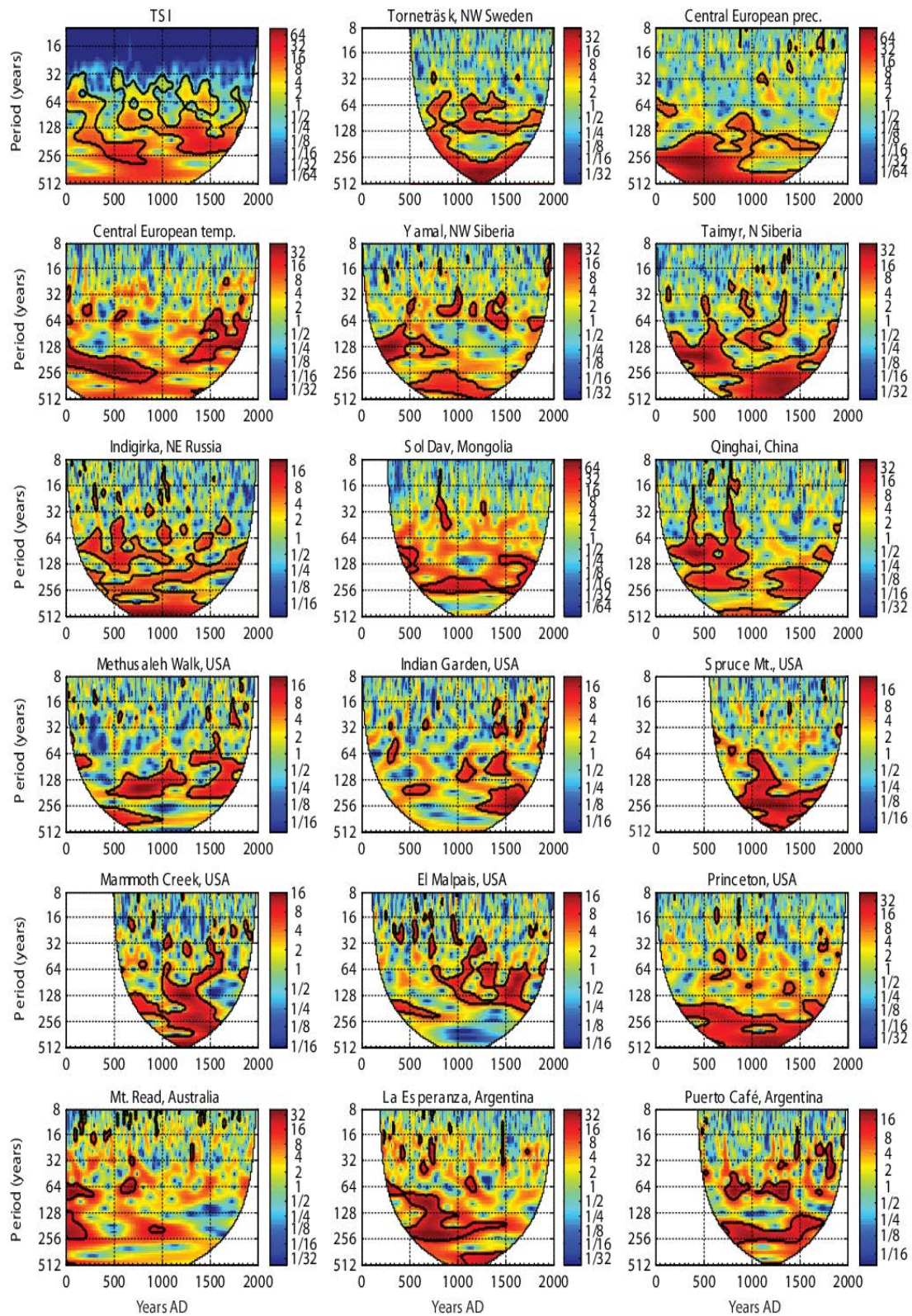
Fig. 2.13: *Wavelet power spectrum (Morlet) of TSI and the tree-ring chronologies. Occurrence of periods with respect to time is given by red to yellow colours. Thick black contours designate the 95% confidence level using a red noise background. The region outside the cone of influence (COI) is shown in white.*
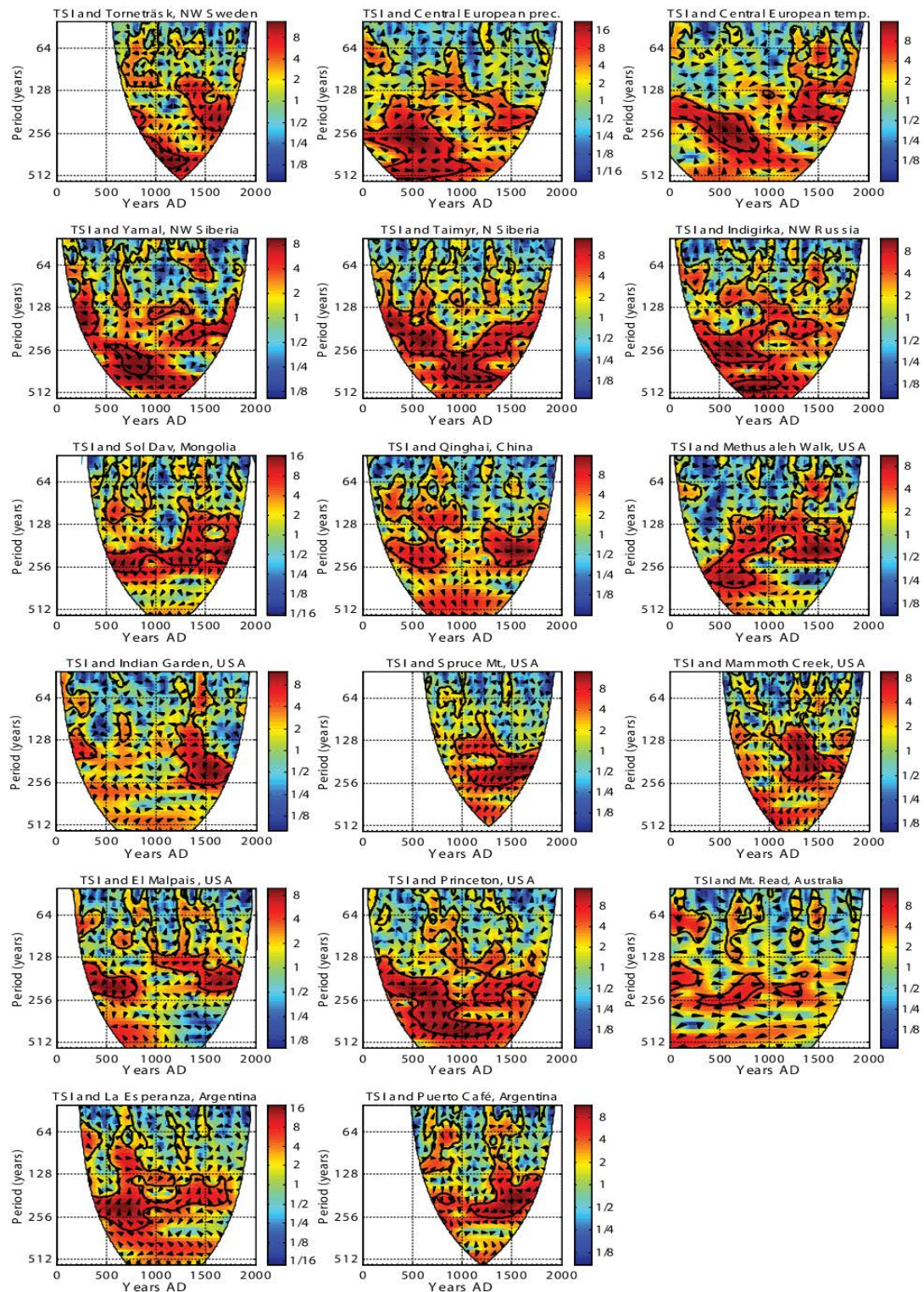
Fig. 2.14: *Power spectrum of the cross wavelet transformation between TSI and each of the tree-ring chronologies. Regions in the time-frequency space with large common power are indicated by red colours. Thick black contours designate the 95% confidence level using a red noise background. The region outside the cone of influence (COI) is shown in white. Vectors indicate the relative phase differences between TSI and a tree-ring chronology. A horizontal vector pointing right (left) implies in-phase (anti-phase) relationships, and a vector pointing down means TSI leading the climate time series by 90°.*

Chapter 3

FORWARD MODELLING OF TREE-RING WIDTH AND COMPARISON WITH A GLOBAL NETWORK OF TREE-RING CHRONOLOGIES

Petra **Breitenmoser** [1,2], Stefan **Brönnimann** [1,2], and David **Frank** [2,3]

[1] *Institute of Geography, Climatology and Meteorology, University of Bern, Switzerland*

[2] *Oeschger Centre for Climate Change Research, University of Bern, Switzerland*

[3] *Swiss Federal Institute for Forest, Snow and Landscape Research (WSL), Birmensdorf, Switzerland*

Abstract

We investigate the relationship between climate and tree-ring data on a global scale using the process-based Vaganov-Shashkin-Lite (VSL) forward model of tree-ring width formation. The VSL model requires as inputs only latitude, monthly mean temperature, and monthly accumulated precipitation. Hence, this simple, process-based model enables ring-width simulation at any location where monthly climate records exist. In this study, we analyse the growth response of simulated tree-rings to monthly climate conditions obtained from the CRU TS3.1 data set back to 1901. Our key aims are (a) to examine the relations among growth simulated due to climatic influences and growth observed in actual tree-ring chronologies at 2287 globally distributed tree sites and (b) to evaluate the potential of the VSL model to reconstruct past climate. A new assessment of the growth-onset threshold temperature of approximately 4-6 °C for most sites and species using a Bayesian estimation approach complements previous observational and geostatistical evidences for the lower temperature limits where plant growth may be sustained. Our results suggest that the VSL model skilfully simulates site level tree-ring series in response to climate forcing for a wide range of environmental conditions and species.

Spatial aggregation of the tree-ring chronologies to reduce non-climatic noise at the site level yielded notable improvements in the coherence between modelled and actual growth. The resulting distinct and coherent patterns of significant relationships between the aggregated and simulated series further demonstrate the VSL model's ability to skilfully capture the climatic signal contained in tree-series. Finally, we propose that the VSL model can be used as an observation operator in data assimilation approaches to reconstruct past climate.

3.1 Introduction

Information derived from tree-rings is one of the most powerful tools available for studying past climatic variability as well as identifying fundamental relationships between tree-growth and climate (e.g. Fritts, 1976; Briffa et al., 2002a,b; IPCC, 2007). Climate reconstructions from trees have many advantages over other proxy archives, including their wide spatial distribution, annual resolution, calendar-exact dating, and high climate sensitivity (Hughes, 2002; Jones et al., 2009). However, relationships between tree-growth and climate are complex and classical calibration methods (i.e. establishing a statistical relationship between instrumental and proxy data during their period of overlap) are often inadequate for a few reasons. Firstly, empirical methods generally treat climate as a function of the proxy rather than quantify how proxy signals are driven by climate variability. Secondly, statistical calibration is bound by assumptions of uniformitarianism and stationarity in the climate-growth system - conditions that may not be adequately met (Raible et al., 2006). Thirdly, most tree-ring based reconstructions of temperature are limited to regions where growth is primarily limited by cold temperatures - leaving the vast areas of the Earth away from high mountains and high latitude environments poorly represented by high-quality proxy data (Wahl and Frank, 2012).

In recent years, data assimilation approaches have found an increasingly important role in paleoclimatic reconstruction efforts (Hughes and Ammann, 2009; Goosse et al., 2010; Widmann et al., 2010; Franke et al., 2011; Bhend et al., 2012; Tingley et al., 2012). Combined information from climate models and proxy archives, including also associated errors and their covariance, provide a physically plausible representation of past climate consistent with available proxy data. An observation operator, which expresses the proxy as a function of the model data, is the formal link between model and proxy data. So-called forward proxy models (process-based or empirical) could potentially be used as an observation operator in data assimilation approaches (Hughes and Ammann, 2009).

The Vaganov-Shashkin (VS; Vaganov et al., 2006, 2011) process-based forward model has been demonstrated to skilfully simulate tree-ring width in North America and Siberia (Anchukaitis et al., 2006; Evans et al., 2006; Vaganov et al., 2011), China (Shi et al., 2008; Zhang et al., 2011), and Tunisia (Touchan et al., 2012). This forward-model of tree-ring growth was developed to establish non-linear and non-stationary relationships between climate variables and tree-ring formation (Vaganov et al., 2006, 2011), yet applications generating "pseudo ring-width" series from global climate models has so far been hindered by the relative complexity. Recently, Tolwinski-Ward et al. (2011a,b) introduced a simplified model version (the so-called Vaganov-Shashkin-Lite; VSL model) that could skilfully reproduce climate-driven variability in North American tree-ring width chronologies. This simple and efficient model of non-linear climatic controls on tree-ring width requires only latitude, monthly temperature, and monthly precipitation as inputs and has the potential to reproduce tree-rings across

a wide range of environments, species, and scales. The VSL model is hence a promising candidate for palaeoclimate reconstruction.

The goals of this study are to i) examine the model's ability to skilfully link climate and tree-ring formation across the globe ii) identify large-scale patterns of the climatic drivers of tree growth and iii) evaluate the suitability of forward modelling of tree-rings in a reconstruction approach. This study is the first report examining the VSL model's worldwide application on a relatively large spatial scale, on a wide range of species and site conditions, using a gridded data set based on direct observations from meteorological stations. For the first time, all freely accessible raw tree-ring width measurements from the International Tree Ring Database (ITRDB) are analysed in a comparable way. Results of such an intercomparison may help to make better use of tree-ring information in climate reconstructions.

The paper is organised as follows: We next provide a brief introduction to the climate data, the structure and parameterisations of the VSL model, and the actual tree-ring chronologies we use to compare with the simulated series. The main results are then presented in Sect. 3.3. Lastly we present conclusions and make suggestions for further analyses.

3.2   Data and methods

3.2.1 Climate data

The climate data used to simulate tree-ring growth are monthly CRU TS3.1 mean near surface temperature and CRU TS3.1.1 precipitation data sets from the Climatic Research Unit (CRU, Mitchell and Jones, 2005). These data cover the global land surface (except for Antarctica) at a 0.5° x 0.5° spatial resolution from 1901-2009 (updated from Mitchell and Jones, 2005, http://badc.nerc.ac.uk/data/cru) and are based on direct observations from meteorological stations. However, the temporal and spatial density of the underlying observations is variable and interpolation over greater distances is routinely performed (Jones et al., 1997). For temperature and precipitation, estimates were made for 80-100% of the land surface, with densely covered areas such as North America, Europe, and Russia having the largest percentages covered. Comparison with the available network of tree-rings (see Fig. 3.4 for locations) shows, for instance, that both the instrumental and tree-ring networks are dense for the European Alps, but very sparse for many tropical regions such as the Amazon. On the other hand, tree-ring chronologies are much more prevalent in the boreal zone, such as in the vast areas of Siberia and northern Canada while instrumental data in India dominate over the available tree-ring network. Hence, caution is needed when interpreting our results.

3.2.2 Forward model description: the VSL model

We use the Vaganov-Shashkin-Lite (VSL) model to produce synthetic tree-ring chronologies (Tolwinski-Ward et al., 2011a,b; version 2.2 accessible from http://www.ncdc.noaa.gov/paleo/softlib/softlib.html). This process-based forward model assumes that climatic influences can be associated directly, but non-linearly with tree-ring growth. In comparison to the full Vaganov-Shashkin model, which depends on daily climate input variables and has over 40 tunable parameters

(Vaganov et al., 2006; 2011), the VSL model is a simplified version. VSL only requires monthly mean temperature, accumulated precipitation, and latitude to model growth. A further 12 adjustable parameters related to climatic limitations on growth, parameterizations for soil moisture availability, and the calendar periods when annual increment is responsive to climate are additionally required. Although detailed mechanistic processes such as photosynthesis, storage, or cambial cellular processes are not modelled directly in VSL, the net effect of the dominating nonlinear climatic controls on tree-growth are implemented in terms of the principle of limiting factors and threshold growth response functions. Despite its simplicity, simulations using VSL have been shown to skilfully reproduce climate-driven variability in North American tree-ring width chronologies (Tolwinski-Ward et al., 2011a,b). The final simulated yearly tree-ring chronology (TRW_{VSL}) is defined as:

$$TRW_{VSL} = \sum_{i \in window, t} G_i(c_i, T_i, P_i) = g_E(c_i) * min\{g_T(T_i), g_M(P_i)\}, \qquad (1)$$

and is produced by summing the growth response function G_i over a specified window of months given by the start and end integration month parameters I_0 and I_f and standardising. The overall growth G_i at a site for the calendar month of i is given by the minimum of the growth responses (g_T) and (g_M) as a function of temperature (T) and precipitation (P) modulated by the response to insolation (g_E) in the calendar month of i (c_i).

In more detail, g_E is the ratio of mean monthly day length relative to that in the summer solstice month - this depends on latitude and is computed using standard trigonometric approximations. The partial growth rates g_T and g_M are defined as ramp functions, with growth parameters representing climate thresholds below which temperature and moisture are not great enough for growth (T_1, M_1), and above which temperature and moisture are high enough for optimal, non-limiting growth (T_2, M_2). Values of these partial growth responses are between zero and one (Tolwinski-Ward et al., 2011a). A Bayesian estimation approach with a uniform prior distribution of the VSL growth response parameters is performed to find the optimal parameters T_1, T_2, M_1, and M_2 for each site. In addition to the Bayesian parameter estimation approach, we also estimated optimal parameters for every site using a simple optimisation procedure as described in Tolwinski-Ward et al. (2011a). Parameters were sampled uniformly across intervals and the parameter set producing the simulation that correlated most significantly with the corresponding observed series was then used to simulate the tree-ring series. Results from both parameter estimation approaches are mostly very similar, with the parameter optimisation approach appearing to result sometimes in model over-fitting due to the correlation constraint imposed. Nevertheless, the comparable results show the validity of the Bayesian parameter estimation approach.

Soil moisture is calculated from monthly temperature and accumulated precipitation data via the empirical Leaky Bucket model of hydrology from the National Oceanic and Atmospheric Administration's Climate Prediction Center (CPS), allowing for sub-monthly updates of soil moisture to account for the non-linearity of the soil moisture response (Huang et al., 1996; Tolwinski-Ward et al., 2011a, codes available from http://www.ncdc.noaa.gov/paleo/softlib/softlib.html).

In addition to the four parameters controlling the simulated growth response to temperature and soil moisture, other parameters are taken from published studies (e.g. Huang et al., 1996; van den Dool et al., 2003; Fan and van den Dool, 2004; Evans et al., 2006; Vaganov et al., 2006; Tolwinski-Ward et al.,

2011a; Zhang et al., 2011; Touchan et al., 2012). The ability to apply the optimal growth response parameters to a wide range of environmental conditions, and thus model generality, is emphasized in the choice of parameters and modelling procedure.

The integration window affects autocorrelation and model skill (Tolwinski-Ward et al., 2011a). We chose the two parameters controlling the integration window for a 16-month interval, starting in previous September and are then summed to the current December for each modelled year (March to June, respectively for the Southern Hemisphere). This integration interval has been selected to (a) account for persistence in tree-ring growth, (b) showed best overall performance in a subset of regions, and (c) has been used successfully by Tolwinski-Ward et al. (2011a) in their simulations of North American tree-ring series. The tree-ring model parameters used in our study are listed in Table1.

Table 3.1: *VSL model parameters*

Parameter description	Parameter	Value
Temperature response parameters		
Threshold temp. for $g_T > 0$	T_1	ϵ [1°C, 9 °C]
Threshold temp. for $g_T = 1$	T_2	ϵ [10°C, 24°C]
Moisture response parameters		
Threshold soil moist. for $g_M > 0$	M_1	ϵ [0.01, 0.035] v/v
Threshold soil moist. for $g_M = 1$	M_2	ϵ [0.1, 0.7] v/v
Soil moisture parameters		
Runoff parameter 1	α	0.093 month^{-1}
Runoff parameter 2	μ	5.8 (dimensionless)
Runoff parameter 3	m	4.886 (dimensionless)
Max. moisture held by soil	W_{max}	0.8 v/v
Min. moisture held by soil	W_{min}	0.01 v/v
Root (bucket) depth	d_r	1000 mm
Integration window parameters		
Integration start month	I_0	-4
Integration end month	I_f	12

3.2.3 Tree ring-chronologies

Raw tree-ring width measurements from 2918 sites from 163 different tree species were obtained from the International Tree Ring Database (ITRDB, Grissino-Mayer and Fritts, 1997; http://www.ncdc. noaa.gov/ paleo/treering.html). Prior to further analysis, we attempted to identify and correct data and metadata errors including repetitive measurements, feet-meter encoding, inappropriate decimal

points and hyphenations, incorrect series labelling, or misplaced series positions (see Table 3.3 in the Appendix).

To remove the biological age-trend and other lower-frequency signals that may be driven by stand dynamics or disturbances, we processed all data sets in the program ARSTAN (AutoRegressive Standardization, Cook, 1985) using standard dendroclimatological methods (i.e. detrending and transformation to dimensionless growth indices). We tested different standardising methods on a subset of 97 locations from all six continents to infer the most applicable detrending option to our data. Methods tested include (a) a negative exponential curve and linear regression fits, (b) a smoothing spline fit with a 50% frequency response cut-off (which is the wavelength at which 50% of the amplitude of a signal is retained) equal to ¾ of a series length, and (c) a smoothing spline with a 200-year frequency response cut-off. These tests and Pearson correlation analyses between the differently standardised series and the monthly climate parameters favour a hierarchical approach: Fitting negative exponential curves and linear regression curves of any slope were applied as first order detrending options but if these two methods were not suitable (e.g. because values of a fitted curve approached zero), a smoothing spline was fit with a 50% cut-off frequency at 75% of each series length. The detrending methods applied will allow retention of climate-related signals in any given chronology on the order of the mean segment length of the constituent tree-ring series (Cook et al. 1995).

Combining multiple measurements into a single ring-width chronology should then ideally represent a coherent climate signal of a particular species at a site (Cook et al., 1990). Standard chronologies (TRW$_{ITRDB}$) of all these sites were developed by a biweight robust mean estimate (Cook et al., 1990) and the variance was stabilized to minimize artefacts from changing sample size through time (Osborn et al., 1997; Frank et al., 2007). Further, we required that the sample depth of a chronology (number of samples from trees used for every point in time) is always ≥8 and that the 1901-1970 interval is fully covered by tree-ring data. These criteria resulted in 2287 chronologies for further analysis

3.3 Results and discussion

3.3.1 Tree-ring chronologies

Understanding of the specific characteristics of the tree network is essential to interpret the modelled tree-ring chronologies. Various chronology characteristics of all 2287 ring-width chronologies (TRW$_{ITRDB}$) for the 1901-1970 common period were computed (Fig. 3.1; see Fig. 3.4 for locations). The average inter-series correlation between all series in a chronology (Rbar) indicates common variance (Cook et al., 1990) while the expressed population signal (EPS) measures the similarity of a chronology to a hypothetical population chronology. The latter is used to determine over which time intervals a chronology can be regarded to meet the population chronology to some acceptable degree (Wigley et al. 1984). An EPS threshold value, following the example in Wigley et al. (1984), of 0.85 is routinely cited in dendrochronological literature. Running Rbar and EPS statistics were calculated over moving 30 year windows with 15 years overlap. 93% of all mean EPS values in our network are above 0.85 and average 1901-1970. Rbar values roughly follow a normal distribution with a mean of 0.39. These statistics suggest that the vast majority of chronologies have a relatively robust signal that should

allow climatic drivers to be inferred. Typical tree-ring chronologies have a mean segment length of 170 years and a sample depth of 30 series per chronology. However, these distributions have relatively long tails reflecting exceptionally well-replicated sites or sites with long-lived tree species (e.g., Bristlecone pine). The mean segment suggest that we should be able to test inter-annual to (at least) multi-decadal variability in our modelling efforts. The geographical distribution of the sites is dominated by low-altitudes and the mid-latitudes, but there are also a considerable amount of high-latitude and high elevation sites particularly in the Northern Hemisphere.
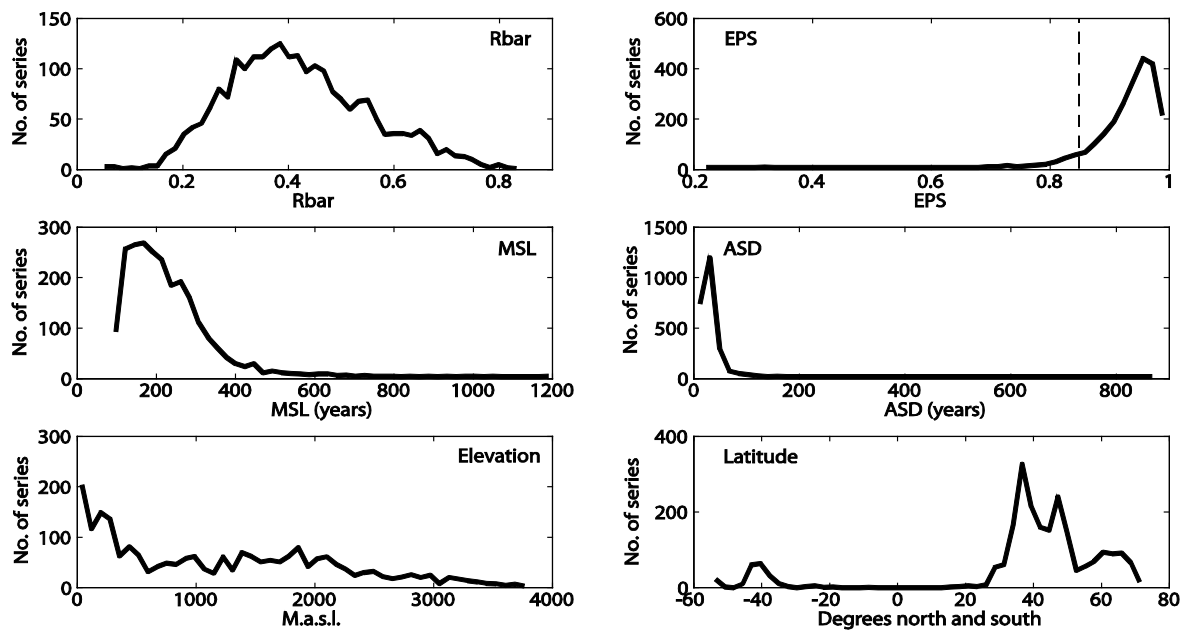
Fig. 3.1: *Frequency plots (calculated in 48 bins) of chronology characteristics for 1901-1970. Rbar is the average inter-series correlation between all series from different trees (Cook et al., 1990); EPS is the expressed population signal and the vertical dashed line denotes the commonly cited 0.85 EPS criterion (Wigley et al., 1984, Cook et al., 1990). Mean 1901-1970 Rbar and EPS values were calculated using a 30-year window that lags 25 years; MSL is the mean segment length; and ASD is the average sample depth.*

3.3.2 Parameter estimation

Site specific growth parameters are necessary due to diverse environmental conditions, site ecologies and species represented in this global network. Accordingly, the VSL growth response function parameters T_1, T_2, M_1, and M_2 were tuned site-by-site via Bayesian parameter estimation. For calibration/verification purposes, we divide the period 1901-1970 into two equal 35-year long intervals and alternately withhold the first or second half for verification. Descriptive statistics of the parameter estimation for the 1901-1935 and 1936-1970 calibration intervals are provided in Table 3.2. Even though the response parameters were calculated independently, the results are very consistent across the two intervals, showing skill in the growth response parameter estimation. In addition, a highest standard deviation of only 1.62 °C for T_2 further shows the good estimation performance and the general applicability of the model for a wide range of environmental conditions.

Table 3.2: *Statistics of the Bayesian estimation of the site-by-site tuned VSL growth response parameters T_1, T_2, M_1, and M_2 for the 1901-1935 and 1936-1970 calibration intervals.*

|	Calib. 1: 1901-1935				Calib. 2: 1936-1970			
	mean	min	max	std	mean	min	max	std
T1 (°C)	4.64	1.80	8.41	0.93	4.75	1.74	7.97	0.89
T2 (°C)	16.34	10.14	22.80	1.62	16.52	10.36	21.87	1.59
M1 (v/v)	0.023	0.02	0.025	0.001	0.023	0.019	0.025	0.001
M2 (v/v)	0.44	0.11	0.64	0.09	0.43	0.11	0.64	0.09

Figure 3.2 further illustrates the estimated temperature and moisture parameters T_1, T_2, M_1, and M_2 for each site grouped according to different tree genera. Interestingly, the site-by-site adjusted Bayesian parameter estimation of the VSL model provides a new quantification for the currently debated (Mann et al., 2012; Anchukaitis et al., 2012) temperature threshold below which growth may no longer take place. We find a growth-onset threshold temperature (T_1) of approximately 4-6 °C for most sites and species with all estimates between 1.80 °C and 8.41 °C (see also Table 3.2). These findings compare favourably with assessments of growing season temperatures at treeline based upon in-situ loggers or remote sensing and interpolated climatic data (Körner and Paulsen, 2004; Körner, 2012), as well as observational studies of wood formation (Rossi et al., 2007).

At the same time, questions arise whether the range of values obtained reflects differential growth limitations as related site conditions or tree species (Fig. 3.2). For instance, Vaganov et al. (2006) reported from the VS-model minimum and optimal temperatures of the primary conifers in the northern taiga of 4 °C and 16 °C for larch, 6 °C and 18 °C for spruce, and 5 °C and 18 °C for Scots pine, respectively. We find comparable results using VSL (Fig. 3.2a-d). Comparison of the growth response parameters for spruce and pine trees in Fig. 3.2 shows for the former tree species higher T_1 and T_2, but generally lower M_2 compared to pine trees. This might reflect the better adaption of pines to lower temperature conditions and drought.

Figure 3.2e illustrates the threshold temperature response parameter T_1 for different pine species. It clearly shows that Ponderosa and Pinyon pines have about 1 to 2 °C reduced mean growth onset temperatures in relation to the other pine species (compare also to Fig. 3.2a in which these two species clearly influence the shape of the pine histogram towards cooler threshold temperatures). Similar conclusions can be drawn for the moisture parameters because species-related differences due to needle structure, frequency and density of stomata influence water loss due to evapotranspiration (Vaganov et al., 2006). Additional uncertainties introduced by the moisture parameterisation and the precipitation input data complicate the clear detection of site environment or species characteristics even more. Hence, a part of the different growth adaptions are related to the climate domain where the trees grow and may also be an expression of the missing representation of winter precipitation stored as snow pack in the CPC Leaky Bucket model and its impact on the timing of snowmelt (Tolwinski-Ward et al., 2011a). Nevertheless, we found clear associations between the four growth parameters. For instance, T_1 and T_2 values and M_1 and M_2 values are clearly associated (r=0.60 and

r=0.47, both p<0.01), while the temperature and moisture growth parameters are negatively related, with the relationship between T_2 and M_2 (r=-0.63, p<0.01) being the most noteworthy. Moreover, temperature-limited sites tend to have higher T_1 and T_2 values in comparison to the moisture-limited sites, whereas higher M_1 and M_2 values can be observed at the moisture-limited sites (see Section 3.3.4). This is again an expression of different climatic conditions, such as trees growing at high altitudes only have a brief season with temperatures high enough to grow.
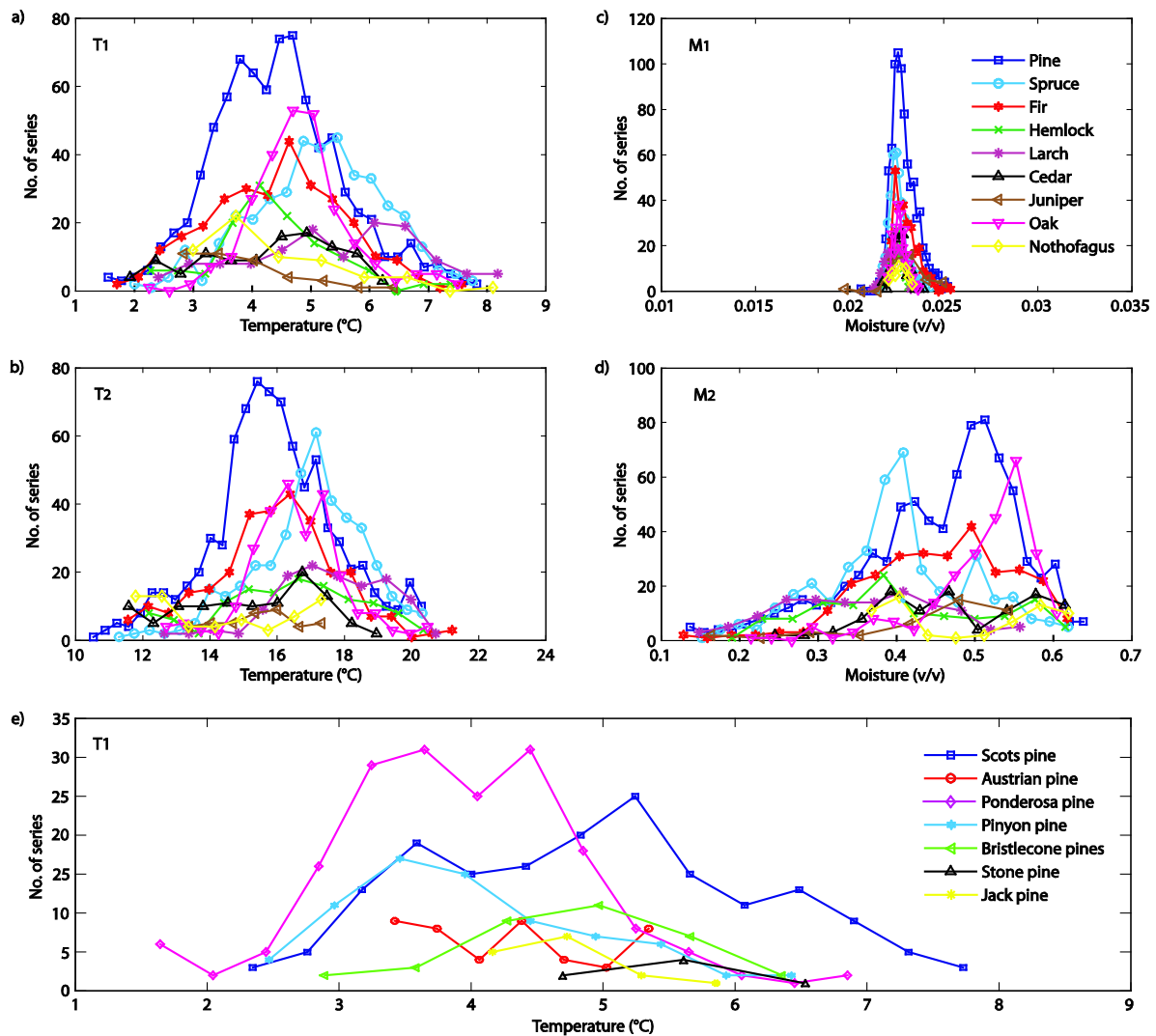
Fig. 3.2: *Frequency plots of the Bayesian estimated VSL growth response parameters: (a) T_1, lowest threshold temperature; (b) T_2, lower bound for optimal temperature; (c) M_1, lowest threshold for moisture; (d) M_2, lower bound for optimal moisture parameters calculated during 1911-1970 for different tree genera: pine (pinus; n=821), spruce (picea; n=407), fir (abies; n=286), hemlock (tsuga; n=124), larch (larix; n=126), cedar (cedrus; n=107), juniper (juniperus; n=40), oak (quercus; n=253), and southern beech (nothofagus; n=62). Histogram of T_1 threshold temperature for different pine species (e): Scots pine (Pinus sylvatica; n=172), Austrian pine (Pinus negra; n=45), Ponderosa pine (Pinus ponderosa; n=181), Pinyon pine (Pinus edulis; n=73), Bristlecone pine (Pinus aristata, Pinus longaeva, and Pinus balfouriana; n=34), Stone pine (Pinus pinea; n=7), and Jack pine (Pinus banksiana; n=15). Numbers in brackets give the series contributing in each group of tree genera. The number of bins for each parameter is determined through the square root of its length.*

To further explore the influence of the individual growth response parameters on the ability to model TRW, we performed a sensitivity study by changing one of the parameters T_1, T_2, M_1, and M_2 while all other parameters are kept constant at their Bayesian determined optimal values (Fig. 3.3). The value of each parameter is varied in steps of ±1 °C and ±5% over the range of ±5 °C for temperature and ±25%, for moisture respectively. Repeated VSL simulations for each parameter set results in a total of 40 new modelled series for each site. The modelled series (TRW$_{VSL}$) are then compared with the measured tree-ring chronology for each site (TRW$_{ITRDB}$) by correlation. Results of these experiments show that all parameters but T_2 have an optimum around the original values. For T_2 slightly higher correlations averaged over all species and environments has a negligible effect on the resulting simulations. On the other hand, increasing the values for T_1 to +5 °C of the original value results in a drop of the correlation coefficient by 0.07 in the mean demonstrating the models relative sensitivity to the lower threshold temperature and again supporting our conclusions for temperature thresholds in the 4-6 °C range and well below 10 °C.
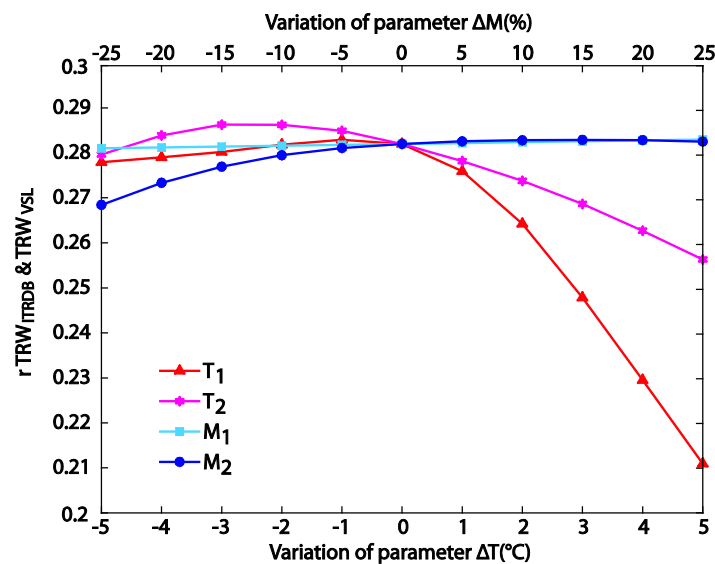
Fig. 3.3: *Mean correlations between TRW$_{ITRDB}$ and TRW$_{VSL}$ during 1911-1970 as a function of T_1, T_2, M_1, and M_2.*

On average, sites of tree-ring chronologies are located 164 m higher than the elevation of the corresponding CRU grid cell (which equals a mean temperature correction of approximately 1°C). Hence, we attempted to correct temperature for elevational differences between the CRU and the tree sites by considering a mean lapse rate of 0.65°C/100m (Wallace and Hobbs, 2006). However, the relative coarse spatial resolution of the climate input data hinders the potential for improved relationships between TRW$_{VSL}$ and TRW$_{ITRDB}$ series using elevation-adjusted climate series. As a result, the average between the elevational-corrected TRW$_{VSL}$ and TRW$_{ITRDB}$ is by 0.02 units lower than the mean between the uncorrected series (which is 0.29). Hence, we do not correct for elevational differences and some of the absolute quantifications for temperature and precipitation may be slightly off by differences in the mean elevation between the grid cell and the tree elevation.

The VSL model was not able to simulate tree-ring series in response to climate forcing in only 16 out of 2287 sites. These were either high-latitude sites in Nepal (3), Siberia (1), and Canada/Alaska (5) for which no growth could be simulated because temperatures never reached the threshold temperature T_1 for growth initiation (hence g_T=0). On the other hand, at a few other (sub-) tropical sites in Florida (1), Mexico (4), Argentina (1), and Indonesia (1), no annual tree-rings could be modelled because neither temperature nor moisture were limiting growth (hence a too low threshold parameter M_2 resulted in g_T=1 and g_M=1). Despite these caveats, we were able to simulate tree-ring growth in 99.3% of the cases, and we could clearly demonstrate that the VSL model can be applied to many different environments and species.

3.3.3 Relationships between actual and simulated tree-ring growth

The degree of similarity between the 2287 actual TRW_{ITRDB} and the corresponding 2287 modelled TRW_{VSL} chronologies were determined by Pearson correlation coefficients during the period 1901-1970 (Fig. 3.4). The Pearson correlation between all TRW_{ITRDB} and TRW_{VSL} is 0.29 and the standard deviation is 0.22 and approximately 41% of the correlation coefficients between TRW_{VSL} and TRW_{ITRDB} are significant at the 95% confidence level. Moreover, significant relationships are globally fairly well distributed, with clusters of correlations >0.6 in the United States. Calibration/verification analysis was performed for two different intervals (1901-1935/1936-1970 and 1936-1970/1901-1935, respectively) and correlation coefficients between TRW_{ITRDB} and TRW_{VSL} at each site are taken as measure of reconstruction skill. We find significant (r>~0.44) correlations during all four calibration/verification intervals at 301 locations, which is 13.2% of all places considered. Further, significant relationships can be found on all continents but Africa which generally shows the weakest model stability. On the other hand, sites with highest correlations (r>0.8) in all four intervals are located in California and locations with r>0.6 are clustered in North America.

Figure 3.5 further illustrates simulations (TRW_{VSL}), as well as the observed chronologies (VSL_{ITRDB}) performed for one high-altitude and one low-altitude site in Switzerland in the right panels and the mean monthly growth response values g_T and g_M over all simulated years in the left panels. Because the simulated growth response is controlled by the point-wise minimum of either temperature or precipitation, the figure clearly shows that growth at the high-altitude site is temperature-limited (g_T<g_M). The lower elevation site, on the other hand, shows a temperature limitation on growth only briefly at the beginning and at the end of the growing season while precipitation limits growth during the summer months (g_M<g_T). Further, the high-elevation site is negatively correlated with growth at the lower-elevation site, for both the observed and modelled chronologies (-0.13 and -0.44, respectively). This relationship demonstrates the VSL model's ability to evaluate the joint influence of temperature and precipitation on growth and that it may be important to separate the effects of the climatic influence on tree-growth. Our simulated growth responses for sites in Switzerland are confirmed by findings from other mountainous regions such as in the south-western USA (Salzer and Kipfmueller, 2005; Tolwinski-Ward et al., 2011).
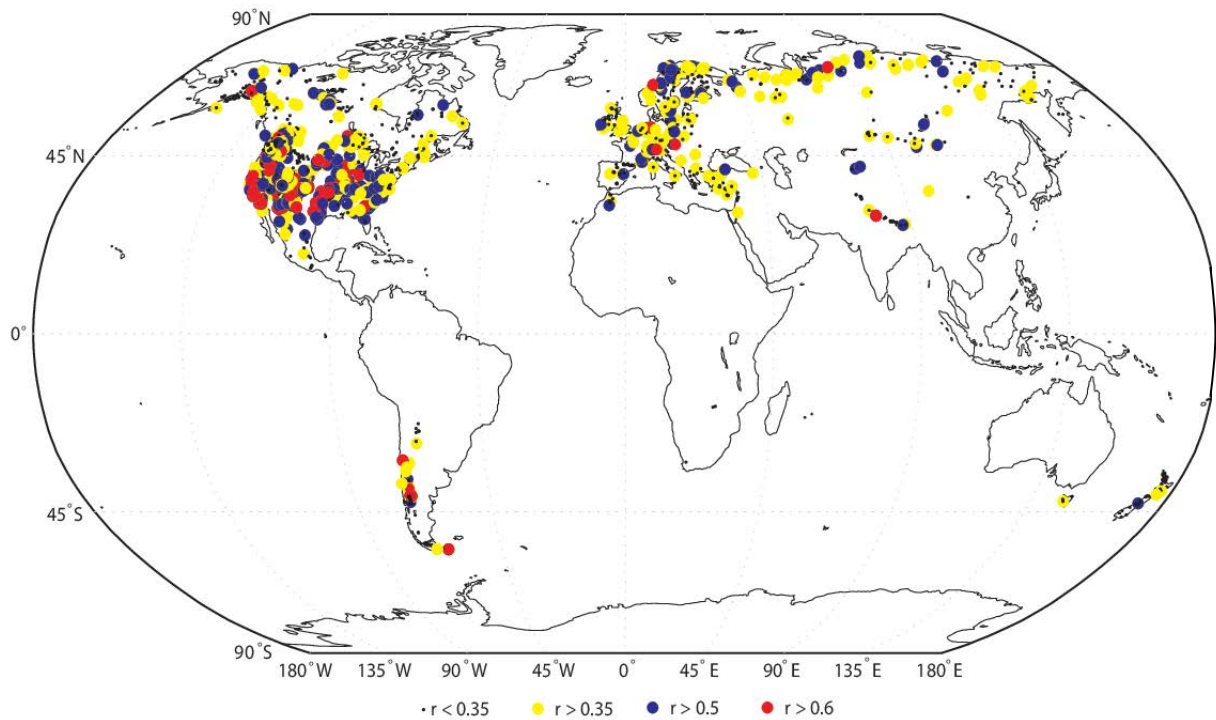
Fig. 3.4: *World map showing the locations of the 2287 tree-ring width chronologies (TRW_ITRDB) and the correlation coefficients between TRW_ITRDB and TRW_VSL for 1911-1970. The four categories correspond to non-significant correlations (r<0.35, p>0.05; black dots), and significant correlations at the 95% (yellow), 99% (blue), and 99.9% (red) confidence levels, respectively. The reduction of degrees of freedom du to autocorrelation was taken into account (Mitchell et al., 1966).*
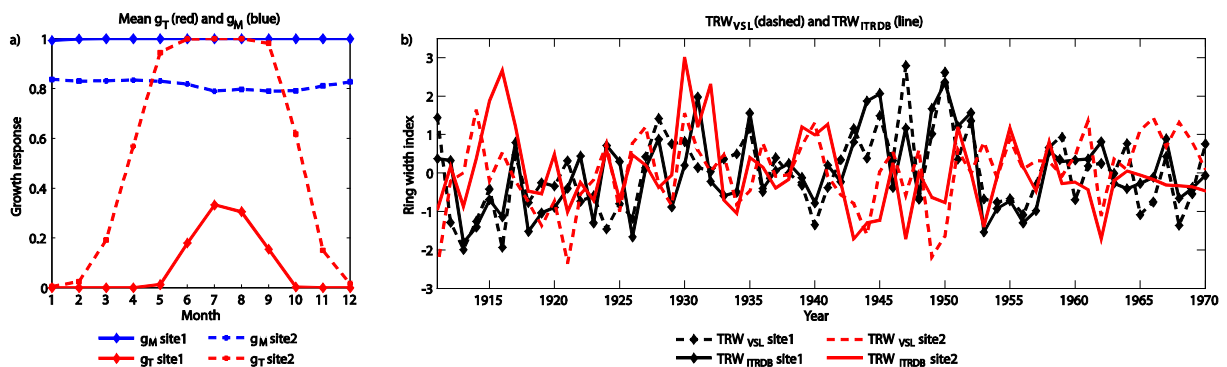
Fig. 3.5: *Left: Simulated growth response curves for temperature (g_T, red lines) and moisture (g_M, blue lines) for two sites in Switzerland. Right: TRW_ITRDB (black lines) and TRW_VSL (red lines) for two sites in Switzerland: site 1: r=0.69, p<0.01, Bergün Val Tuors, European larch, 2065 m; site 2: r=0.44, p<0.01, Krauchthal, Scots pine, 550 m.*

One-year lagged autocorrelation coefficients (AR1) were assessed from TRW$_{ITRDB}$ and TRW$_{VSL}$ series at all sites. Mean coefficients of 0.46 and 0.42, respectively over all series clearly reveal persistence, i.e. 21% and 18%, respectively of the variance in the width of the ring in the current year can be explained by the conditions influencing tree-ring growth in the past year. This highlights the importance of including last year's growing season for growth simulation in the VSL model in order to retain potentially useful climate information contained in tree-rings (see Table 3.1). Similarly, Wettstein et al. (2011) report a median AR1 of 0.47 for 762 ITRDB derived tree-ring width series located poleward of roughly 30° to 40° northern latitude while Tingley et al. (2012) found AR1 coefficients of approximately 0.6 found for the tree-ring width series used in Mann et al. (2008).

3.3.4 Site aggregation and regional comparisons of regional growth variation

Increasing the signal to noise ratio

So far, the tree-ring chronologies were compared individually with the corresponding CRU grid cell with the underlying assumption that direct proximity is the best estimate for the climate conditions over a region (note the 0.5° or ~55 km spatial resolution of the CRU data set at the equator). These analyses allowed exploration of the direct climate-tree ring growth relationship in as many cases as possible using the VSL model. Non-climatic noise contained in individual tree-ring chronologies, however, can hinder the detection of clear climate-growth relationships. Hence, we aggregated the tree-ring chronologies to reduce non-climatic noise and extract regional growth signals. Aggregation is performed using a search radius of 200 km and 600 km, respectively, centred at each land grid cell of the CRU climate data set. The former radius approximates the grid resolution of many global climate models and the latter takes spatially coherent precipitation and especially temperature patterns more into account. We do not use greatly expanded search radii like Cook et al. (2010) or Ljungqvist et al. (2012), for instance, whose work were motivated by the construction of a gridded climate reconstruction from spatially sparsely distributed proxy series under considerations of long-range teleconnections (Jones et al., 1997).

We created aggregated, weighted mean tree-ring series from every TRW$_{ITRDB}$ found within a specified search circle around each grid node by assigning weights relative to four factors: (a) mean Rbar of each chronology, (b) mean EPS of each chronology, (c) distances between the site location and the grid node, and (d) significance (minimum p-value) of the correlation between temperature/precipitation and TRW$_{ITRDB}$ (equations 2-5). With this approach, we do not only consider distance, and climate signal, but also account for information contained in the tree-ring series. The four relative weighting factors are based on the premise that high Rbar/EPS values and small distances and minimal p-values are likely indicative of high-quality climate-tree growth relationships and reduce non-climatic noise. Correlation coefficients between the tree-ring chronologies and the climate parameters temperature and precipitation are calculated for different time windows: a 12-month period from January to December (July to June, respectively for the SH), and during a 5-month growing season interval from May to September (November to March, respectively for the SH). Doing so, we account for persistence while we capture the summer months when climate generally dominates tree growth (Briffa et al., 2002a) and also account for variable growing season lengths at different locations. The relative weight is then selected from the smaller p-value of these two correlation analyses.

Relative weights are given by to following weight functions:

$$weight\ Rbar\ =\ e^{-2x^5} \tag{2}$$

$$weight\ EPS\ =\ e^{-2x} \tag{3}$$

$$weight\ significance\ =\ e^{-3x} \tag{4}$$

$$weight\ distance\ =\ e^{-2x^2/R^2} \tag{5}$$

The relative weights decrease from a maximum of one at the exact grid node location to minimum values at the search periphery (Fig. 3.6). There is no a priori reason to choose any particular weighing function but we determined the functions based on theoretical considerations (e.g. Ljungqvist et al., 2012) and the parameter distribution as shown in Table 3.1. The Gaussian distance weight function was used successfully in Ljungqvist et al. (2012). Multiplication of the four relative weights gives the weight value we apply to each individual tree-ring series within the search radius. Ultimately, we used the average of these weighted series (and scaled so that the sum of all weights is equal to 1) as the weighted mean tree-ring series (TRW$_{ITRDB\ 200km}$ or TRW$_{ITRDB\ 600km}$).
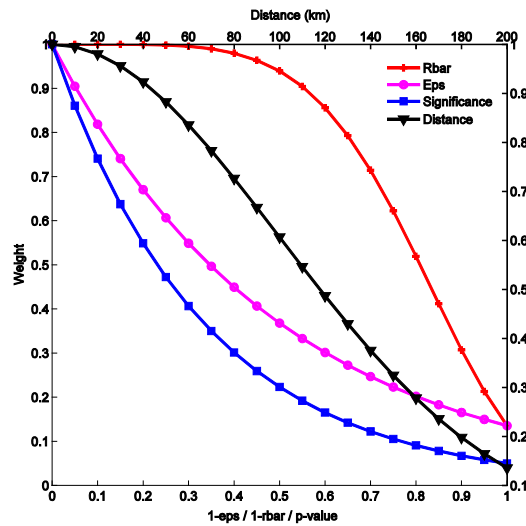
Fig. 3.6: *Weight functions for tree-ring chronologies located within a 200 km search circle around grid node, as derived from Eqs. (2-5). Note that 1-rbar and 1-EPS values are used because high Rbar and EPS values correspond to high relative weights, while distance values and p-values close to zero correspond to high relative weights.*

We further differentiate the sites based upon their principal climatic drivers and thus aggregate separately all temperature and moisture-limited chronologies located within the search radius around each grid cell node. This is particularly important in mountainous terrain with more complex climatic conditions (see Fig. 3.5). In detail, we classify temperature and moisture sensitive chronologies using the simulated monthly growth responses g$_T$ and g$_M$. Temperature-sensitive chronologies are hence series which have more temperature-limited months during the growing season (months with g$_T$ and

$g_M > 0$). Precipitation-sensitive chronologies are determined vice versa (i.e. more or equally moisture-limited months than temperature-limited months). In accordance with the above weighting scheme, we compute one aggregated "temperature" and one aggregated "moisture" series for every cell with temperature and/or moisture-limited tree-ring chronologies located within the given search radius. With this separation at 200 km (600 km, respectively), 35% (14%) of all land grid cells contain only temperature-limited series, 24% (11%) are only moisture-limited, and 41% (75%) of the cells include both temperature- and moisture-limited chronologies, respectively.

Regional model simulations

We perform VSL simulations for each of the grid cell points containing at least one aggregated tree-ring series, using monthly temperature and precipitation series from CRU and with the same VSL model parameter set up described in Table 3.1. These resulting simulated series (TRW$_{VSL\ 200km}$) are compared with the aggregated tree-ring series (TRW$_{ITRDB\ 200km}$). For instance, the mean of the correlation coefficients between TRW$_{VSL\ 200km}$ and TRW$_{ITRDB\ 200km}$ during the common interval 1901-1970 is 0.34 for the temperature-limited series and 0.38 for the moisture-limited series. Hence, aggregation clearly improves the climatic signal in comparison to the correlations for the individual tree-ring sites (which was 0.29).

In order to employ tree-ring data for climate reconstruction in a data assimilation approach, it is necessary to test if the growth and climate coefficients/relationships apply prior to the calibration period. Accordingly, Fig. 3.7 shows a scatter plot of the correlation coefficients between TRW$_{VSL\ 200km}$ and TRW$_{ITRDB\ 200km}$ series during the different calibration/verification intervals (1901-1935/1936-1970, and 1936-1970/1901-1935). Points along the 1:1 line are sites for which VSL produces simulations that are stable in time whereas points below this line represent sites for which the model yields a higher correlation during the calibration period. Our findings do not change when the temperature and moisture-limited sites are compared separately. We find model skill in the Pearson correlation coefficients in 9% of all temperature-limited grid cells, in 40% of all moisture-limited grid cells, and in 2% of all the grid cells which are influenced by both climatic parameters. The model skill is stable for moisture-limited sites in large areas of the United States and central Canada, the lower elevation-sites in west-central Europe, Turkey, Mongolia, western Himalayas, and in mid-Chile whereas temperature-limited sites dominate Scandinavia, Siberia, eastern Himalayas, central Europe, southern-south America, and parts of the western United States. The relative stability of the VSL model outside the calibration window and its ability to skilfully simulate growth for a wide range of environments promote to use of the model for data assimilation based climate reconstructions, but care must be taken in the selection of sites.

To explore the potential of the tree-ring chronologies to capture the main climate signal over beyond 200 km, we performed aggregation using a 600 km search radius. Aggregation at 600 km includes 50% of all land grid cells in contrast to 28% with a 200 km search radius. The maximum number of individual tree-ring chronologies used for aggregation at radii 200 km and 600 km is 111 and 316, while the average number of tree chronologies aggregated at a grid node is 7 and 31, respectively.
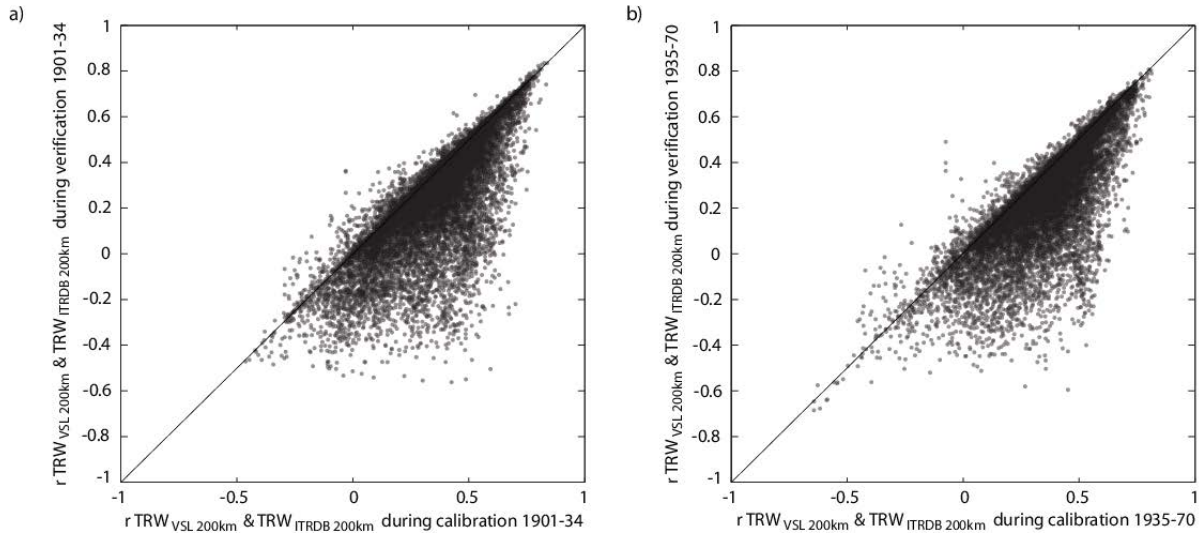
Fig. 3.7: *Scatter plot of correlation coefficients between TRW$_{VSL\ 200km}$ and TRW$_{ITRDB\ 200km}$ series for two different calibration/verification intervals (a) 1901-1935/1936-1970; and (b) 1936-1970/1901-1935.*

The world maps in Figure 3.8 show the spatial patterns of the correlation coefficients between the aggregated TRW$_{VSL}$ and TRW$_{ITRDB}$ series for temperature and moisture-limited grid cells within a search radius of 200 km and 600 km. The 600 km aggregation improves the relationships for both temperature and precipitation where there was coverage at 200 km but also extends the geographical range which results in lower correlation coefficients. Coherent large scale spatial variability of highly significant correlation coefficients for inferred temperature limited sites can be found in Scandinavia, western/central Siberia, and along western and eastern United States (Fig. 3.8a and 3.8c). On the other hand, large-scale patterns of highest correlation coefficients (largely r>0.5) are present at moisture-sensitive sites throughout the United States and central Canada (Fig. 3.8b and 3.8d). Regions such as central Europe, Turkey, central Asia, or the Andes are characterised by both temperature and moisture limitations, which is an expression of a complex terrain with small-scale climatic features and large climatic gradients. High correlation coefficients between TRW$_{VSL}$ and TRW$_{ITRDB}$ are present in all those regions, with a clear tendency towards temperature-limited, high-elevation sites. Aggregation using 600 km search radii (Fig. 3.8c and 3.8d) produces similar results as for 200 km (Fig. 3.8a and 3.8b). Correlations coefficients generally increase for those area already covered by the 200 km search radius, with extensions to new grid cells also yielding often positive significant correlations (e.g., the Eurasian boreal forest zone). The broad scale patterns we obtain such as the temperature limited growth at high latitudes and high altitude is in agreement with previous large-scale studies (e.g. Briffa et al., 2002a; Wettstein et al., 2011; Babst et al. in press) which show a distinct belt of temperature-sensitive and non-significant relationships with precipitation at northern higher latitudes (e.g., Taymir peninsula, Russia), and high altitudes (e.g., the European Alps). Such sites with relatively high correlations are probably due to a misclassification of sites and/or climate drivers due to elevational differences. Our findings furthermore largely matches the distribution of potential climatic constraints to plant growth in Nemani et al. (2003) and Beer et al. (2010) or the climate classification based on Köppen-Geiger by Kottek et al. (2006). Hence, these correlations between TRW$_{VSL}$ and

TRW$_{ITRDB}$ show spatial coherency and are a clear indicator of the potential of the tree-ring chronologies as well as the simulated series to capture the main climate signals and thus their suitability for data assimilation approaches.
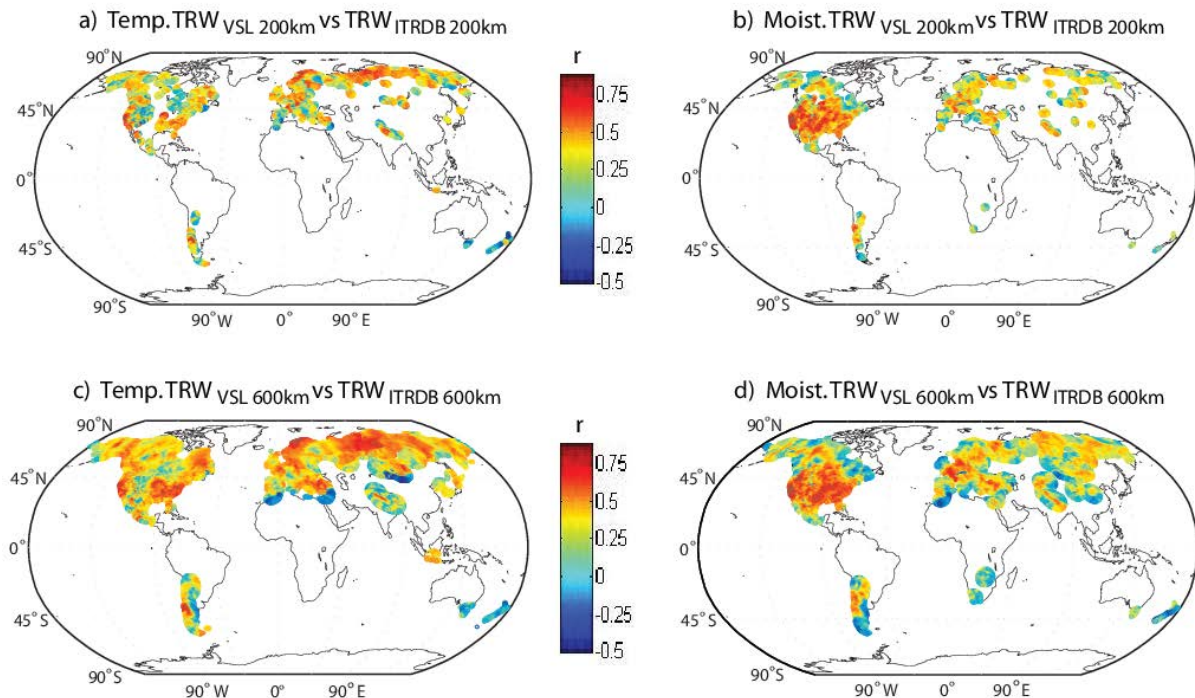
Fig. 3.8: *World map displaying correlation coefficients between TRW$_{VSL\ 200km}$ and TRW$_{ITRDB\ 200km}$ (Fig. 3.8a,b) and TRW$_{VSL\ 600km}$ and TRW$_{ITRDB\ 600km}$ (Fig. 3.8c,d) at temperature-limited (Fig. 3.8a,c) and moisture-limited (Fig. 3.8b,d) grid cells.*

3.4 Conclusions

We investigated relationships between climate and tree-ring data on a global scale using the non-linear, process-based Vaganov-Shashkin-Lite (VSL) forward model of tree-ring width formation (Tolwinski-Ward et al., 2011a). A network of 2287 globally distributed ring-width chronologies provided a large, high-quality sample space from which relations among actual tree-ring growth and growth simulated due to climatic influences could be analysed. Bayesian estimation of the VSL growth response parameters performed well for a wide range of species, environmental conditions, and time intervals, showing the model's general applicability for worldwide studies using CRU climate input data. A benefit from this parameterization approach was also a new global assessment of the growth-onset threshold temperature (T_1) of approximately 4-6 °C for most sites and species, thus providing new evidence for on-going debates regarding the lower temperatures at which growth may take place (Anchukaitis et al. 2012, Mann et al. 2012; Körner 2012). Moreover, our results for a wide range of environments, species, and different time intervals suggest that the VSL model can skilfully simulate tree-ring series in response to climate forcing. Further, the model performed well at sites with extreme climate (i.e. classical dendroclimatological sites at treelines) but, in addition, could

also reveal notable skill at locations with a less extreme climate due to the models explicit consideration of joint temperature and moisture controls on modelled tree growth. Spatial aggregation of tree-ring chronologies based upon chronology quality, climate response, and proximity reduced non-climatic noise contained in the tree-ring data and resulted in improved relationship between actual and modelled tree-growth as well as a spatial extension of regions where simulations can be validated. The resulting distinct and coherent spatial variability of significant relationships between VSL simulated tree growth and actual tree growth aggregated at 200km (TRW$_{ITRDB\ 200km}$) and 600km (TRW$_{ITRDB\ 600km}$) further demonstrate the potential of the VSL model to successfully capture the climate signal across large regions. We propose that the VSL model can be used as an observation operator in data assimilation approaches to reconstruct past climate.

Acknowledgements

References

Anchukaitis, K. J., Evans, M. N., Kaplan, A., Vaganov, E. A., Hughes, M. K., Grissino-Mayer, H. D., and Cane, M. A., 2006. Forward modeling of regional scale tree-ring patterns in the southeastern United States and the recent influence of summer drought. Geophys. Res. Lett. **33**, L04705, doi:10.1029/2005GL025050.

Anchukaitis, K. J., Breitenmoser, P., Briffa, K. R., Buchwal, A., Büntgen, U., Cook, E. R., D'Arrigo, R. D., Esper, J., Evans, M. N., Frank, D., Grudds, H., Gunnarson, B., Hughes, M. K., Kirdyanov, A. V., Körner, C., Krusic, P. J., Luckman, B., Melvin, T. M., Salzer, M., W., Shashkin, A. V., Timmreck, C., Vaganov, E. A., and Wilson, R. J. S., 2012. Tree rings and volcanic cooling. Nat. Geosc., doi:10.1038/ngeo1645.

Babst, F., Poulter, B., Trouet, V., Tan, K., Neuwirth, B., Wilson, R., Carrer, M., Grabner, M., Tegel, W., Levanic, T., Panayotov, M., Urbinati, C., Bouriaud, O., Ciais, P., and Frank, D., in press. Climatic drivers of forest productivity derived from 1000 sites across Europe. Global Ecology and Biogeography.

Beer, C., Reichstein, M., Tomelleri, E., Ciais, P., Jung, M., Bonan, G. B., Bondeau, A., Cescatti, A., Lasslop, G., Lindroth, A., Lomas, M., Luyssaert, S., Margolis, H., Oleson, K. W., Roupsard, O., Veenendaal, E., Viovy, N., Williams, C., Woodward, F. I., and Papale, D., 2010. Terrestrial gross carbon dioxide uptake: global distribution and covariation with climate. Science **329**, 834-838.

Bhend, J., Franke, J., Folini, D., Wild, M., and Brönnimann, S., 2012. An ensemble-based approach to climate reconstructions. Clim. Past **8**, 963-976.

Briffa, K. R., Osborn, T. J., Schweingruber, F. H., Jones, P. D., Shiyatov, S. G., and Vaganov, E. A., 2002a. Tree-ring width and density data around the Northern Hemisphere: Part 1, local and regional climate signals. Holocene **12**(6), 737-757.

Briffa, K. R., Osborn, T. J., Schweingruber, F. H., Jones, P. D., Shiyatov, S. G., and Vaganov, E. A., 2002b. Tree-ring width and density data around the Northern Hemisphere: Part 2, spatio-temporal variability and associated climate patterns. Holocene **12**(6), 759-789.

Cook, E. R., 1985. A time series approach to tree-ring standardization, Ph.D. thesis, University of Arizona, 171pp.

Cook, E. R., Briffa, K. R., Shiyatov, S., Mazepa, V., and Jones, P. D., 1990. Data analysis. In: Cook, E. R. and Kairiukstis, L. A. (eds.), Methods of dendrochronology: applications in the environmental sciences, Kluwer Academic Publishers, Dordrecht.

Cook, E. R., Briffa, K. R., Meko, D. M., Graybill, D. A., and Funkhouser, F., 1995. The 'segment length curse' in long tree-ring chronology development for palaeoclimatic studies. Holocene **5**(2), 229-237.

Cook, E. R., Anchukaitis, K. J., Buckley, B. M., D'Arrigo, R. D., Jacoby, G. C., and Wright, W. E., 2010. Asian monsoon failure and megadrought during the last millennium. Science **328**, 486-489.

Evans, M. N., Reichert, B. K., Kaplan, A., Anchukaitis, K. J., Vaganov, E. A., Hughes, M. K., and Cane, M. A., 2006. A forward modeling approach to paleoclimatic interpretation of tree-ring data. J. Geophys. Res. **111**, G03008, doi:10.1029/2006JG000166.

Fan, Y. and van den Dool, H., 2004. Climate Prediction Center global monthly soil moisture data set at 0.5° resolution for 1948 to present. J. Geophys. Res. **109**, D10102, doi:10.1029/2003JD004345.

Frank, D., Esper, J., and Cook, E. R., 2007. Adjustment for proxy number and coherence in a large-scale temperature reconstruction. Geophys. Res. Lett. **34**, L16709, doi:10.1029/GL030571.

Franke, J., Gonzáles-Rouco, J. F., Frank, D., and Graham, N. E., 2011. 200 years of European temperature variability: insights from and tests of the Proxy Surrogate Reconstruction Analog Method. Clim. Dyn. **37**, 133-150.

Fritts, H. C., 1976. Tree rings and climate. Academic Press, London.

Goosse, H., Crespin, E., de Montety, A., Mann, M. E., Renssen, H., and Timmermann, A., 2010. Reconstructing surface temperature changes over the past 600 years using climate model simulations with data assimilation. J. Geophys. Res. **115**, D09108, doi:10.1029/2009JD012737.

Grissino-Mayer, H. D. and Fritts, H. C., 1997. The International Tree-Ring Data Bank: an enhanced global database serving the global scientific community. Holocene **7**, 235-238.

Huang, J., van den Dool, H. M., and Georgankakos, K. P., 1996. Analysis of model-calculated soil moisture over the United States (1931-1993) and applications to long-range temperature forecasts. J. Clim. **9**, 1350-1362.

Hughes, M. K., 2002. Dendrochronology in climatology: the state of the art. Dendrochronologia **20**, 95-116.

Hughes, M. K. and Ammann, C. M., 2009. The future of the past - An Earth system framework for high resolution paleoclimatology: editorial essay. Clim. Change **94**, 247-259.

IPCC , 2007. Climate Change 2007: The physical science basis. Contribution of working group I to the Forth Assessment Report of the Intergovernmental Panel on Climate Change. In: Solomon, S., Qin, D., Manning, M., Chen, Z., Marquis, M., Averyt, K. B., Tignor, M., Miller, H. L. (eds), Cambridge University Press, Cambridge, United Kingdom and New York, NY, USA.

Jones, P. D., Osborn, T. J., and Briffa, K. R., 1997. Estimating sampling errors in large-scale temperature averages. J. Climate **10**, 2548-2568.

Jones, P. D., Briffa, K. R., Osborn, T. J., Lough, J. M., van Ommen, T. D., Vinther, B. M., Luterbacher, J., Wahl, E. R., Zwiers, F. W., Mann, M. E., Schmidt, G. A., Ammann, C. M., Buckley, B. M., Cobb, K. M., Esper, J., Goosse, H., Graham, N., Jansen, E., Kiefer, T., Kull, C., Küttel, M., Mosley-Thompson, E., Overpeck, J. T., Riedwyl, N., Schulz, M., Tudhope, A. W., Villalba, R., Wanner, H., Wolff, E., and Xoplaki, E., 2009. High-resolution palaeoclimatology of the last millennium: a review of current status and future prospects. Holocene **19**(1), 3-49.

Körner, C., 2012. Alpine treelines - Functional ecology of the global high elevation tree limits. Springer, Basel.

Körner, C. and Paulsen, J., 2004. A world-wide study of high altitude treeline temperatures. J. Biogeogr. **31**, 713-732.

Kottek, M., Grieser, J., Beck, C., Rudolf, B., and Rubel, F., 2006. World map of the Köppen-Geiger climate classification updated. Meteorol. Z. **15**, 259-263.

Ljungqvist, F. C., Krusic, P. J., Brattström, G., and Sundqvist, H. S., 2012. Northern Hemispheric temperature patterns in the last 12 centuries. Clim. Past **8**, 227-249.

Mann, M. E., Zhang, Z., Hughes, M. K., Bradley, R. S., Miller, S. K., Rutherford, S., and Ni, F., 2008. Proxy-based reconstructions of hemispheric and global surface temperature variations over the past two millennia. P. Natl. Acad. Sci. USA **105**(36), 13252-13257.

Mann, M. E., Fuentes, J. D., and Rutherford, S., 2012. Underestimation of volcanic cooling in tree-ring based reconstructions of hemispheric temperatures. Nat. Geosc., doi:10/1038/NGEO1394.

Mitchell, J. M. Jr., Dzerdzeevskii, B., Flohn, H., Hofmeyr, W. L., Lamb, H. H., Rao, K. N., and Wallen, C. C., 1966. Climatic change. Technical Note **79**, World Meteorological Organization, Geneva.

Mitchell, T. D. and Jones, P.D., 2005. An improved method of constructing a database of monthly climate observations and associated high-resolution grids. Int. J. Climatol. **25**, 693-712.

Nemani, R. R., Keeling, C. D., Hashimoto, H., Jolly, W. M., Piper, S. C., Tucker, C. J., Myneni, R. B., and Running, S. W., 2003. Climate-driven increase in global terrestrial net primary production from 1982 to 1999. Science **300**, 1560-1563.

Osborn, T. J., Briffa, K. R., and Jones, P. D., 1997. Adjusting variance for sample-size in tree-ring chronologies and other regional time series. Dendrochronologia **15**, 89-99.

Raible, C. C., Casty, C., Luterbacher, J., Pauling, A., Esper, J., Frank, D., Büntgen, U., Roesch, A. C., Tschuck, P., Wild, M., Vidale, P.-L., Schär, C., and Wanner, H., 2006. Climate variability - observations, reconstructions, and model simulations for the Atlantic-European and Alpine region from 1500-2100 AD. Clim. Change **79**, 9-29.

Rossi, S., Deslauriers, A., Anfodillo, T., and Carraro, V., 2007. Evidence of threshold temperatures for xylogenesis in conifers at high altitudes. Oecologia **152**, 1-12.

Salzer, M. W. and Kipfmueller, K. F., 2005. Reconstructed temperature and precipitation on a millennial timescale from tree-rings in the southern Colorado Plateau, USA. Clim. Change **70**, 465-487.

Shi, J., Liu, Y., Vaganov, E. A., Li, J., and Cai, Q., 2008. Statistical and process-based modeling analyses of tree growth response to climate in semi-arid area of north central China: A case study of *Pinus tabulaeformis*. J. Geophys. Res. **113**, G01026, doi:10.1029/2007JG000547.

Tingley, M. P., Craigmile, P. F., Haran, M., Li, B., Mannshardt, E., and Rajaratnam, B., 2012. Piecing together the past: statistical insights into paleoclimatic reconstructions. Quaternary Sci. Rev. **35**, 1-22.

Tolwinski-Ward, S. E., Evans, M. N., Hughes, M. K., and Anchukaitis, K. J., 2011a. An efficient forward model of the climate controls on interannual variation in tree-ring width. Clim. Dyn. **36**, 2419-2439.

Tolwinski-Ward, S. E., Evans, M. N., Hughes, M. K., and Anchukaitis, K. J., 2011b. Erratum to: An efficient forward model of the climate controls on interannual variation in tree-ring width. Clim. Dyn. **36**, 2441-2445.

Touchan, R. Shishov, V. V., Meko, D. M., Nouiri, I., and Grachev, A., 2012. Process based model sheds light on climate sensitivity of Mediterranean tree-ring width. Biogeosciences **9**, 965-972.

Vaganov, E. A., Hughes M. K., and Shashkin, A. V., 2006. Growth dynamics of conifer tree rings. In: Growth dynamics of tree rings: Images of past and future environments. Ecological studies **183**, Springer, New York.

Vaganov, E.A., Anchukaitis, K. J., and Evans, M. N., 2011. How well understood are the processes that create dendroclimatic records? A mechanistic model of climatic control on conifer tree-ring growth dynamics. In: Hughes, M. K., Swetnam, T., Diaz, H. (eds.), Dendroclimatology, Developments in Paleoenvironmental Research **11**, Springer, New York.

van den Dool, H., Huang,J., and Fan, Y., 2003. Performance and analysis of the constructed analogue method applied to U.S. soil moisture over 1981–2001. J. Geophys. Res. **108**, 8617, doi:10.1029/2002 JD003114.

Wahl, E. and Frank, D., 2012. Evidence of environmental change from annually-resolved proxies with particular reference to dendroclimatology and the last millennium. In: Matthews, J. A. (ed.), The SAGE handbook of environmental change **1**, Sage, 320-344.

Wallace, J. M. and Hobbs, P. V., 2006. Atmospheric Science: an Introductory Survey. 2nd edition. International geophysics series **92**, Elsevier Academic Press, Amsterdam.

Wettstein, J. J., Littell, J. S., Wallace, J. M., and Gedalof, Z., 2011. Coherent region-, species-, and frequency-dependent local climate signals in Northern Hemisphere tree-ring widths. J. Clim. **24**, 5998-6012.

Widmann, M., Goosse, H., van der Schrier, G., Schnur, R., and Barkmeijer, J., 2010. Using data assimilation to study extratropical Northern Hemisphere climate over the last millennium. Clim. Past **6**, 627-644.

Wigley, T. M. L., Briffa, K. R., and Jones, P. D., 1984. On the average value of correlated time series, with applications in dendroclimatology and hydrometeorology. J. Clim. Appl. Meteorol. **23**, 201-213.

Zhang, Y. X., Shao, X. M., Xu, Y., and Wilmking, M., 2011. Process-based modelling analyses of *Sabina przewalskii* growth response to climate factors around the northeastern Qaidam Basin. Chinese Sci. Bull. **56**(14), 1518-1525.

3.5 Appendix

Table 3.3: *Raw-ring width series from the ITRDB with identified errors.*

File	Series	Problem	What has been done
ak051.rwl		Arstan cannot read in files	Remove hyphens at the end of each label in each line
aust004.rwl	108400, 108410, 108430, 108440, 108450, 108460, 108470, 108480, 108490, 108500, 108510, 108520, 108530, 108540, 108550, 108560, 108570, 108580, 108590, 108610, 108620, 108630	22 of 59 series are redundant Decimal points Chronology up into the future	File not used
aust005.rwl-aust008.rwl		Arstan cannot read in files	Remove hyphens at the end of each header line
brit015.rwl-brit026.rwl, brit048w.rwl, brit049w.rwl		Arstan cannot read in files	Remove hyphens at the end of each header line
brit020.rwl	568112	Chronology up into the future	Delete -999 in last row
ca580.rwl-ca597.rwl		Arstan cannot read in files	Remove underlines in header
cana038.rwl, cana039.rwl, cana041.rwl-cana098.rwl, cana111.rwl-cana114.rwl, cana168w.rwl-cana173w.rwl		Arstan cannot read in files	Remove hyphens at the end of each header line
cana165.rwl-cana167.rwl		Chronology up into the future	File not used
cana262.rwl		Arstan cannot read in files	Remove hyphen in middle header line
cana275.rwl	bs480a1, bs480a2	Chronology up into the future	Change position of -9999
chil012.rwl	AGU261	Chronology up into the future	Change position of the line with 1940-1949 data to the right place in the series
co562.rwl	BLA08B	Arstan cannot read in files	Add 999 at end of series
czec.rwl		Units in ITRDB are given in feets	Conversion from feet into metres
czec2.rwl		Units in ITRDB are given in feets	Conversion from feet into metres
czec3.rwl		Units in ITRDB are given in feets	Conversion from feet into metres
fran015.rwl-fran028.rwl, fran032w.rwl, fran033w.rwl		Arstan cannot read in files	Remove hyphens at the end of each header line
germ014.rwl		Units in ITRDB are given in feets	Conversion from feet into metres
germ018.rwl		Units in ITRDB are given in feets	Conversion from feet into metres
germ1.rwl		Units in ITRDB are given in feets	Conversion from feet into metres
germ12.rwl		Units in ITRDB are given in feets	Conversion from feet into metres
germ15.rwl		Units in ITRDB are given in feets	Conversion from feet into metres
germ16.rwl		Units in ITRDB are given in feets	Conversion from feet into metres
germ17.rwl		Units in ITRDB are given in feets	Conversion from feet into metres
germ18.rwl		Units in ITRDB are given in feets	Conversion from feet into metres

Table 3.3: *Raw-ring width series from the ITRDB with identified errors (continued).*

germ21.rwl		Chronology up into the future Decimal points	File not used
germ3.rwl		Units in ITRDB are given in feets	Conversion from feet into metres
germ301.rwl		Units in ITRDB are given in feets	Conversion from feet into metres
germ4.rwl		Units in ITRDB are given in feets	Conversion from feet into metres
germ5.rwl		Units in ITRDB are given in feets	Conversion from feet into metres
ital006.rwl-ital017.rwl		Arstan cannot read in files	Remove hyphens at the end of each header line
ital022.rwl		Units in ITRDB are given in feets	Conversion from feet into metres
ital023.rwl	VIG641	Chronology up into the future	Add 999 at end of series
ital027.rwl		Units in ITRDB are given in feets	Conversion from feet into metres
ital2.rwl		Units in ITRDB are given in feets	Conversion from feet into metres
mt115.rwl		No data available because it has not been added yet	File not used
nc4.rwl		Arstan cannot read in files	Remove hyphens at the end of each header line and Add a break before year date
nc5.rwl-nc11.rwl, nc016.rwl		Format problems	File not used
neth005.rwl		No header info and chronology up into the future	File not used
neth005.rwl		Chronology up into the future	File not used
newz076.rwl		Arstan cannot read in files Cchronology up into the future	Remove hyphen in series Add break after series name Change 9999 into 999
nv505.rwl	Q43102	Chronology up into the future	Add 999 at end of series
ny.rwl		Format problems	File not used
or015b.rwl		Subgroup of series from or015.rwl	File not used
or082.rwl-or084.rwl		Hyphens in series names cause format problems	File not used
or088.rwl		Arstan cannot read in files	Remove hyphens at some of the series names
russ020w.rwl, russ022w.rwl		Arstan cannot read in files	Remove hyphens at the end of each header line
russ023w.rwl	863122	Chronology up into the future	Change position of 999
russ024w.rwl	864101, 864162, 864172	Chronology up into the future	Change position of 999
russ027w.rwl	870062	Chronology up into the future	Change position of 999
russ030w.rwl	873282	Chronology up into the future	Change position of 999
russ031w.rwl	874032, 874091	Chronology up into the future	Change position of 999
russ032w.rwl	875143	Chronology up into the future	Change position of 999
russ033w.rwl	876102	Chronology up into the future	Change position of 999
russ035w.rwl	878021, 878131	Chronology up into the future	Change position of 999
russ036w.rwl	879382	Chronology up into the future	Change position of 999
russ039w.rwl	882091,882111, 82112, 882451	Chronology up into the future	Change position of 999
russ040w.rwl	884091	Chronology up into the future	Change position of 999
russ042w.rwl	886032, 886232	Chronology up into the future	Change position of 999
russ043w.rwl	892081, 892082	Chronology up into the future	Change position of 999
russ044w.rwl	892242	Chronology up into the future	Change position of 999
russ046w.rwl	895271	Chronology up into the future	Change position of 999
russ051w.rwl	911102	Chronology up into the future	Change position of 999
russ053w.rwl	913132	Chronology up into the future	Change position of 999
russ055w.rwl	914122	Chronology up into the future	Change position of 999
russ056w.rwl	915071	Chronology up into the future	Change position of 999

Table 3.3: Raw-ring width series from the ITRDB with identified errors (continued).

russ059w.rwl	919012, 919061, 919122	Chronology up into the future	Change position of 999
russ060w.rwl	920161	Chronology up into the future	Change position of 999
russ062w.rwl	923412, 923421	Chronology up into the future	Change position of 999
russ064w.rwl	925432	Chronology up into the future	Change position of 999
russ065w.rwl	926092	Chronology up into the future	Change position of 999
russ066w.rwl	927272, 927362	Chronology up into the future	Change position of 999
russ068w.rwl	928020, 928050, 928090, 928121, 928122, 928170, 928261, 928262, 928640, 928740, 928750	Chronology up into the future	Change position of 999
russ073w.rwl	933051, 933052, 933072, 933112	Chronology up into the future	Change position of 999
russ084w.rwl	952212, 952281	Chronology up into the future	Change position of 999
russ087w.rwl	954172	Chronology up into the future	Change position of 999
russ089w.rwl	956041, 956042, 956122	Chronology up into the future	Change position of 999
russ090w.rwl	957051, 957081, 957131	Chronology up into the future	Change position of 999
russ093w.rwl	960152	Chronology up into the future	Change position of 999
russ098w.rwl	965181, 965262	Chronology up into the future	Change position of 999
russ099w.rwl	966051, 966111	Chronology up into the future	Change position of 999
russ152w.rwl	977191	Chronology up into the future	Change position of 999
spai002.rwl	493062	Chronology up into the future	Add 999 at end of series
swed019w.rwl-swed023w.rwl		Arstan cannot read in files	Remove hyphens at the end of each header line
swit102.rwl-swit120.rwl, swit138w.rwl-swit140w.rwl		Arstan cannot read in files	Remove hyphens at the end of each header line
swit177w.rwl		0 in data gaps	File not used
turk033.rwl		Arstan cannot read in files	Remove hyphens at the end of each label in each line
tx040.rwl		Data has been removed from ITRDB	File not used
ut510.rwl-ut512.rwl		Arstan cannot read in files	Remove hyphens at the end of each header line
va20.rwl	3996	Chronology up into the future	Add 999 at end of series
wa034.rwl	711091	Chronology up into the future	Add 999 at end of series Delete double years 1730-1890
wa043.rwl	66041	Chronology up into the future	Add 999 at end of series

Chapter 4

PAST CLIMATE RECONSTRUCTION USING FORWARD-MODELLING OF TREE-RING WIDTH WITH AN ANALOGUE APPROACH

Petra **Breitenmoser** [1,2], Stefan **Brönnimann** [1,2], David **Frank** [2,3] , and Jörg **Franke** [1,2]

[1] *Institute of Geography, Climatology and Meteorology, University of Bern, Switzerland*

[2] *Oeschger Centre for Climate Change Research, University of Bern, Switzerland*

[3] *Swiss Federal Institute for Forest, Snow and Landscape Research (WSL), Birmensdorf, Switzerland*

Abstract

We use an analogue approach to reconstruct global summer climate from 1600 to present using climate model simulations and tree-ring data. Tree-ring width data from a global network are used to select, for each 6-month-period, the best member among an ensemble of climate model simulations. The resulting reconstruction is thus consistent with model physics, forcings, and proxy data. A 30 member initial-condition ensemble performed with the ECHAM5.4 general circulation model for the period 1600-2005 forms the basis of the study. The model was forced with observed and reconstructed sea-surface temperatures as well as with time series of the main external forcing factors. The Vaganov-Shashkin Lite (VSL) forward model of tree-ring growth was used to simulate tree growth in these model simulations. Tree-ring growth was simulated at 405 grid points as a function of monthly mean temperature, monthly accumulated precipitation, and latitude. The best member was then selected according to the mean squared error between modelled and observed tree-ring width. The skill of the approach was estimated in the 1911-1970 period using CRU TS3 temperature and precipitation as a reference. Our reconstruction is, especially at the interannual time scale, in good agreement with an

instrumental record of past temperature and precipitation at the site level. However, we are not able to provide skilful reconstructions in the Southern Hemisphere, which we mainly attribute to biases in the climate input data series. Nevertheless, the quality of our first-order reconstruction is sufficient for meaningful interpretation and to reduce uncertainty about past climate despite potential for further improvements. The greatest advantage of our reconstruction using the climate model's best ensemble member is its potential for climate impact studies (such as summer heat waves). Due to the physical consistency, data for such studies is not only limited to temperature and precipitation on a monthly time scale, but is available for all model parameters and down to 6-hourly resolution back to 1600 AD, if desired.

4.1 Introduction

Detailed knowledge of past climate variability provides a crucial context for understanding the ongoing and future climate change. Analysis in the pre-industrial era relies strongly on climatic information stored in natural proxy archives or on climate modelling studies (Jansen et al., 2007). Global climate models (GCMs) that are driven by both natural and anthropogenic forcings (e.g. changes in solar irradiance, land cover atmospheric aerosol and greenhouse gas concentrations) allow addressing physically consistent responses of the model climate to forcing factors (e.g. Crowley, 2000; Gonzáles-Rouco et al., 2003; Ammann et al., 2007; Gao et al., 2008; Steinhilber et al., 2009; Jungclaus et al., 2010). Therefore, models help to quantitatively understand the mechanisms of past climatic changes and to place the recent 20th and 21st century warming trends into a longer-term perspective (Jansen et al., 2007; Wanner et al., 2008).

Comparisons of large-scale analyses of multi-proxy reconstructions with simulations using GCMs and systematic model intercomparisons have greatly improved our understanding of externally and internally forced past climate variability (Crowley, 2000; Shindell et al., 2003; Ammann et al., 2007; Wanner et al., 2008; Gray et al., 2009; Wahl and Frank, 2012). However, uncertainties from i) the forcing applied, ii) the model response, and iii) internal variability still challenge the determination of differences between model results and observations (Goosse et al., 2010).

In recent years, novel approaches have found an increasingly important role in palaeoclimate reconstruction efforts, combining climate models and proxy data to achieve improved reconstructions with reduced uncertainty (e.g. Guiot et al., 2009; Hughes and Ammann, 2009; Goosse et al., 2010; Widmann et al., 2010; Franke et al., 2011; Bhend et al., 2012; Tingley et al., 2012). These approaches are sometimes referred to as data assimilation approaches, but this term is not yet standard in palaeoclimatology. Common to these approaches is that they are designed to combine the information content in proxy data with the physical consistency in climate model simulations to achieve improved past climate reconstructions. These approaches offer a more complete and quantitative understanding of processes linking proxy information, such as tree-ring growth, with environmental variables, including the evaluation of uncertainties.

These approaches allow replacing the statistical transfer functions common to conventional climate reconstruction approaches with proxy forward models driven by the simulation output. Proxy forward models describe the proxy as a function of climate and can be anything from simple, empirically calibrated functions to complex numerical models (e.g. Goosse at al., 2010; Thompson et

al. 2011) One of the greatest strengths of these forward models is the explicit treatment of i) non-linearity, ii) that the parameters have a clear biological or physical meaning, iii) and that they are not restricted to one single climate variable nor to sites limited by extreme climate. In the following we focus on models for tree-ring width.

The high requirements of many forward models have so far greatly limited model verification by comparison with dencrochronological data in worldwide networks (Vaganov et al., 2006, 2011). But Tolwinski-Ward et al. (2011a) recently developed an efficient alternative version, the so-called Vaganov-Shashkin-Lite (VSL) model. This VSL model is simple and efficient in terms of its monthly resolution and relatively few tunable parameters, but complex in terms of its non-linear transformation of climate variability into a tree-ring index. A subsequent study by Breitenmoser et al. (to be submitted) confirmed the potential of the VSL model as a forward modelling approach in climate reconstruction.

In this study, we use the VSL model in an analogue approach to reconstruct summer season (i.e. April to September in the Northern Hemisphere (NH) and October to March in the Southern Hemisphere (SH), respectively) climate by constraining the internal variability contained in simulations with an ECHAM5.4 general circulation model variant. We use the mean square error (MSE) to quantify the difference between modelled and observed tree-ring series and therefrom select the best model ensemble member for every year. This procedure greatly reduces climate uncertainty compared to the initial 30 ensemble member simulations while maintaining physically plausible results. This approach opens possibilities to study the climate of the past in great detail with all the advantages model data offers.

4.2 Data and methods

4.2.1 Climate data

The reconstruction is based on simulations performed with the ECHAM5.4 general circulation model (Roeckner et al., 2003, 2004). We ran a 30 member initial-condition ensemble in T63L31 resolution (approx. 2° or 200 km horizontal grid resolution) with all series spanning the 1600 to 2005 period. The ECHAM5.4 model was forced with reconstructed sea surface temperature (SST, Mann et al., 2009) and with an ENSO-dependent intra-annual variability (reconstructed NINO3.4 index by Cook et al., 2008). Climatological sea ice is from HadISST (Rayner et al., 2004). The reconstructed solar irradiance is from Lean (2000) and land surface parameters were derived from the land-use reconstruction of Pongratz et al. (2008). Volcanic aerosol loads are from Crowley et al. (2008), concentrations of greenhouse gases are according to Yoshimori et al. (2010 and references therein), and tropospheric sulphate concentrations were prescribed according to Koch et al. (1999). We used the 30 simulations (hereafter referred to as CCC400) as climate input series to the forward model. The boundary conditions for the model were prescribed and identical across all 30 ensemble simulations. The spread of the different ensemble simulations reflects one fraction of the internal variability of the atmosphere. Note that by not allowing sea-surface temperatures to react to the atmosphere, the ensemble likely gives a low estimate for internal atmospheric variability, which however is not important for this specific application.

The monthly CRU TS3.1 mean near surface temperature and CRU TS3.1.1 precipitation data sets from the Climatic Research Unit (CRU, Mitchell and Jones, 2005) are used to validate our reconstruction. These data cover the global land surface (except for Antarctica) at a 0.5° x 0.5° spatial resolution from 1901-2009 (updated from Mitchell and Jones, 2005, http://badc.nerc.ac.uk/data/cru) and are based on direct observations from meteorological stations. However, the temporal and spatial density of the underlying observations is variable and interpolation over greater distances is routinely performed (Jones et al., 1997). Geographic locations with long and reliable climate series are not necessarily regions with a dense network of tree-ring chronologies and vice-versa (see below). Hence, we consider the validation results a conservative estimate for the skill in the data assimilation approach.

4.2.2 Spatially aggregated tree-ring series

We used spatially aggregated, weighted mean tree-ring series from Breitenmoser et al. (to be submitted). They have been shown to skilfully represent a coherent climate signal. To create these series, raw tree-ring width measurements from 2918 sites were obtained from the International Tree Ring Database (ITRDB, Grissino-Mayer and Fritts, 1997; http://www.ncdc.noaa.gov/paleo/treering. html), checked and corrected for consistency, and then processed in the program ARSTAN (AutoRegressive STANdardization, Cook, 1985) using classical dendroclimatological detrending methods to produce tree-ring chronologies (Breitenmoser et al., to be submitted). All chronologies were required to have sample replication ≥8 for every year during the 1901-1970 interval, reducing the number of available series to 2287 chronologies. Subsequently, spatial aggregation was performed on temperature and moisture-sensitive sites separately using a search radius of 200 km centred at each land grid cell of the CRU climate input. This resulted in a total of 18550 grid cells (0.5° x 0.5°) containing at least one tree-ring chronology. Of these, aggregated ring-width series ($TRW_{ITRDB\ agg}$) at 2498 grid cells possess significant (p<0.05) relationships with tree-rings simulated with the VSL model (TRW_{VSL}) using monthly CRU temperature and precipitation series during the different calibration/verification intervals (1901-1935/1936-1970, and 1936-1970/1901-1935) (Breitenmoser et al., to be submitted). Average Pearson correlations at these sites between the observed $TRW_{ITRDB\ agg}$ and CRU are 0.46 for temperature and 0.58 for precipitation during the summer season. It shows that climatic information is indeed recorded in the tree-rings. We included some sites in New Zealand (n=3), Tasmania (n=1), South Africa (n=4), Indonesia (n=4), and Morocco (n=34 sites) where we did not obtain stable relationships between simulated and actual tree-ring series in all of the four calibration/verification intervals to maintain a global distribution with sites on each continent.

4.2.3 Model data extraction

We extracted monthly near surface temperature and precipitation of all 30 ensemble members of the CCC400 simulations at locations closest to the 2498 selected CRU grid points (Sect. 4.2.2). Due to the coarser spatial resolution of the model, sometimes more than one TRW grid cell fell within each CCC400 grid cell. In such cases, we used the centremost TRW grid cell. In CCC400, 405 grid cells from the total possible 6170 terrestrial grid cells (382 in the Northern Hemisphere (NH) and 23 in the Southern Hemisphere (SH), respectively) were covered by tree-ring locations.

4.2.4 Forward model description: the VSL model

We use the Vaganov-Shashkin-Lite (VSL) model to simulate tree-ring chronologies (Tolwinski-Ward et al., 2011a,b; version 2.2 accessible from http://www.ncdc.noaa.gov/paleo/softlib/softlib.html). In this process-based forward model, net effects of the dominating nonlinear climatic controls on tree-growth are implemented in terms of the principle of limiting factors and threshold growth response functions. VSL only requires monthly mean temperature, monthly precipitation totals, and latitude to model growth. A further 12 adjustable parameters related to climatic limitations on growth, parameterizations for soil moisture availability, and the calendar periods when annual increment is responsive to climate are additionally required. A detailed description of the VSL model can be found in Tolwinski-Ward et al. (2011a). We do not use the soil moisture of the CCC400 model simulations due to incorrect incorporation of the forest fraction (Pongratz et al., 2008) into the CCC400 run. Instead, soil moisture is calculated from monthly temperature and precipitation data via the empirical Leaky Bucket model of hydrology from the National Oceanic and Atmospheric Administration's Climate Prediction Center, allowing for sub-monthly updates of soil moisture to account for the non-linearity of the soil moisture response (Huang et al., 1996; Tolwinski-Ward et al., 2011a, codes available from http://www.ncdc.noaa.gov/paleo/softlib/softlib.html).

Results of the Bayesian estimation of the VSL growth response parameters described in Breitenmoser et al. (to be submitted) showed the VSL model's applicability using CRU climate input data for a wide range of environments and species (codes for the Bayesian growth response parameter estimation are available from http://www.ncdc.noaa.gov/paleo/softlib/softlib.html; codes by Tolwinski-Ward et al., 2011a). Hence, we employed these individually estimated optimal parameters and performed the VSL forward model for each of the 405 grid cells which showed strong and stable associations between simulated and actual tree-ring series in a prior analysis (Breitenmoser et al., to be submitted). We used monthly temperature and monthly precipitation series of all 30 CCC400 ensemble members during 1911-1970 to model tree-ring series (TRW$_{VSL}$). The two parameters controlling the integration window in the VSL model were chosen for two 6-month periods, from April to September and October to March, respectively to best possibly capture the growing season months. All other parameters were taken Breitenmoser et al. (to be submitted).

4.2.5 Definition of the measure of quality

In order to quantify the difference between the standardised modelled tree-rings (TRW$_{VSL}$) and the standardised aggregated tree-ring series (TRW$_{ITRDB\ agg}$), we defined the mean square error (MSE) as a measure of goodness to fit between every ensemble member (e) at the 405 grid cells (n) for each comparison time step during 1911-1970:

$$MSE_e = \frac{\sum_{i=1}^{n}\left((TRW_{VSL_e} - TRW_{ITRDB\ agg}\right)^2}{n_e}\ with\ e = 1{:}30. \tag{1}$$

Calculations were performed separately for each hemisphere, considering only series contributing to the corresponding summer hemisphere. In other words, we only considered ring-width series from

trees growing in the NH for the Northern Hemispheric summer season and vice versa for the SH, resulting in two "summer" quality measures in each year. This approach has similarities to the assimilation technique by Goosse et al. (2010) who compared model results with observations using a cost function. Finally, we ranked the MSE for the 30 ensemble members.

4.2.6 Reconstruction using the best ensemble member

Our reconstruction approach aims to reduce the uncertainty contained in the 30 ensemble members of the CCC400 model with information from simulated and actual tree-rings. Hence, we determined which realisation among all possibilities was the one closest to the actual past climate conditions using the quality measures. For each year and location, we extracted and averaged summer temperature and precipitation from the best ensemble member (i.e. lowest MSE) of a particular year as well as from the prior summer season to take persistence into account which is not accounted for in the model. The standard deviation of the best five members at each year and location is used to quantify uncertainty (grey boxes in Fig. 4.2). This approach yields summer season temperature and precipitation fields (CCC400$_{reconstruction}$) for all 405 locations during the 1911-1970 time period.

4.3 Results

4.3.1 Comparison of CRU and CCC400 climate data

In a first step, we tested how well the CCC400 ensemble series represent historical temperature and precipitation patterns from the CRU observations. We accordingly characterise trends, variability and absolute temperature and precipitation bias at all 405 grid cells where we have tree-ring data

The summer season temperature average (standard deviation) over all 405 locations is 15.4 °C (0.8 °C) for the CRU series, and 14.6 °C (0.8 °C) over all CCC400$_{ensemble\ members}$. Similarly, the summer season precipitation average (standard deviation) over all 405 sites is 60.0 mm/month (14.2 mm/month) for the CRU series- and 55.8 mm/month (13.5 mm/month) for all CCC400$_{ensemble\ members}$. These numbers suggest reasonably small biases, however, spatial patterns reveal quite significant discrepancies at local to regional scales (Fig. 4.1). Results are presented for temperature (left panels) and precipitation (right panels) during the summer season of each hemisphere and only for those 405 grid cells in which we performed our reconstruction. An interesting feature observed in Figure 4.1c is the pattern of the difference in the temperature and precipitation trends between the western and eastern North American locations. This pattern has similarities to ENSO imprints expected on climate and the difference may be related to the model not being able to capture ENSO patterns adequately (Huang et al., 2005; Mo, 2010).

Another interesting feature are pronounced differences at mountainous regions, notably in the Himalayas, the European Alps, and the Andes. To assess the influence of elevational differences in the two data sets, we performed linear regression of the temperature and precipitation biases on altitudinal differences between the CRU series and the CCC400$_{ensemble\ mean}$ series at all 405 grid cells. We found that 28% of the variance in temperature differences can be explained by altitude but only 0.4% of the variance in precipitation differences.

These discrepancies in the input data sets stem from poor replication of highly complex mountainous terrain in a model with relatively coarse spatial resolution and highlight potential difficulties in the interpretation of the VSL simulation results. These biases likely place limitations on the goodness of fit improvements when assimilating tree-ring data.
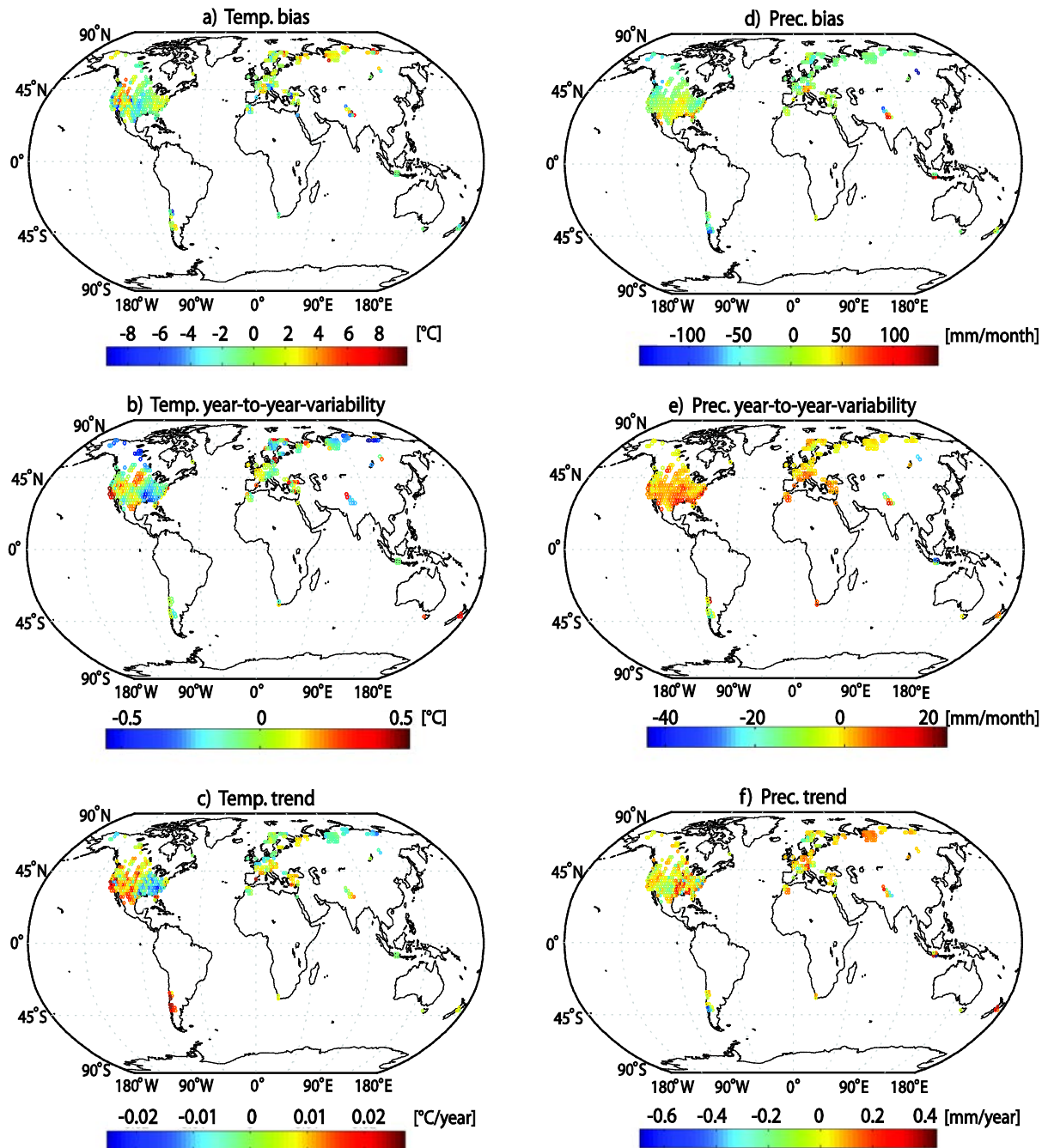
Fig. 4.1: *World map showing differences between CRU and CCC400ensemble mean (CRU minus CCC400) for temperature (left panels) and precipitation (right panels) during April to September in the NH, and October to March in the SH, respectively during 1911-1970: (a) temperature bias; (b) temperature year-to-year variability (i.e. difference of the mean standard deviation of CRU and CCC400ensemble member series); (c) temperature trend; (d) precipitation bias; (e) precipitation year-to-year variability; and (f) precipitation trend. Negative values denote higher values of the CCC400 ensemble mean than the CRU series at a location.*

4.3.2 Goodness of fit of MSE calculations

Figure 4.2 shows the quality of the MSE calculations for each ensemble member, for every year, and for both hemispheres. We notice, for instance, a greater spread for the SH as well as better fits for the best members and worse fits for the worst members which is related to the degrees of freedom and data points that constrain model behaviour. Interestingly, there are years where all ensemble members tended to produce worse fits, such as the year 1914 in the NH (topmost light blue line in Fig. 4.2a) or the year 1936 in the SH (topmost dark blue line in Fig. 4.2b). Similar findings were found by Franke et al. (2011) and seem to be a result of unusual synoptic patterns.
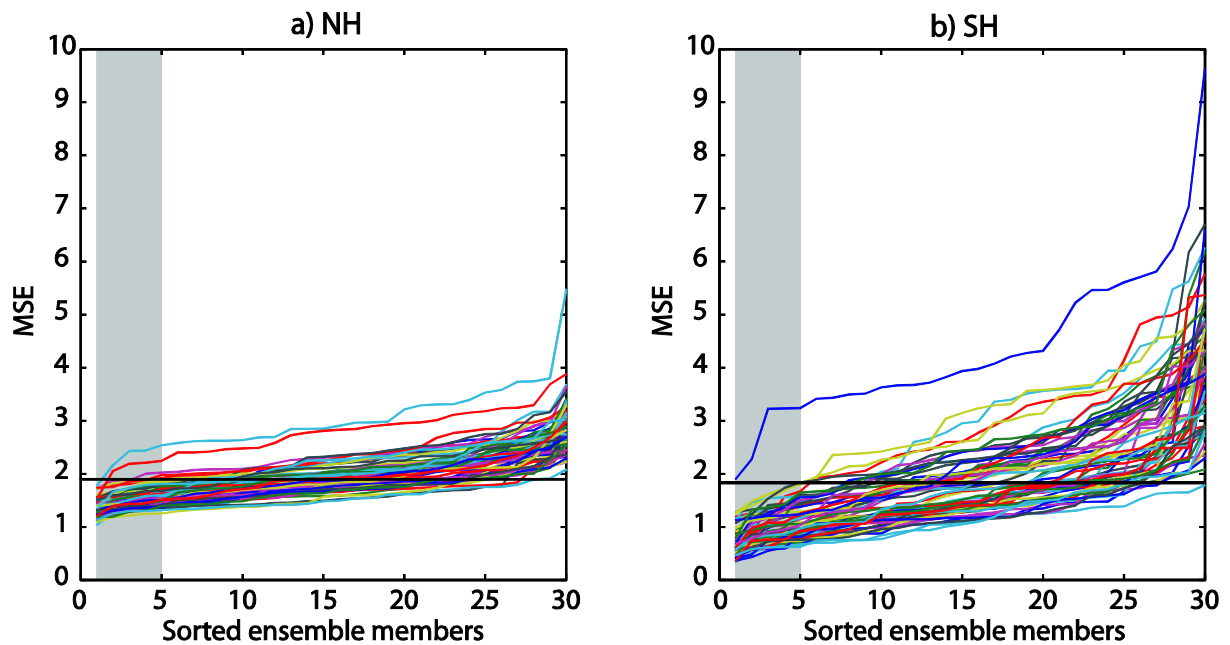
Fig. 4.2: *Quality measures of the MSE calculations sorted in ascending ensemble member order and for every individual year (coloured lines) in the Northern and Southern Hemisphere. The grey box highlights the best five ensemble members from which we calculated the standard deviation to take uncertainty into account. The horizontal line illustrates the quality of the model ensemble mean average over the period 1911-1970.*

4.3.3 Summer mean temperature and precipitation reconstruction

The time series of Northern summer temperatures (Fig. 4.3a) and precipitation (Fig. 4.3b) averaged over all available sites illustrates the importance of internal variability. As expected, our reconstruction has stronger interannual variability than the ensemble mean of CCC400 and the low-frequency variability is strongly bound to the model by methodological constraints. Goosse et al. (2005a,b) and Bhend et al. (2012) found similar results in their analyses in which they clearly demonstrated that averaging of different model runs tends to remove internal variability and accentuates the forced response of the system. These observations indicate the suitability of our approach to constrain the ensemble mean with additional tree-ring data.
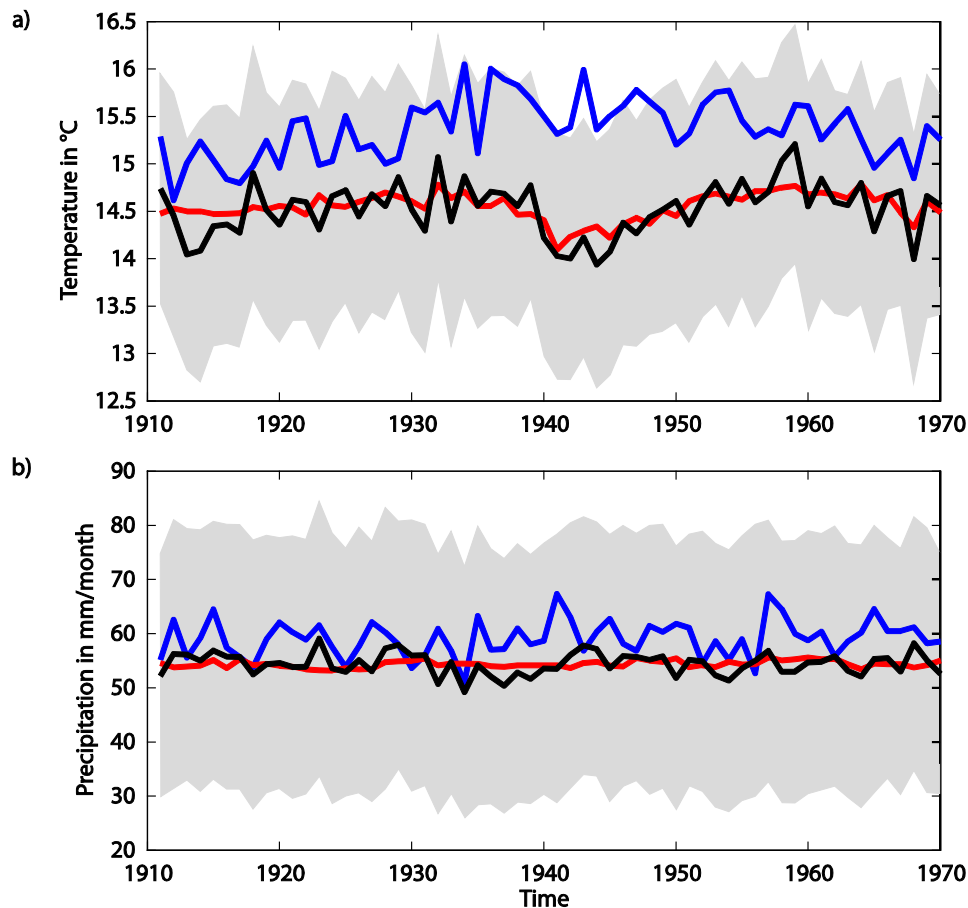
Fig. 4.3: *Summer (April to September) average temperature (top panel) and precipitation (lower panel) for all available sites in the Northern Hemisphere in the analogue reconstruction (black line). The red line is the CCC400 ensemble average and the blue line is CRU. The grey area denotes the standard deviation of the best five selected ensemble members.*

The world maps in the right panels of Fig. 4.4 show the Pearson correlation coefficient between temperature in CRU and temperature in CCC400$_{reconstruction}$ (Fig. 4.4c) and between precipitation in the two data sets (Fig. 4.4d) for the NH and SH summer seasons of 1911-1970. Likewise, the left panels of Fig. 4.4 display the Pearson correlation coefficient between temperature in CRU and temperature in CCC400$_{ensemble\ mean}$ (Fig. 4.4a) and between precipitation in CRU and precipitation in CCC400$_{ensemble\ mean}$ (Fig. 4.4b) for comparison. Comparison of these world maps shows that our reconstruction approach was successful at improving skill of temperature fields over Europe and Siberia, with more limited improvements over much of North America. Comparison of the temperature correlation coefficients over North America in Fig. 4.4a and Fig. 4.4c reveals that climate was already well captured over most of this El Niño-Southern Oscillation (ENSO) influenced region, and hence, we did not gain much improvement. On the other hand, temperature fields obtained by assimilating tree-ring data show notable improvements compared to the ensemble mean for central North America. In contrast, patterns of precipitation correlation coefficients are spatially more heterogeneous. Largest improvements in precipitation fields from the tree-ring assimilations were obtained over central Europe and the central/eastern United States. Note, however, that locations particularly in the

southeastern United States could not be reconstructed skilfully due to large uncertainties here in the GCM ensemble (see Fig. 4.1d/e). Moreover, we were not able to provide skilful reconstructions in the Southern Hemisphere which we attribute to i) the more limited amounts of tree-ring data and ii) biases in the GCM representation of Southern Hemisphere climate variability and thus greater difficulties in mimicking CRU variability as well as faithfully simulating tree-ring chronologies
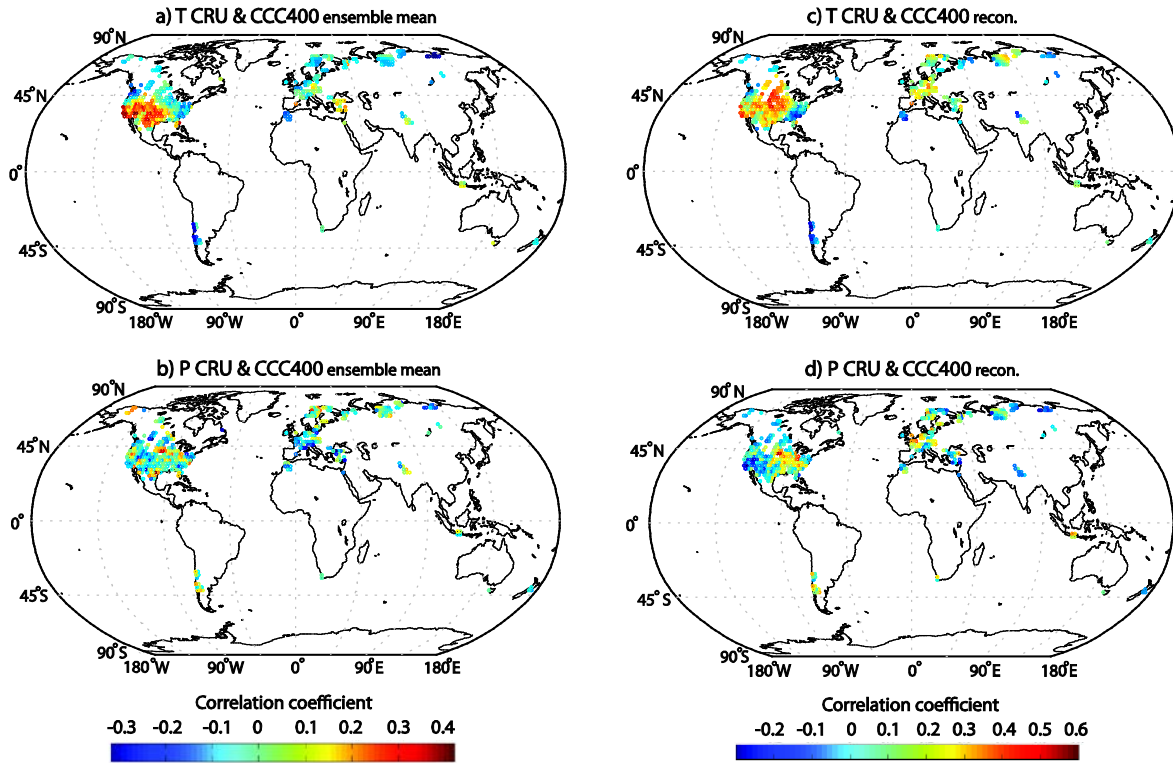
Fig. 4.4: *Pearson correlation coefficients between CRU and CCC400$_{ensemble\ mean}$ (left panels) and between CRU and CCC400$_{reconstruction}$ (right panels) for temperature (top panels) and for precipitation (lower panels). Results are shown for all 405 locations, with correlation analyses performed for the summer season April to September in the NH, and October to March in the SH, respectively during 1911-1970.*

4.4 Discussion

In order to assess the potential of our reconstruction approach, we determined lower and upper skill bounds hypothesising that correlations between the CCC400$_{reconstruction}$ and CRU data should be higher than between CCC400$_{ensemble\ member}$ and CRU and lower than correlations obtained by assimilating actual CRU data instead of simulated tree-ring series. The upper limits (CCC400$_{upper\ reconstruction}$) for the reconstruction methodology are based on MSE calculations using the summer season means of CCC400$_{ensemble\ member}$ series and CRU instead of TRW$_{VSL}$ and TRW$_{ITRDB\ agg}$, as described in eq (1). Hence, we neither incorporated proxy information nor the VSL forward model in this CCC40$_{upper\ reconstruction}$ to reconstruct past climate. The histograms in Fig. 4.5 illustrate the correlation coefficients between temperature and precipitation of CRU and CCC400 for the lower limit (Fig. 4.5a/b), for the upper limit
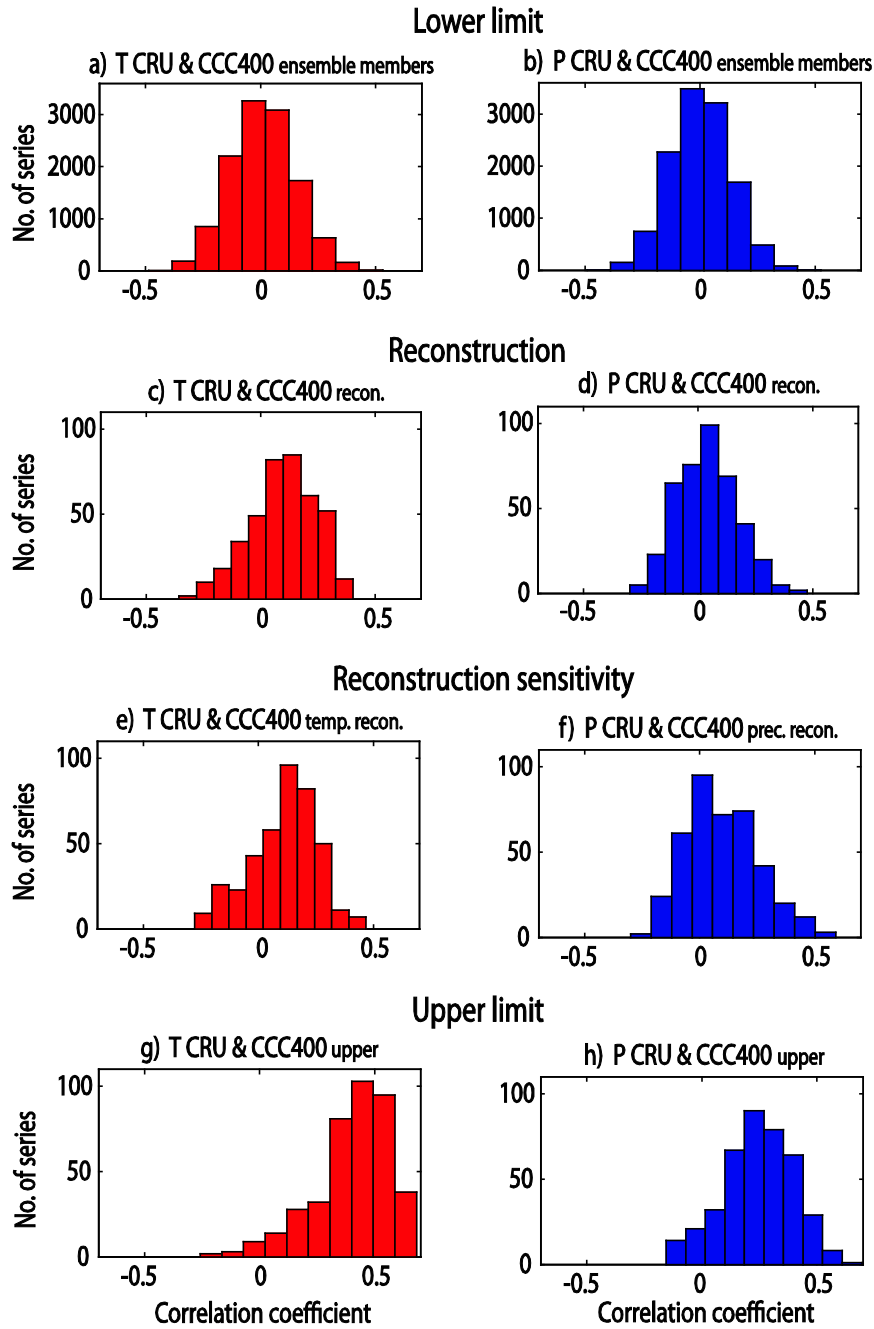
(Fig. 4.5g/h), and for the actual reconstruction (Fig. 4.5c/d). The results are as expected; the median and the upper tail of the distribution of our reconstruction are between the lower and upper limit. However, we are missing the high correlation coefficients in the upper limit precipitation reconstruction (Fig. 4.5h) which clearly imposes a limit for our precipitation reconstruction using CCC400 precipitation input data.

In a next step, we tested a reconstruction approach whereby we applied temperature and moisture-limited $TRW_{ITRDB\ agg}$ series separately for the calculation of the MSE in eq. (1) to select the best ensemble members for summer season temperature and precipitation, respectively. In short, we only used information from temperature-limited tree-ring series to reconstruct temperature (Fig. 4.5e) and vice-versa for precipitation (Fig. 4.5f). Note, however, that most grid cells have $TRW_{ITRDB\ agg}$ where modelled growth is limited by both temperature and moisture variation. Of all grid cells in the NH (SH), 64.7% (82.6%) VSL simulated growth is mainly driven by temperature fluctuations, 81.9% (69.6%) by moisture, and 45.6% (52.2%) of all the grid cells have modelled tree growth influenced by both temperature and moisture.

Improvements of the reconstruction skill between temperature fields using all VSL simulated sites (Fig. 4.5c) only temperature-sensitive tree-ring series (Fig. 4.5e) are driven in part by correlation coefficients up to 0.45 in the Midwest of the United States (compare also with Fig. 4.4c/d). On the other hand, reductions of correlation coefficients approaching -0.2 are found for some high latitudes sites in Canada, Scandinavia and north-central Siberia. Comparable results are also obtained for precipitation fields using all (Fig. 4.5d) or only moisture-limited sites (Fig. 4.5f) with increased correlation coefficients up to 0.35 obtained for sites in Morocco and western Europe. These results from the sensitivity analyses clearly show one of the biggest advantages of the VSL forward model to explicitly account for the joint influences of temperature and hydroclimatic stress as fingerprinted on actual tree-ring proxies.

We obtain skill comparable to classical regression approaches in our analogue approach. However, some caveats apply. For instance, we did not consider uncertainties contained in the actual tree-ring data and therefore treated our proxy data as "truth". While this was a reasonable first approximation, future refinement of our approach should take uncertainties into account. Second, we did not apply any weighting. Weighting of individual ensemble members, such as biases between the CRU and CCC400 series, could use the information contained in the model more efficiently, and hence, improve the reconstruction.

Some of the low correlations between CRU and CCC400 can be explained by the number of ensemble model simulations available. Our calculations were restricted to 30 due to computational resources and more model ensembles would certainly be desirable. We average the best 5 of 30 ensemble members for each summer season in our approach to represent uncertainty, but this number of analogues clearly does not cover the full envelope of climate variability (van den Dool, 1994).

Fig. 4.5: *Lower limit, actual reconstruction skill, reconstruction sensitivity, and upper limit for temperature and precipitation shown in histograms of Pearson correlation coefficients performed for the summer seasons April to September in the NH, and October to March in the SH, respectively during 1911-1970. Upper panels: Correlation coefficients between CRU and CCC400ensemble member series (i.e. 30 ensemble simulations at 405 sites) for a) temperature and b) precipitation. Upper middle panels: Correlation coefficients between CRU and CCC400reconstruction climate series for c) temperature, d) precipitation. Lower middle panels: Correlation coefficients between CRU and e) CCC400 temperature reconstruction using only information from temperature-limited tree-ring series, f) CCC400 precipitation reconstruction using only information from precipitation-limited tree-ring series. Lowest panels: Correlation coefficients between CRU and CCC400upper reconstruction for g) temperature, and h) precipitation for all 405 locations.*

4.5 Conclusions and outlook

The main goal of this study was to examine an analogue approach relying upon a forward model of tree-ring growth and actual tree-ring chronologies to constrain a GCM model ensemble and ultimately reduce the uncertainty about past climate variation. We used the so-called Vaganov-Shashkin Lite forward model of tree-ring growth in order to compare GCM output to observed tree-ring growth during the 1911-1970 period. We could show that our approach yields notable improvements in skill compared to the ensemble mean, especially at inter-annual time-scales, based upon comparisons with CRU TS3.1 temperature and precipitation observations. Biases in the GCM climatology and variation, however, may impact the ability to accurately simulate tree growth and thus limit the quality of the reconstruction. Combining forward models from ensemble model simulations and actual tree-ring data offers great possibilities to study the climate of the past. The best analogue from high resolution model ensemble simulations yields global climatic fields of diverse parameters (e.g., pressure, wind speed, temperature at 6-hourly resolution) consistent with model physics and climate forcing. We believe one primary benefit of such data is their suitability for climate impact studies. For instance, summer heat wave or drought statistics could be studied where climatic information is not available in the required resolution.

Application of the reconstruction approach to all model grid cells and extension of the reconstruction to the full CCC400 model length back to 1600 AD will likely reduce uncertainties in our understanding of past climate. Additionally, applying our reconstruction to regions with good climate input data and a large network of very high-quality tree-rings, such as for Europe, may yield notable improvements in reconstruction skill. Comparison with conventional past climate reconstruction approaches as well as applying our reconstruction approach with other global climate models will help provide even more reliable estimations of uncertainty. Ultimately, inclusion of information from other archives such as from documentary data, corals, ice cores, or speleothems in a full assimilation approach would extend the reconstruction to other seasons and may help to identify inconsistencies between the different proxies.

References

Ammann, C. M., Joos, F., Schimel, D. S., Otto-Bliesner, B. L., and Tomas, R. A., 2007. Solar influence on climate during the past millennium: Results from transient simulations with the NCAR Climate System Model. P. Natl. Acad. Sci. USA **104**, 3713-3718.

Bhend, J., Franke, J., Folini, D., Wild, M., and Brönnimann, S., 2012. An ensemble-based approach to climate reconstructions. Clim. Past **8**, 963-976

Breitenmoser, P., Brönnimann, S., and Frank, D. Forward modelling of tree-ring width and comparison with a global network of tree-ring chronologies, to be submitted.

Cook, E. R., 1985. A time series approach to tree-ring standardization, Ph.D. thesis, University of Arizona, 171pp.

Cook, E. R., D'Arrigo, R., and Anchukaitis, K., 2008. ENSO reconstructions from long tree-ring chronologies: Unifying the differences?, talk presented at a special workshop on "Reconciling ENSO Chronologies for the Past 500 Years", held in Moorea, French Polynesia on 2–3 April.

Crowley, T. J., 2000. Causes of climate change over the past 1000 years. Science **289**, 270-277.

Crowley, T., Zielinski, G., Vinther, B., Udisti, R., Kreutz, K., Cole-Dai, J., and Castellano, E., 2008. Volcanism and the Little Ice Age. PAGES newsletter 22–23.

Franke, J., Gonzáles-Rouco, J. F., Frank, D., and Graham, N. E., 2011. 200 years of European temperature variability: insights from and tests of the Proxy Surrogate Reconstruction Analog Method. Clim. Dyn. **37**, 133-150.

Gao, C. C., Robock, A., and Ammann, C., 2008. Volcanic forcing of climate over the past 1500 years: An improved ice core-based index for climate models. J. Geophys. Res.-Atm. **113**, D23111, doi:10.1029/2008jd010239.

Gonzáles-Rouco, F., von Storch, H., and Zorita, E., 2003. Deep soil temperature as proxy for surface air-temperature in a coupled model simulation of the last thousand years. Geophys. Res. Lett., **30**(21), 2116, doi1029/203GL018264.

Goosse, H., Crowley, T., Zorita, E., Ammann, C., Renssen, H., and Driesschaert, E., 2005s. Modelling the climate of the past millennium: what causes the differences between the simulations? Geophys. Res. Lett. **32**, L06710, doi:10.1029/2005GL022368.

Goosse, H., Renssen, H., Timmermann, A., and Bradley, R. S., 2005b. Internal and forced climate variability during the last millennium: a model-data comparison using ensemble simulations. Quat. Sci. Rev. **24**, 1345-1360.

Goosse, H., Renssen, H., Timmermann, A., Bradley, R. S., and Mann, M. E., 2006. Using paleoclimate proxydata to select optimal realisations in an ensemble of simulations of the climate of the past millennium. Clim. Dyn. **27**(2–3), 165-184.

Goosse, H., Crespin, E., de Montety, A., Mann, M. E., Renssen, H., and Timmermann, A., 2010. Reconstructing surface temperature changes over the past 600 years using climate model simulations with data assimilation. J. Geophys. Res. **115**, D09108, doi:10.1029/2009JD012737.

Gray, L. J., Beer, J., Geller, M., Haigh, J. D., Lockwood, M., Matthes, K., Cubasch, U., Fleitmann, D., Harrison, G., Hood, L., Luterbacher, J., Meehl, G. A., Shindell, D., Van Geel, B., and White, W., 2010. Solar influences on climate. Rev. Geophys. **48**, RG4001, doi:10.1029/2009 RG000282.

Grissino-Mayer, H. D. and Fritts, H. C., 1997. The International Tree-Ring Data Bank: an enhanced global database serving the global scientific community. Holocene **7**, 235-238.

Guiot, J., Wu, H. B., Garreta, V., Hatte, C., and Magny, M., 2009. A few prospective ideas on climate reconstruction: from a statistical single proxy approach towards a multi-proxy and dynamical approach, Clim. Past. **5**, 571-583.

Huang, H-P., Seager, R., and Kushnir, Y., 2005. The 1976/77 transition in precipitation over the Americas and the influence of tropical seas surface temperature. Clim. Dyn. **24**, 721-740.

Huang, J., van den Dool, H. M., and Georgankakos, K. P., 1996. Analysis of model-calculated soil moisture over the United States (1931-1993) and applications to long-range temperature forecasts. J. Clim. **9**, 1350-1362.

Hughes, M. K. and Ammann, C. M., 2009. The future of the past - An Earth system framework for high resolution paleoclimatology: editorial essay. Clim. Change **94**, 247-259.

Jansen, E., Overpeck, J., Briffa, K., Duplessy, J., Joos, F., Masson-Delmotte, V., Olago, D., Otto-Bliesner, B., Peltier, W., Rahmstorf, S., Ramesh, R., Raynaud, D., Rind, D., Solomina, O., Villalba, R., and Zhang, D., 2007. Paleoclimate. In: Solomon, S., Qin, D., Manning, M., Chen, Z., Marquis, M., Averyt, K., Tignor, M., and Miller, H. (eds.), Climate Change 2007: The physical science

basis, Contribution of working group I to the Fourth Assessment Report of the Intergovernmental Panel on Climate Change, Cambridge University Press, Cambridge, United Kingdom and New York, NY, USA.

Jones, P. D., Osborn, T. J., and Briffa, K. R., 1997. Estimating sampling errors in large-scale temperature averages. J. Climate **10**, 2548-2568.

Jones, P. D., Briffa, K. R., Osborn, T. J., Lough, J. M., van Ommen, T. D., Vinther, B. M., Luterbacher, J., Wahl, E. R., Zwiers, F. W., Mann, M. E., Schmidt, G. A., Ammann, C. M., Buckley, B. M., Cobb, K. M., Esper, J., Goosse, H., Graham, N., Jansen, E., Kiefer, T., Kull, C., Küttel, M., Mosley-Thompson, E., Overpeck, J. T., Riedwyl, N., Schulz, M., Tudhope, A. W., Villalba, R., Wanner, H., Wolff, E., and Xoplaki, E., 2009. High-resolution palaeoclimatology of the last millennium: a review of current status and future prospects. Holocene **19**(1), 3-49.

Jungclaus, J. H., Lorenz, S. J., Timmreck, C., Reick, C. H., Brovkin, V., Six, K., Segschneider, J., Giorgetta, M. A., Crowley, T. J., Pongratz, J., Krivova, N. A., Vieira, L. E., Solanki, S. K., Klocke, D., Botzet, M., Esch, M., Gayler, V., Haak, H., Raddatz, T. J., Roeckner, E., Schnur, R., Widmann, H., Claussen, M., Stevens, B., and Marotzke, J., 2010. Climate and carbon-cycle variability over the last millennium. Clim. Past **6**, 723-737, doi:10.5194/cp-6-723-2010.

Koch, D., Jacob, D., Tegen, I., Rind, D., and Chin, M., 1999. Tropospheric sulfur simulation and sulfate direct radiative forcing in the Goddard Institute for Space Studies general circulation model. J. Geophys. Res.-Atmos. **104**, 799–822.

Lean, J., 2000. Evolution of the sun's spectral irradiance since the Maunder Minimum. Geophys. Res. Lett. **27**, 2425–2428.

Mann, M. E., Woodruff, J. D., Donnelly, J. P., and Zhang, Z. H., 2009. Atlantic hurricanes and climate over the past 1500 years. Nature **460**, 1256–1260.

Mitchell, T. D. and Jones, P.D., 2005. An improved method of constructing a database of monthly climate observations and associated high-resolution grids. Int. J. Climatol. **25**, 693-712.

Mo, K. C., 2010. Interdecadal modulation of the impact of ENSO on precipitation and temperature over the United States. J. Clim. **23**, 3639-3656.

Pongratz, J., Reick, C., Raddatz, T., and Claussen, M., 2008. A reconstruction of global agricultural areas and land cover for the last millennium. Global Biogeochem. Cy. **22**, GB3018, doi:10.1029/2007GB003153.

Rayner, N. A., Parker, D. E., Horton, E. B., Folland, C. K., Alexander, L. V., Rowell, D. P., Kent, E. C., and Kaplan, A., 2003. Global analyzes of sea surface temperature, sea ice, and night marine air temperature since the late nineteenth century. J. Geophys. Res. Atmos. **108**, 4407, doi:10.1029/2002 JD002670.

Roeckner, E., Bäuml, G., Bonaventura, L., Brokopf, R., Esch,M., Giorgetta, M., Hagemann, S., Kirchner, I., Kornblueh, L., Manzini, E., Rhodin, A., Schlese, U., Schulzweida, U., and Tompkins, A., 2003. The atmospheric general circulation model ECHAM5 Part I: model description. Tech. rep. **349**, Max Planck Institute for Meteorology.

Roeckner, E., Brokopf, R., Esch, M., Giorgetta, M., Hagemann, S., Kornblueh, L., Manzini, E., Schlese, U., and Schulzweida, A., 2004. The atmospheric general circulation model ECHAM5 Part II: Sensitivity of simulated climate to horizontal and vertical resolution. Tech. rep. **354**, Max Planck Institute for Meteorology.

Shindell, D. T., Schmidt, G. A., Miller, R. L., and Mann, M. E., 2003. Volcanic and solar forcing of climate change during the preindustrial era. J.Clim. **16**(24), 4094-4107.

Steinhilber, F., Beer, J., and Fröhlich, C., 2009. Total solar irradiance during the Holocene. Geophys. Res. Lett. **36**, L19704. doi:10.1029/2009gl040142.

Thompson, D. M., Ault, T. R., Evans, M. N., Cole, J. E., and Emile-Geay, J., 2011. Comparison of observed and simulated tropical climate trends using a forward model of coral $\delta^{18}O$. Geophys. Res. Lett. **38**, L14706, doi:10.1029/2011GL048224.

Tingley, M. P., Craigmile, P. F., Haran, M., Li, B., Mannshardt, E., and Rajaratnam, B., 2012. Piecing together the past: statistical insights into paleoclimatic reconstructions. Quaternary Sci. Rev., 35, 1-22.

Tolwinski-Ward, S. E., Evans, M. N., Hughes, M. K., and Anchukaitis, K. J., 2011a. An efficient forward model of the climate controls on interannual variation in tree-ring width. Clim. Dyn. **36**, 2419-2439.

Tolwinski-Ward, S. E., Evans, M. N., Hughes, M. K., and Anchukaitis, K. J., 2011b. Erratum to: An efficient forward model of the climate controls on interannual variation in tree-ring width. Clim. Dyn. 36, 2441-2445.

Vaganov, E. A., Hughes M. K., and Shashkin, A. V., 2006. Growth dynamics of conifer tree rings. In: Growth dynamics of tree rings: Images of past and future environments. Ecological studies **183**, Springer, New York.

van den Dool, H. M., 1994. Searching for analogues, how long must we wait? Tellus **46A**, 314-324.

Wahl, E. and Frank, D., 2012. Evidence of environmental change from annually-resolved proxies with particular reference to dendroclimatology and the last millennium. In: Matthews, J. A. (ed.), The SAGE handbook of environmental change **1**, Sage, 320-344.

Wanner, H., Beer, J., Bütikofer, J., Crowley, T. J., Cubasch, U., Flückiger, J., Goosse, H., Grosjean, M., Joos, F., Kaplan, J. O., Küttel, M., Müller, S. A., Prentice, I. C., Solomina, O., Stocker, T. F., Tarasov, P., Wagner, M., and Widmann, M., 2008. Mid- to Late Holocene climate change: an overview. Quaternary Sci. Rev. **27**, 1791-1828.

Widmann, M., Goosse, H., van der Schrier, G., Schnur, R., and Barkmeijer, J., 2010. Using data assimilation to study extratropical Northern Hemisphere climate over the last millennium. Clim. Past **6**, 627-644, doi:10.5194/cp-6-627-2010.

Yoshimori, M., Raible, C. C., Stocker, T. F., and Renold, M., 2010. Simulated decadal oscillations of the Atlantic meridional overturning circulation in a cold climate state. Clim. Dynam. **34**, 101-121.

Acknowledgements

Chapter 5

CONCLUSION AND OUTLOOK

This thesis presented three studies analysing various aspects of climatic growth signals in observed and modelled tree-rings in a global network of tree-rings to deepen our understanding of past climate variability and to provide a first attempt to combine model and proxy data. The following conclusions can be drawn:

- Solar and volcanic fingerprints could be identified in a global compilation of all presently available tree-ring chronologies covering the past about 2000 years.
- The coincidence of solar and volcanic events during the LIA complicated attribution, but nevertheless, physically plausible and significant climate response lags of approximately 0 to 20 years relative to solar forcing and significant periodicities near the about 200 years DeVries frequency point to a possible solar imprint in the tree-ring chronologies.
- Moreover, evidences of synchronous cooling events in respect to highly explosive tropical volcanic eruptions could be described.
- Bayesian estimation of the VSL growth response parameters performed well for a wide range of species, environmental conditions, and time intervals, confirming the model's general applicability for worldwide studies using CRU climate input data. Global assessment of the growth-onset threshold temperature (T_1) of approximately 4-6 °C for most sites and species, thus providing new evidence for on-going debates regarding the lower temperatures at which growth may take place.
- Performing spatial aggregation of ring-width chronologies based upon chronology quality, climate response and proximity reduced non-climatic noise and resulted in improved relationships between observed and modelled tree-growth as well as a spatial extension of regions where simulations could be validated.
- The VSL model's ability to skilfully simulate tree-ring series with historical climate data was demonstrated.
- The use of the VSL model as an observation operator in a novel analogue approach proofed concept to reconstruct past summer season temperature and precipitation from ensemble member simulations of an ECHAM5.4 general circulation model variant. This methodology represented a first, but significant step toward data-assimilation.
- Comparison with CRU data showed that constraining the model ensemble simulations with proxy information could be used to skilfully reduce uncertainty in a network of 405 locations,

especially at the interannual time scale, while maintaining physically plausible results. However, biases in climatology and variability inherent to current generation climate models significantly impacted the quality of the reconstruction.

- The research demonstrated opportunities to skilfully reconstruct climate using tree-ring data far away from the more typical locations where growth is limited by one climate parameter. The VSL model makes this possible by explicitly integrating joint temperature and moisture variation in a non-linear way.

These studies contributed to an enhanced understanding of past climate variability and provided valuable knowledge to the advancement of combining model and proxy data. It could be shown that successful implementation of forward models in future assimilation approaches strongly rely on continued efforts to improve climate models and proxy data.

This research uncovered many limitations which need to be addressed in future research. For instance, challenges for climate research in general, and dendroclimatology in particular are: First, new and long chronologies need to be acquired, especially in the so far underrepresented regions of the mid-latitudes of both hemispheres. There are presently less than 20 series globally that go back about two millennia to estimate past climate variability and its relation to external forcings. Second, it is imperative to continuously update the major tree-ring networks. Unfortunately, many high-quality chronologies stop in the late 70s of the last century and have not been updated. Hence, they do not contain the rapid global warming of the last decades nor can the shift in recent growth responses of trees (known as "divergence"; Jacoby and D'Arrigo, 1995; Briffa et al., 1998; D'Arrigo et al., 2008) be in terms of potential changes biasing the climate response in tree-rings.

Besides efforts to continuously improve global climate models and reconstruction methodologies, advances in the development of forward models are imperative. Such dynamical forward models should, of course, be as simple as possible, while still capturing all relevant features between climate and tree growth to adequately describe all relevant climatic processes in the past, present, and in the future.

Possible future applications of the results of this thesis are:

- The VSL forward model could be used to study what kind of fingerprint can be expected in the global network of tree-rings in response to external perturbations of the climate system. For instance, the effect of increased temperature and changes in precipitation on tree growth could be analysed in the context of global warming but also by comparison with observed tree-rings displaying non-stationarities in the climate-growth relationships (Jacoby and D'Arrigo, 1995; Briffa et al., 1998; D'Arrigo et al., 2008). Likewise, growth thresholds could be studied in relation to climatic extremes such as after large volcanic eruptions. This is especially important in terms of variable integration windows and in an extensive global network of tree-rings. At the same time, a thorough examination of the Bayesian growth response estimation approach would significantly contribute to the ongoing scientific debate about threshold levels for growth initiation (Anchukaitis et al., 2012; Mann et al., 2012). This could be achieved by using different priors than the uniform distribution applied in this

analysis or by more sophisticated sampling approaches than Hastings-within-Gibbs sampling algorithm.

- The analogue reconstruction of summer temperature and precipitation represents a first step toward more sophisticated data-assimilation oriented approaches. Results showed that this approach is suitable for climate impact studies, providing detailed information at sites and with variables that are not directly available from proxy data, but which is consistent with model physics and climate forcing. Further optimization will likely reduce uncertainties in our understanding of climate since 1600. Direct incorporation of more sophisticated hydrology schemes, which better represents moisture storage and delayed moisture supply through snow processes, may be an improvement. Uncertainties contained in the observed tree-ring data, the input climate model, the climate validation data set, and the forward model should be included within more sophisticated assimilation approaches. Additionally, the analogue reconstruction can be validated against regression-based reconstructions and other data-assimilation approaches when they become increasingly available. This comparison could lead to new, improved approaches integrating as many different data sources as possible across space, time and proxy types (including other tree proxies), benefiting from the reconciliation of proxy and model data and enhancing the confidence of estimates of past climate change and help identify inconsistencies between the different proxies.

References

Anchukaitis, K. J., Evans, M. N., Kaplan, A., Vaganov, E. A., Hughes, M. K., Grissino-Mayer, H. D., and Cane, M. A., 2006. Forward modeling of regional scale tree-ring patterns in the southeastern United States and the recent influence of summer drought. Geophys. Res. Lett. **33**, L04705, doi:10.1029/2005GL025050.

Anchukaitis, K. J., Breitenmoser, P., Briffa, K. R., Buchwal, A., Büntgen, U., Cook, E. R., D'Arrigo, R. D., Esper, J., Evans, M. N., Frank, D., Grudd, H., Gunnarson, B. E., Hughes, M. K., Kirdyanov, A. V., Körner, C., Krusic, P.J., Luckman, B., Melvin, T. M., Salzer, M. W., Shashkin, A. V., Timmreck, C., Vaganova E. A., and Wilson, R. J. S., 2012. Tree rings and volcanic cooling. Nature Geoscience, doi:10.1038/ngeo1645.

Briffa, K. R., Schweingruber, F.H., Jones, P. D., Osborn, T. J., Shiyatov, S. G., and Vaganov, E. A., 1998. Reduced sensitivity of recent tree-growth to temperature at high northern latitudes. Nature **391**, 678-682.

D'Arrigo, R., Wilson, R., and Cherubini, P., 2008. On the 'Divergence Problem' in Northern Forests: A review of the tree-ring evidence and possible causes. Global Planet. Change **60**, 289-305.

Jacobey, G. C. and D'Arrigo, R. D., 1995. Tree-ring width and density evidence of climatic and potential forest change in Alaska. Global Biogeochem. Cy.**9**, 227-234.

Mann, M. E., Fuentes, J. D., and Rutherford, S., 2012. Underestimation of volcanic cooling in tree-ring based reconstructions of hemispheric temperatures. Nat. Geosc., doi:10.1038/NGEO1394.

Acknowledgements

First of all, I would like to acknowledge Prof. Dr. Heinz Wanner for offering me the opportunity to do a PhD in Bern. You were always interested and supportive in the initial phase of my thesis and a great motivator of the KLIMET group. My other just as warm thanks go to Prof. Dr. Stefan Brönnimann for being my supervisor but especially for your support, trust, and all your valuable comments and discussions. Thanks for giving me the opportunity to attend numerous conferences and workshops in which I could connect to different climate research communities. Dr. David Frank, heartfelt thanks for introducing me into the world of trees, for always being interested in my work and for the supply of vital support in the tree-ring work. You've also spent a lot of time for critical examinations of my papers and provided very important and constructive criticism throughout my PhD, which I am very thankful for. I thank Prof. Dr. Martin Grosjean, from the Oeschger Center who made it possible to do this thesis within the Graduate School of Climate Sciences and for giving me the opportunity to connect to the climate research community very early in my PhD. Marlis Röthlisberger and Isa Geissmüller, I always appreciated your help in any administrational matters. I would like to extend my thanks to all current and past colleagues from KLIMET and FERKL, for all the good times and the lively discussions during the coffee breaks, mensa lunches, or funny evening events. You guys are too numerous to mention here all by name but you made the 5th floor a great place to work. Nevertheless, special thanks go to my fellow office dweller Reni, for the plenty of good times in the office and Dr. Jörg Franke, who solved all problems arising from the model data and provided me with critical inputs to some parts of this thesis. I am most thankful to my family and friends from near and far. You enriched my life so much, thanks for your support, welcome distractions, positive energy, and warm friendships. Sarah and Tamara, I am especially thankful to have your friendship and ongoing encouragement during the last two months after my accident. Unfortunately, my beloved "Nini" and "Grosi" were not allowed to see this thesis to be completed but I am grateful for all your love. I am missing you. Last but not least, I am deeply grateful to my parents and sister, for your love and support whatever I do.

Declaration

under Art. 28 Para. 2 RSL 05

Last name, first name:	Breitenmoser, Petra Daniela
Matriculation number:	03-702-321
Programme:	PhD of Science in Climate Sciences
	Bachelor ☐ Master ☐ Dissertation ☒
Thesis title:	Climatic growth signatures in observed and modelled tree-rings – constraints from a global tree-ring network
Thesis supervisor:	Prof. Dr. Stefan Brönnimann

I hereby declare that this submission is my own work and that, to the best of my knowledge and belief, it contains no material previously published or written by another person, except where due acknowledgement has been made in the text. In accordance with academic rules and ethical conduct, I have fully cited and referenced all material and results that are not original to this work. I am well aware of the fact, on the basis of Article 36 Paragraph 1 Letter o of the University Law of 5 September 1996, the Senate is entitled to deny the title awarded on the basis of this work if proven otherwise.

Bern, December 17, 2012

Signature

Curriculum Vitae

Personal	Petra Daniela Breitenmoser	
	Am Landsberg 7, 8330 Pfäffikon, Switzerland	
	Born 24th April 1978 in Wetzikon, Switzerland	

Education	2009-2013	PhD student in Climate Sciences, Institute of Geography and Oeschger Centre for Climate Change Research, University of Bern
	2003-2009	B.Sc and M.Sc student in Geography, University of Zurich
	2007-2008	B.Sc (hons) student in Antarctic and Southern Ocean Studies, University of Tasmania
	1998-2001	Teacher training, primary school teacher diploma
	1991-1998	Kantonsschule Zürcher Oberland, Wetzikon
	1995	Cashmere High School, Christchurch, New Zealand
	1985-1991	Primary School, Saland and Pfäffikon

Professional experience	2009-2013	Assistant at the Institute of Geography, University of Bern
	2006-2007	Assistant at the Institute of Geography, University of Zurich
	2001-2003	Teacher at Primary School Hittnau